

UiO : **University of Oslo**

Karolina Spustova

Membranous Protocell Superstructures

Thesis submitted for the degree of Philosophiae Doctor

Department of Chemistry

Faculty of Mathematics and Natural Sciences

Centre for Molecular Medicine Norway

Faculty of Medicine



2021

© **Karolina Spustova, 2021**

*Series of dissertations submitted to the
Faculty of Mathematics and Natural Sciences, University of Oslo
No. 2467*

ISSN 1501-7710

All rights reserved. No part of this publication may be
reproduced or transmitted, in any form or by any means, without permission.

Cover: Hanne Baadsgaard Utigard.
Print production: Representralen, University of Oslo.

Preface

This thesis is submitted in partial fulfillment of the requirements for the degree of *Philosophiae Doctor* at the Department of Chemistry, Faculty of Mathematics and Natural Sciences, University of Oslo. The research presented here was conducted in the time period October 2018 to December 2021 under the supervision of Dr. Irep Gözen, and co-supervision of Dr. Reidar Lund and Dr. Andreas Carlson.

The thesis is collection of four original papers presented in chronological order of writing. The papers are preceded by introductory chapters that provide background information for the reader and explain the motivation behind the work. Additional publications that are not included in this thesis are listed.

Karolina Spustova

Oslo, September 2021

Table of Contents

List of publications	vii
Author's contributions	ix
Abstract	xi
1 Introduction	1
2 Primitive cell models for the origin of life	3
2.1 Hypotheses on the origins of life	3
2.1.1 The RNA world	5
2.1.2 Lipid world.....	6
2.2 Prebiotic compartments	7
2.2.1 Membranous protocells.....	8
2.3 Surface adhered membranous compartments.....	11
2.4 Prebiotic subcompartmentalization.....	11
3 Surface energy and wetting phenomena	13
3.1 Surface free energy	13
3.2 Wetting phenomena and interfacial energies	14
3.3 Micro- and nanoengineered surfaces	15
3.4 Natural mineral surfaces	16
4 Membrane mechanics	19
4.1 Lipid molecules and lipid polymorphism	19
4.2 Self-assembly.....	21
4.3 Lipid membrane fluidity	22
4.4 Lipid membrane mechanics	23
4.5 Formation of vesicles from lipid bilayers	23
4.6 Phospholipid vesicles	25
4.7 Supported membranes	26
4.8 Nanotube formation and protocell nucleation	27
4.9 Van der Waals Interactions	28
4.10 Membrane permeability and transient pores	29

5	Methods.....	31
5.1	Preparation of lipid vesicles	31
5.1.1	Preparation of small unilamellar vesicles	32
5.2	Surface fabrication	32
5.3	Characterization of surfaces.....	35
5.4	Epifluorescence and confocal fluorescence microscopy	36
5.5	Fluorescence recovery after photobleaching	39
5.6	Near infrared laser heating	39
5.7	Microfluidics.....	40
5.8	DNA strand displacement reactions	42
5.9	Analytical models	42
5.9.1	Finite element model for uptake through transient pores	43
6	Summary of the main findings.....	45
7	Conclusion and future outlook	47
	Acknowledgments.....	49
	References	51

List of publications

- Paper I S. Jõemetsa, K. Spustova, K. Kustanovich, A. Ainla, S. Schindler, S. Eigler, T. Lobovkina, S. Lara-Avila, A. Jesorka, I. Gözen
Molecular Lipid Films on Microengineering Materials
Langmuir 2019, 35, 32, 10286 – 10298
- Paper II K. Spustova, E. S. Köksal, A. Ainla, I. Gözen
Subcompartmentalization and Pseudo-Division of Model Protocells
Small 2020, 17, 2005320
- Paper III K. Spustova, C. Katke, E. Pedrueza Villalmanzo, R. Ryskulov, C. N. Kaplan, I. Gözen
Colony-like Protocell Superstructures
Submitted manuscript
- Paper IV I. J. Schanke, L. Xue, K. Spustova, I. Gözen
Transport among Protocells via Tunneling Nanotubes
Submitted manuscript

List of related publications by the author that are not included in this thesis

Paper V K. Spustova, L. Xue, R. Ryskulov, A. Jesorka, I. Gözen

Manipulation of Lipid Membranes with Thermal Stimuli

In press, book chapter in *Methods in Molecular Biology* 2021

Paper VI E. S. Köksal, I. Põldsalu, L. Xue, K. Spustova, R. Ryskulov, F. Meng, E. Pedrueza Villalmanzo, A. Jesorka, I. Gözen

Milestones and Recent Advances in Protocells

Submitted review article, *Small*

Author's contributions

- Paper I K.S. contributed to the data collection shown in Fig. 4, Tab. 1 and SI. Developed a zeta potential measurement method for custom sample sizes, performed zeta-potential measurements of solid surfaces used in the study, and analyzed the associated experimental data. K.S. contributed to the first reported measurement and calculation of graphene monolayer zeta potential. K.S. prepared all movies in SI, analyzed fluorescence recovery after photobleaching experiments, and prepared Fig. S3.2, S3.3 and S4. She contributed to the writing of the manuscript, and prepared the revised submission, including manuscript and response letter.
- Paper II K.S. carried out all the experiments showing the spontaneous subcompartmentalization and pseudo-division of surface-adhered protocells. Performed all the microscopy and microfluidics-associated experiments at room temperature and at elevated temperatures. K.S. analyzed the experimental data: the time dependent changes in membrane area, number and size of the subcompartments, and the fluorescent intensity analyzes. She contributed to the writing of the manuscript.
- Paper III K.S. carried out all the experiments showing formation and development of surface-adhered protocell colonies. Author performed all the confocal microscopy experiments of the time dependent changes in protocell structures in both at room temperature and at elevated temperatures. K.S. proposed and carried out the mechanical stability experiments shown in Fig. 3. Author performed microfluidic experiment showing encapsulation of fluorescein and DNA molecules, and non-enzymatic DNA reactions. She analysed the time dependent changes in subcompartments and colony number, size and area, and the fluorescent intensity analyses and prepared Fig. 1, 2, 4, 5, and supplement information. Author contributed to the writing of the manuscript.
- Paper IV K.S. performed the control experiments with confocal microscopy and prepared Fig. 1, she assisted the analysis of Fig. 2 and contributed to the writing of the manuscript.

Abstract

This thesis focuses on the shape transformations of biomembrane assemblies on solid surfaces as models featuring primitive, cell-like compartments at the origin of life: the protocells. On solid substrates the biomembranes are able to spontaneously perform non-trivial morphological transformations resulting in formation of protocell-nanotube networks, or subcompartmentalized protocells. The work includes a detailed characterization of the interaction of lipid membranes with surfaces made of various micro-engineering materials including silica-based substrates, metal oxides, polymers and graphene. The networks are utilized for investigating possible communication among protocells through the nanotubes. The special emphasis has been put on membranous superstructures which are reminiscent of bacterial colonies with hundreds to thousands of adjacent compartments. In contrast to the widely accepted membranous protocell models consisting of single unilamellar vesicles, the surface-based biogenesis provides alternative routes to sophisticated primitive membrane systems both in terms of structure and function.

1 Introduction

How first living cells emerged on the early Earth is still an unanswered question. In fact, the exact criteria of living have not been conclusively defined. A 2012 paper by Trifonov¹ analyzed the mutual words among 123 published definitions of life which led to nine main groups of terms: *system, matter, chemical, complexity, reproduction, evolution, environment, energy and ability*. It is evident that sufficient amount of our understanding of life, represented by these keywords, are associated with the characteristics of biological cells, the earliest and basic entity of all living organisms capable of self-sufficiency and reproduction. One theoretical model, the chemoton, has laid out three essential characteristics of a minimal cell to be considered as living²: a heritable form of information; a metabolic system producing energy and building components; and a membranous physical boundary. Contemporary living cells carry all these features including the membrane boundary termed 'the plasma membrane'.

A substantial amount of the experimental effort in origin of life research has been put into combining membranous compartments with other prebiotic materials and environmental conditions representing early Earth. The aim is to build an understanding of the response of the primitive compartments to the external components and conditions, and ultimately instigate the development and self-reproduction of compartments mimicking the origin of life. A commonly utilized model of membranous compartments comprises single-shelled lipid vesicles freely suspended in aqueous media. These vesicular compartments are formed via self-assembly of lipid monomers upon dispersion into aqueous environments.

In this thesis, I investigated a different route to the formation of protocells: solid surface-based pathways with a special focus on autonomous compartmentalization ability of lipid assemblies. Surfaces intrinsically have excess energy which can be harnessed by soft materials upon contact, specifically with lipid agglomerates. On surfaces, lipid compartments can perform complex shape transformations resulting in interactive compartmentalized structures and protocell populations. The experimental systems I developed require only a minimal number of prebiologically-relevant components: mineral-like solid surfaces, amphiphilic molecules and suitable aqueous environments³. Along with amphiphiles and water, surfaces naturally existed on the early Earth in form of minerals and rocks.

In the light of these ideas, the diverse behavior of lipid membranes on various solid surfaces was investigated and reported in **Paper I**⁴. In **Paper II**⁵ a subcompartmentalization mechanism mediated by solid surfaces was introduced, resulting in formation of tens of micro-compartments inside a single surface-adhered protocell, reminiscent of intra-cellular organelles. In **Paper III** colony-like protocell superstructures were shown to emerge from simple lipid assemblies via mechanisms described in Paper II, and perform non-enzymatic DNA strand displacement

reactions. Finally, in **Paper IV** the capability of protocell compartments to communicate via tunneling nanotubes was investigated and reported.

In the subsequent chapter (Part 2) of my thesis, I provide an overview of the origin of life problem, and describe the widely accepted hypotheses as well as the features of commonly utilized forms of the prebiotic compartments and their development.

In Part 3, I introduce the concept of surface and interfacial energies, and explain surface tension as well as the features of the micro-engineered and natural surfaces suitable for research described in this thesis.

In Part 4 I describe the properties of lipid molecules, their self-assembly and lipid membrane mechanics, which are highly relevant for the membrane transformations. Various forms of lipid vesicles and films as key structures in the experiments presented in this thesis are described. Details of the membrane-surface interactions, and the transient pore hypothesis are explained.

Methods and techniques utilized in the papers included in this thesis are explained in Part 5. These include preparation of lipid samples, surface fabrication and characterization, confocal microscopy, microfluidics applications, infrared laser-based systems for localized heating, and analytical modeling.

In Part 6 I summarize the main findings of each of the published and submitted research papers.

In Part 7 I conclude my thesis and discuss some of my future perspectives.

2 Primitive cell models for the origin of life

The Origin of Life, i.e., abiogenesis, represents the phase in early evolution during which non-living matter transformed to living matter⁶. What makes an entity living? There is no well-defined answer to this question. However, the three basic criteria suggested by Gánti provide a plausible model². According to Gánti, a unit containing all basic elements of living -a chemoton- includes: (i) a metabolism producing energy and building components, (ii) a replicator unit which can store information that can be copied and passed on; (iii) an outer membrane barrier, a compartment which contains (i) and (ii), which prevents internalized compounds from getting diluted, and supports the system's growth. The National aeronautics and space administration (NASA) of the USA has a broader definition of life: "a self-sustaining chemical system capable of Darwinian evolution"⁷. Darwin suggested that evolution of organisms happen through the inheritance of physical and behavioral traits over generations and that diverse life-forms could have arisen from a common ancestor⁸. This means that the information stored in a chemoton should be open to adaptations which are beneficial for the living entity, i.e. ensures its survival.

Protocells are thought to have been a stepping stone to the origin of life⁹, first assembling in the form of primitive compartments from available materials on the early Earth, and later going through increasingly more complex steps over time, such as growth, replication and division. This chapter summarizes the current hypotheses about the origin of life and aims to give an overview of the environmental conditions on the early Earth, available materials and possible clues which may have led to the emergence of life.

2.1 Hypotheses on the origins of life

Radiometric dating of rocks indicates that the Earth is approximately 4.5 billion years old^{10, 11}. The life, as we know it, is water-based, therefore the emergence of water on the early Earth was a crucial requirement for life. Water on Earth dates back as early as the Hadean Eon (~4.5 to ~3.8 billion years ago (Gya))¹² and is possibly of extraterrestrial origin¹³. Analyses from the Greenstone Belt in Isua, Greenland, indicates that permanent oceans have existed since ~3.7 Gya¹⁴.

The earliest evidence of life are 3.5 billion years old stromatolites discovered in Western Australia^{15, 16}, the sedimentary layers in rocks formed by photosynthetic cyanobacteria. Experimental studies indicate that there was at least one common ancestor (LUCA)¹⁷ before life diverged to different domains including bacteria. The first bacterium had already been a relatively complex organism and had simpler descendants, e.g. LUCA, or even more primitive cells. Since there is currently no fossil evidence of such structures, many hypotheses have been produced, taking into account the possible ambient conditions on the early Earth.

One of the earliest hypothesis about origin of life is the **panspermia** theory which assumes the life exists throughout the universe and was delivered as 'seeds' to the Earth by space dust, meteorites, and other extraterrestrial objects¹⁸. The presence of the organic materials in meteorites supports this hypothesis^{19, 20}. The idea of panspermia is, however, based on a starting point of an already living entity and does not address the question of abiogenesis.

The gradual emergence of life from a '**primordial soup**' was proposed in 1920s. Oparin²¹ and Haldane²² independently formulated hypothesis that life emerged from an aqueous suspension of inorganic molecules under the oxygen-poor atmosphere of the primitive Earth. Through this gradual chemical evolution, organic compounds were synthesized and gave rise to prebiotic reactions and complex molecules essential for survival and reproduction of first forms of life. According to Oparin, the macromolecules such as proteins were clustered together in the soup to form 'bits of gel', i.e., coacervates²¹. Haldane described the accumulation of substances until the oceans adapted to the consistency of hot dilute soup and that prebiotic molecules concentrated within microcontainers with physical boundaries²².

In 1953 the **Miller-Urey experiment** provided the first evidence for the formation of organic compounds from inorganic molecules in an artificial environment feasible to have existed on the early Earth²³. The experiment was performed in a chamber containing a heated pool of water, mixture of gases considered to be present on the early Earth (H₂O, NH₃, CH₄ and H₂) and artificial lightning. As a result of this interaction, several organic molecules was formed and detected, among them number of amino acids²³. The relevance of Miller's composition of gases with respect to the early Earth atmosphere, however, was questioned, as the concentration of methane and ammonia is considered to have been low²⁴. Later it was shown that in conditions which better reflected the early Earth environment, with a mixture of gasses dominated by CO₂ and N₂²⁵, significant amounts of amino acids could still form²⁶. The Miller-Urey experiment alone does not explain the way of a possible emergence of life, but it is considered one of the important developments elucidating how organic matter from inorganic materials could have been hypothetically produced on the early Earth.

Hydrothermal vents at the sea-floor, which are typically located near volcanically active places have been proposed to be plausible locations for the emergence of life^{27, 28}. They are particularly interesting, as the environment contains, due to high temperature and high pressure, minerals, dissolved compounds and gasses in addition to water. These black smoker type hydrothermal vents, which form due to volcanic eruptions at the sea-floor, reach temperatures up to 405 °C inside the vent and cool down to 2 °C at the tip of the vent, creating a temperature gradient²⁹. The acidic environment (pH 2-3) is rich with dissolved CO₂, H₂S and metal ions such as Fe(III)²⁸, a combination which causes precipitation of iron sulfides - hence the black color. White smoker type hydrothermal vents, for example the Lost city hydrothermal fields (LCHF)³⁰, feature a lower temperature range 40-90 °C and alkaline pH 9-11. The white color is caused by precipitation of

magnesium carbonate, which can grow chimneys of heights up to 60 meter above the sea-floor. The water circulation at the tip of the white smokers is driven by heat and exothermic reactions, which can result in production of simple abiotic molecules, e.g. H₂ and CH₄³⁰. Hydrothermal vents are populated by archaeal microbiomes^{31,32}, and could have been a possible location for the first cells to appear.

In an environment with high temperature and pressure, metal ions could have been extracted from minerals and rocks and entered the oceans on the early Earth³³. Metal sulfides rich in zinc and iron among other elements have been found in the proximity of the vent sites of deep-sea hydrothermal vents³⁴. The hypotheses associated with the origin of life are often based on special environmental conditions and chemical compositions, commonly referred to as 'worlds'. The **zinc world** hypothesis, for example, suggests that the first life forms were utilizing ZnS formations of hydrothermal origin to drive photosynthesis³⁵. The specific role of Zn²⁺ in biochemical reactions, specifically in RNA folding and metabolic processes in modern cells constitute support for the zinc world hypothesis. The **iron-sulfur world** hypothesis, also associated with hydrothermal environments, proposes that surface of iron sulfide minerals could facilitate early forms of prebiotic reactions, e.g. autotrophic carbon fixation resulting in producing of small molecules of inorganic gasses³⁶.

On dry land, similar environments, e.g. **warm little ponds**, were proposed by Darwin as suitable environment for beginning of life^{37, 38}. Warm little ponds accommodate dry-wet cycles due to water evaporation and subsequent precipitation, which concentrates otherwise dilute organic molecules³⁹.

In the context of this thesis work, one prominent hypothesis -the **lipid world**-⁴⁰is highly relevant. Since the lipid world supports, and is complementary to, the **RNA world**⁴¹, another prominent hypothesis on the origin of life, both hypotheses will be explained in detail in the following.

2.1.1 The RNA world

The RNA world ^{41,42} hypothesizes that primitive life was based on RNA as an information carrier, not on DNA as in contemporary cells. RNA can act both as a genetic information carrier and as a ribozyme, enabling its own replication⁴³. Due to the fact that it can self-replicate, and due to its relevance for cellular life, structural and functional versatility, RNA is thought to be the earliest genetic molecule in the prebiotic world⁴⁴. Some cofactors and vitamins that are crucial for a working cellular metabolism, such as acetyl CoA, have ribonucleotides as a structural component which do not have a functional role in the biochemistry they are involved in^{45, 46}. This is considered as evidence that modern biomolecules carry relics of RNA, hence supporting an RNA world. Hypothetically, in an environment where complex cellular machinery did not exist, a primitive cells capable of forming daughter cells with identical content in some way, combined

with a relatively simple molecule capable of self-replicating, could be a feasible milestone on the road to the first living cell.

The RNA world has received significant support⁴⁷ but is also facing criticism partly due to the lack of experimental evidence on the synthesis of ribonucleotides under prebiotic conditions⁴⁸. In recent years, prebiotically plausible syntheses of ribonucleotides have been achieved^{39, 49, 50}. Powner *et al.* demonstrated that pyrimidine nucleotides could be prepared from prebiotic molecules such as cyanamide, glyco- and glyceraldehyde and inorganic phosphate⁴⁹. Becker *et al.* showed the production of both purine and pyrimidine nucleotides from a reaction network containing prebiotically feasible components (e.g. cyanoacetylene, NH₂, urea, formic acid), driven by fluctuations in temperature, pH and dry-wet cycles³⁹. The formation of sugar component of RNA backbone, the ribose, was also shown to be feasible under prebiotic conditions⁵⁰.

The translation of a RNA sequence into peptides would be challenging for primitive cells, therefore self-replication without the need for translation would be beneficial. Ligase, a ribozyme, can self-replicate from short precursors creating a self-sustaining system^{51, 52}. RNA polymerase, another ribozyme, can synthesize ligase, although with lower fidelity⁵³, and also amplify other RNAs⁵⁴. In general, prebiotic ribozymes are speculated to have been 'promiscuous', meaning having little specificity such that a single molecule could catalyze several types of reactions⁵⁵. A sequence of one RNA template has been shown to control the translation of RNA sequence into dipeptides in the absence of ribosome or enzymes⁵⁶.

2.1.2 Lipid world

In 2001 Segré and Lancet *et al.*⁴⁰ proposed the lipid world hypothesis as an early evolutionary step in the emergence of cellular life. The lipid world concept is motivated by the ability of amphiphiles to spontaneously aggregate and to perform diverse functions that are relevant to the origin of life.

Compartmentalization is the primary role of lipid molecule membrane assemblies in biology as well as at the emergence of life. Lipid compartments could emerge by self-assembling and internalizing reactants in a confined volume⁵⁷. A membranous boundary would have kept the molecules in close proximity, and increase the probability of reactants to interact, thus enhancing the reaction rates⁵⁸. It was shown that encapsulation inside a lipid compartment can promote the formation of peptides from amino acids, and effectively protect the process from hydrolysis⁵⁹. Compartmentalization enhanced the affinity of RNA aptamers compared to those only dispersed in bulk solution⁶⁰.

Lipid aggregates display **catalytic activity** and therefore can be referred to as lipozymes⁴⁰ (note that lipozymes should not be confused with the commercial class of industrial enzymes under the same name). It has been shown that lipids promote polycondensation of amino acids into

peptides^{61, 62}, increase binding of nucleotides⁶³, significantly enhance the rate of chemical reactions⁶⁴⁻⁶⁶. Lancet discusses in his review lipid catalytic networks capable of Darwinian evolution and replication⁶⁷.

Lipid assemblies are autopoietic⁶⁸, which means that they are capable of reproducing and maintaining themselves by creating their own components which can assemble into forms similar to the original structure^{69, 70}. Lipids are recycled throughout growth and division instead of being synthesized *de novo*. In other words, the compositional repertoire of one primitive cell could transfer to next generations⁶⁷. This can be considered as a **compositional genome**^{67, 71}, that allows to store and transfer information. Therefore, lipids have a direct influence on growth and reproduction, hence the system evolution. A detailed discussion about the molecular structure of lipids and features of lipid membranes is included in chapter 4. *Membrane mechanics*.

Lipid compartments are able to grow and divide. For example, lipid vesicles can grow by enzyme-free incorporation of new amphiphilic molecules⁷² and divide as a result of mechanical agitation⁷³. Chen and Szostak *et al.*⁷⁴ reported lipid vesicle growth caused by osmotic pressure. Fatty acid vesicles encapsulating RNA molecule swell due to the imbalance in osmotic pressure, which results in an increase in membrane tension. If more fatty acids are available in the environment, the molecules are incorporated into the vesicle, resulting in growth over time^{74, 75}.

Several models of RNA-based life proposed that enzymatic functions would evolve more rapidly inside an enclosed compartment^{58, 66, 76}. This offers a perspective on how life could emerge as coordinated evolution of nucleic acids, proteins and lipid moieties, rather than individually evolving^{48, 77}.

2.2 Prebiotic compartments

Prebiotic compartments separate two aqueous environments with a physical boundary that is a result of aggregation or assembly of available materials during that time. One possible form of compartments has been suggested to be **solid compartments** in form of micro cavities in minerals and rocks^{78, 79} (*cf.3.4 Natural mineral surfaces*). Besides providing confinement and crowding inside micro pores, minerals facilitate prebiotic reactions. It has been shown that adsorption of molecules on the minerals can catalyze polymerization reactions⁸⁰. Clay minerals were shown to adsorb, concentrate and catalyze the synthesis or formation of organic molecules⁸¹. Clay surface are known to facilitate polymerization of RNA⁸²⁻⁸⁴ and peptides⁸⁵, and could potentially act as chelating agents due to their affinity to mono- or divalent ions⁸⁶, capable of altering the ionic ambient environment.

Various types of soft primitive compartments have been proposed as model protocells, with different levels of structural complexity, such as aqueous droplets, coacervates and lipid vesicles (**Figure 2.2.1**).

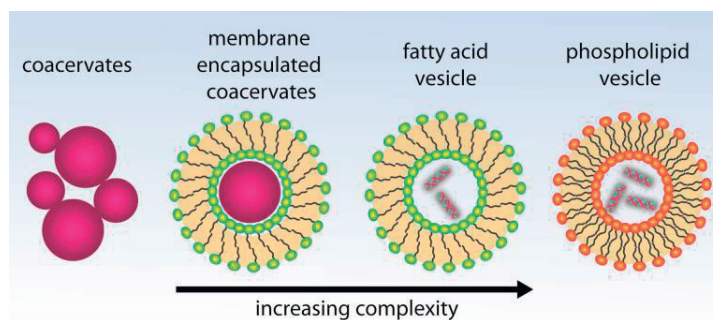


Figure 2.2.1 Prebiotic compartment models in increasing complexity.

Oparin suggested that a mixture of oppositely charged polyelectrolytes could form ‘bits of a gel’, small liquid phase droplets separated from water, as possible protocell compartments²¹. These droplets, later termed **coacervates**, are formed by liquid-liquid phase separation due to changes in polymer or salt concentration, pH or temperature, and are capable of spontaneously accumulating solutes^{87, 88}. Commonly, one of these phases have a dilute concentration of compounds, whereas the other phase is concentrated with these compounds⁸⁹. The absence of an enclosing membrane allows free diffusion of molecules between different droplets and the dilute phase^{90, 91}. Strong accumulation and high stability of RNA oligonucleotides⁹², and enhanced ribozyme reactions^{91, 93} have been observed in coacervates. Coacervates can be surrounded by colloidal particles, for example clay⁹⁴, and can later be chemically or thermally stabilized to form colloidosomes⁹⁵. Compared to coacervates, colloidosomes are able to perform a more controlled uptake and release of cargo molecules through nanospaces in the boundary formed by the particles⁹⁶. Phase separated coacervates can serve as a template for adsorption of lipid molecules, and formation of a membrane between concentrate and dilute phase^{97, 98}. Fatty acid coated coacervates were shown to mediate the selective uptake of molecules and despite the dense phase disintegrates, the fatty acid membrane maintains its integrity⁹⁸. A drawback of the coacervate models is the necessity of the conditions for phase separation, e.g. extreme pH or temperature, which can negatively affect the encapsulated biocompounds, e.g. genetic fragments. In contrast, amphiphilic membranes form via self-assembly without the need of external stimuli.

2.2.1 Membranous protocells

In the work leading to this thesis, membranous compartments^{99, 100} have been employed as protocell models. There are multiple reasons which motivated this choice. The ability to self-assemble, and simultaneously compartmentalize ambient compounds, as well as other unique features of lipids that characterize a “lipid world”, have been described in previous chapters. Besides, all modern cells are enveloped in a lipid bilayer. Therefore, if amphiphiles were available on the early Earth, it is rather plausible that at least some primitive cells were **lipid membranous compartments**.

A number of sources of lipids have been suggested in the prebiotic world. One is the direct delivery through meteorites during heavy late bombardment¹⁰¹. This corresponds to the time period approximately 4.0 billion years ago, where a high frequency of failed planets and asteroids collided with objects in the Solar System, e.g. the Earth moon and Mars¹⁰¹. In carbonaceous chondrite meteorites, a wide selection of hydrocarbons, carboxylic, sulfonic and phosphonic acids, alcohols, sugars, amines and over 70 amino acids were identified^{102, 103}. Analyses of fatty acids extracted from Murchison and Tagi Lake meteorites show chain lengths up to 12 carbons¹⁰⁴ (cf. 4.1 *Lipid molecules and lipid polymorphism*). This is sufficient for assembly of stable liposomes¹⁰⁵. In fact, formation of lipid vesicles from hydrocarbons extracted from the Murchison meteorite were observed¹⁰⁶. The simple phospholipid head group molecule ethanolamine was identified in diamond-bearing Almahata Sitta meteorite from Sudan¹⁰⁷.

Delivery of organic matter can possibly also occur via interstellar dust particles (IDP)¹⁰⁸. The extraterrestrial dust was shown to carry organic matter¹⁰⁹⁻¹¹¹. Approximately 5,200 tons of extraterrestrial dust per year reaches the Earth¹⁰⁸, and more than 14,000 organic compounds have been detected on interstellar material and meteorites^{112, 113}. Approximately 320 tons of organic matter per year is estimated to be delivered to Earth via IDPs alone¹¹⁴. Larsen and coworkers pioneered the work on the compositional analyses of IDPs collected from urban areas in Norway¹¹⁵.

The structurally simplest lipid-like molecules are fatty acids with a single molecular chain composed of hydrocarbons terminated with a carboxylic acid group. Evidence shows that fatty acids can be directly delivered via meteorites. They can also be synthesized under prebiotic conditions¹¹⁶⁻¹¹⁸. It was also experimentally shown that structurally more advanced phospholipids, e.g. phosphatidylcholine¹¹⁹ and phosphatidylethanolamine¹²⁰, could possibly be synthesized under prebiotic conditions. Recently, Devaraj *et al.*¹²¹ succeeded in the nonenzymatic synthesis of diacylphospholipids in water.

The collected evidence on the early presence of lipids and the known ability of amphiphilic molecules to form compartments suggest that membranous compartments are feasible in the protocell context¹²². Lipid compartments can undergo shape deformations and adapt various morphologies as a response and adaptation to the external stimuli¹²³, thus keep the compartment intact and effectively protect encapsulated cargo.

Fatty acids have been shown to assemble in aqueous environment into micelles¹²⁴ or bilayer structures^{74, 75, 125}. Bilayer vesicles made of fatty acids can spontaneously grow by incorporation of the free fatty acids from the aqueous environment⁷². An emergent fatty acid vesicle can adapt an elongated, thread-like shape, which upon agitation divides into several smaller vesicles, setting a new growth cycle^{73, 126}. Spontaneous vesicle division has been induced by addition of oleic anhydride monomers into a vesicle suspension, which upon hydrolysis transform into oleic acids and incorporate into the vesicles. This leads to formation of vesicle inside a vesicle later

diving into two separate compartments¹²⁷. Another division example involving oleic acid vesicles has been presented when oleic micelles were pipetted into the vicinity of the vesicles¹²⁸.

Replacement of fatty acids by the structurally more complex phospholipids has been suggested to have occurred during evolution. Phospholipid molecules typically consist of two fatty acids chains connected with a charged phosphate-containing head group (*cf. 4.1 Lipid molecules and lipid polymorphism*). Fatty acid membranes are more permeable and more dynamic compared to pure phospholipid membranes. Fatty acid molecules can rapidly flip between the leaflets and incorporate¹²⁹. In contrary, phospholipid membranes are far less prone to spontaneously incorporate lipid molecules or exhibit inter-leaflet exchange, and are also less permeable. In the presence of vesicles containing low amounts of phospholipids (10 mol%), the mixed vesicles incorporated fatty acid easier than pure fatty acid vesicles¹²⁹. Incorporation of phospholipid has been reported to inhibit permeation by molecules, e.g. sugar ribose, and provide better stability in the presence of divalent cations¹²⁹. Maintaining integrity, retaining important components for prebiotic RNA chemistry and excluding the components that are detrimental to the process is advantageous for primitive cells in RNA world¹³⁰. Over the course of evolution, the amount of phospholipids in the membrane is thought to have increased, eventually transforming to purely phospholipid membranes.

Recently, mixed lipid vesicles made from fatty acids and phospholipids (1:1) were shown to provide faster evolutionary adaptation of encapsulated ribozymes compared to ribozymes in bulk. This results support that membranous protocells would provide functional and evolutionary benefits for the encapsulated contents instead of acting as passive containers⁶⁶.

Under certain pH conditions and in the presence of pre-formed phospholipid vesicle, self-replication of fatty acids exhibits a 'matrix effect'^{131, 132}. In general, fatty acids can spontaneously form vesicles of various size, but if phospholipid vesicles are present in the system, the size of fatty acid vesicles approximate the size of the phospholipid vesicles, hence the matrix effect¹³³.

Encapsulation and self-replication are more challenging in the case of phospholipid vesicles, simply due to the above mentioned features of phospholipids. Diffusion through the phospholipid membrane is limited by the size and charge of the diffusing molecules. In Paper II we describe a plausible pathway for the internalization of non-permeable fluorescent compounds through transient pores¹³⁴. During the short pore opening time, the external solutes can enter the phospholipid protocell¹³⁵. This uptake path was also demonstrated to be suitable for RNA and DNA fragments (Paper III-IV). The phospholipid compartments can hold the encapsulated molecules for a period of time and even host simple prebiotically plausible chemical reactions (Paper III).

Division of phospholipid compartments requires energy as well as material input (*cf. 4. Phospholipid membrane mechanics*). In contemporary cells, fission of the membrane can be

achieved in several ways, e.g. membrane-adhering proteins¹³⁶. For the earliest prebiotic cells, such proteins or chemical energy sources were not available. Some plausible mechanisms for division of prebiotic cell have been proposed, it was reported that scission of cell-sized vesicles can be induced by mechanical agitation⁷³, continuous addition and incorporation of lipid material¹²⁸ and osmotic changes or UV light triggering¹³⁷. Solid surfaces, abundant on the early Earth, were lately proposed as a possible contributor in the development of primitive cells, specifically as energy source for spontaneous membrane shape transformations¹³⁸.

2.3 Surface adhered membranous compartments

The previous subchapter was focusing on membranous compartments freely suspended in bulk solution. Surface energy of minerals and rocks could have been utilized by membranous assemblies to achieve functions that would not be possible to consistently achieve in bulk. Intrinsic energy of surfaces will be explained in detail in chapter 3. *Surface energy and wetting phenomena*. Briefly, solid surfaces, which includes minerals or nanoengineered mineral-like surfaces, possess a form of intrinsic physico-chemical energy which can be harnessed to effect the transformation of surface-adhered membranes¹³⁸.

Experiments in which mineral microparticles were combined with lipid monomers in aqueous environments support that surface interactions are favorable for compartment formation^{113, 139-141}: In the presence of mineral microparticles, the formation of lipid vesicles is amplified compared to the environment containing the same concentration of lipid monomers, but free of minerals.

Solid surface areas that are much larger than microparticles (dimensions of a microscope cover slide) allow monitoring of all possible unique shape transformations, e.g. the formation of protocell nanotube networks^{142, 143}, which has been shown both for phospholipids and fatty acids¹²⁵ and was reported to happen on natural mineral surfaces and a sample of a Martian meteorite¹⁴⁴. The full set of possibilities arising from protocell structures that form through surface-mediated pathways remain to be fully elucidated. One example has been a new division hypothesis¹⁴⁵. The work contained in this thesis is based on surface-supported routes, in particular their capability in forming numerous subcompartments.

2.4 Prebiotic subcompartmentalization

Cellular subcompartmentalization features spatially distinct environments in which reactants co-localize and specific functions take place⁴³. Subcompartments are usually contained in a unit cell and termed 'organelles'. There exist some exceptions where organelles are functioning between the cells, e.g. exosomes¹⁴⁶, or migrasomes¹⁴⁷.

Cellular compartments can be membrane-bound, or formed by liquid-liquid phase-separation¹⁴⁸. Experiments focusing on the formation of membraneless compartments are based on coacervate models which were explained earlier. Simply, the formation of coacervate droplet inside lipid compartments have been achieved as a result of changes in pH^{88, 149}, temperature¹⁵⁰, or can be formed as a result of immiscible aqueous phases and protein partitioning¹⁵¹.

Membranous organelles have been previously associated solely with eukaryotic cells. In the last decade it was reported that the evolutionary simpler bacteria and archaea also contain membranous compartments^{152, 153}. It is therefore plausible that membranous compartments have existed in protocells and are evolutionary conserved. The simplest model of a protocell with membrane-enveloped inner compartments is a vesosome, a vesicle containing internal non-concentrically arranged vesicles¹⁵⁴. Vesosomes can form randomly as a result of mechanical agitation during self-assembly or prepared with advanced techniques such as microfluidics¹⁵⁴.

The formation of compartmentalized structures from the 'mother' protocell requires shape transformation of the membrane and therefore external stimuli. Upon osmotic shock, vesicles were shown to shrink and form multiple daughter compartments by the formation of membrane invaginations from the outside inwards¹⁵⁵. A similar effect was seen on giant vesicles tethered to a solid surface via streptavidin-biotin coupling¹⁵⁶.

In this thesis it is hypothesized that protocell colonies could have possibly formed on solid surfaces on the early Earth. Multicellular organisms benefit from the close proximity of individual cells, which enhances chemical cell-to-cell communication, and stability in difficult environments. Protocell colonies could have had an advantageous position over individual protocells in osmotically and mechanically challenging ambient environments, and therefore would likely possess an advantage towards Darwinian evolution. Colony-like collection of protocells could have facilitated the chemical communication and exchange of components between the protocells within the colony. Small molecules can diffuse through the membrane boundaries without getting diluted and might initiate chemical communication among the protocells¹⁵⁷. The formation of 'vesicle colonies' might have been a likely step in the emergence of the first cells¹²², but experimentally could only be induced by molecules or cues that are not compatible with prebiotic chemistry, e.g. streptavidin-biotin couples¹⁵⁸, poly-L-arginine¹⁵⁹, oppositely charged biopolymers¹⁶⁰, or magnetic manipulation¹⁶¹.

In Paper III we show a prebiotically feasible, consistent pathway for the formation of protocell colonies on solid surfaces. The reported colonies are feature rich and exhibit advantages over isolated protocells. The system is overall based on only a few necessary assumptions: the presence of lipid agglomerates, the presence of solid substrates, e.g. minerals or rocks, and a suitable aqueous environment.

3 Surface energy and wetting phenomena

Solid surfaces are one of the key components of the phenomena reported in this thesis. Solid surfaces were abundant on the early Earth in the form of minerals and rocks. Mineral surfaces have been experimentally shown to promote adsorption of organic molecules and to enhance their polymerization^{80, 83, 84} (*cf.* 2.1 *Hypotheses on the origins of life*). They also can drive membrane shape transformations resulting in lipid nanotubes networks¹⁴², protocells with subcompartments⁵ or protocell colonies^{125, 142, 144, 162}. It is therefore plausible that surfaces could have facilitated the formation and further development of primitive cells on the early Earth.

In this chapter, I introduce the concept of surface energy and wetting phenomena, and give a brief account of the features of the nano-/microfabricated and natural surfaces. Surface energy is critical for lipid membrane-surface interactions that govern the shape transformations of adhered membranes (*cf.* 0. *Membrane mechanics*) described in this thesis.

3.1 Surface free energy

Surface energy is defined as the excess energy at the surface of a material compared to the bulk. The atoms or the molecules in bulk of a material have balanced interactions with the neighboring atoms or molecules (**Figure 3.1.1**) in all directions equally, resulting in a net force of zero. In contrast, atoms on the surface of the material miss cohesive interactions, i.e., attraction between the molecules of the same type. The lack of cohesion on one side of the surface atoms causes an imbalance of interactive forces, resulting in increase in free energy.

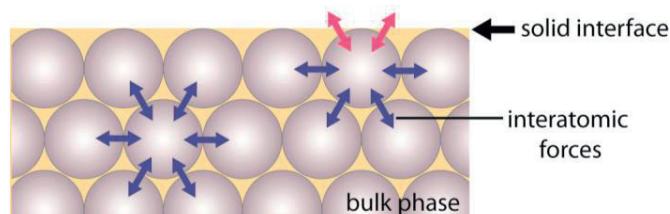


Figure 3.1.1 Schematic drawing of the surface and bulk atoms of a solid material. Atoms in bulk experience balanced interatomic interactions, while surface atoms lack these interactions at the solid-air interface.

Another way to visualize the surface energy is in relation to the force needed to break the bulk of a material. Separation of a block of solid material into two pieces requires breakage of the molecular bonds between neighboring atoms¹⁶³. The amount of work applied is proportional to the amount of molecules on the newly created surface. The surface free energy (σ , in units of N/m or J/m²) is formulated as a function of work (W) per unit of the newly created surface area (A).

$$\sigma = \frac{1}{A} W$$

The magnitude of the surface energy depends on the strength of the intermolecular forces between the atoms in the bulk. For high energy surfaces like metal or glasses (silica), the surface free energy is high, due to the strong covalent or metallic bonds between the atoms. Strong chemical bonds affect the boiling point of the material, e.g. high boiling point of metals ($T_B > 2000\text{ }^\circ\text{C}$) usually correlates with their high surface energy ($\gamma > 1000\text{ mJ m}^{-2}$)¹⁶⁴. The atoms of low energy surfaces ($\gamma \sim 0.05\text{ mJ m}^{-2}$)¹⁶⁵, e.g. plastics, are attached to each other with relatively weaker bonds, e.g. van der Waals or hydrogen bonds.

3.2 Wetting phenomena and interfacial energies

Surfaces have a tendency to minimize their excess energy. Liquids adapt to the smallest possible surface-to-volume ratio by forming spherical droplets. Solids cannot easily minimize their surface by physical deformations; therefore, they form interfaces with air or liquids. Molecules on the solid surface aim to establish physico-chemical interactions with the available neighboring molecules at the interface. Contact with a liquid, for example, causes spreading of the liquids on the surfaces in a process termed *surface wetting*¹⁶⁶.

During wetting of a solid substrate, water (liquid) molecules create interactions with the solid surface at the atomistic scale (**Figure 3.2.1 a**). Wettability can be measured with contact angle (θ), which is the angle at the intersection of the contour of a liquid drop with the plane of the surface (**Figure 3.2.1 b-d**). The contact angle results from equilibrium of three different surface tensions, each of which strives to minimize the interface: liquid and solid surface (γ_{LS}), liquid and vapor (air) (γ_{LV}) and solid surface and vapor (γ_{SV}).

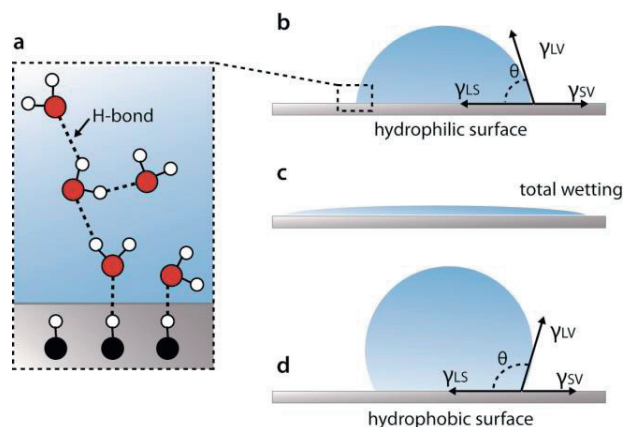


Figure 3.2.1 Wetting. (a) Hydrogen bonding between water-water and surface-water molecules. A liquid droplet on (b-c) hydrophilic, (d) hydrophobic surface. (c) Shows total wetting on a high energy surface.

Young's equation relates the contact angle to the interfacial tensions (γ) and serves as a quantitative description of the wetting phenomena:

$$\gamma_{LV} \cos \theta = \gamma_{SV} - \gamma_{LS}$$

If the interfacial tension of the solid-vapor interface is higher than the solid-liquid ($\gamma_{SV} > \gamma_{SL}$), $\cos\theta$ must be positive and the contact angle lower than 90° (**Fig. 3.2.1 b**). For contact angles less than 90° wetting is favorable and the adhesive forces between the liquid and the surface cause the liquid to spread (**Figure 3.2.1 b**). A finite contact angle between liquid and a high energy solid surface is established ($\theta = 0^\circ$), means perfect- or total wetting (**Figure 3.2.1 c**). Contact angles above 90° indicate unfavorable surface wetting. This typically occurs on hydrophobic surfaces on which liquid drops ball up in order to minimize the contact with the surface (**Figure 3.2.1 d**).

Simulations showed that water on a silica surfaces exhibit higher wettability with increased density of hydroxyl groups present on the surface¹⁶⁷. In addition to the surface free energy and its chemical nature, the wettability is closely related the roughness. Certain degree of roughness enhances surface wettability¹⁶⁸. On the other hand, extreme roughness can turn a high energy surface into *super-hydrophobic* and repel the water¹⁶⁹. Such surfaces entrap air between the pillars, resulting in only a fraction of the solid surface being exposed to the droplet¹⁶⁹. Super-hydrophobic surfaces have wide applications in nanotechnology, such as unwettable textiles and self-cleaning surfaces¹⁷⁰.

3.3 Micro- and nanoengineered surfaces

Diverse membrane assemblies can be formed on solid surfaces with different surface chemistry and structure. As mentioned previously, surface energy, materials properties and roughness play important roles in behavior of liquids and lipid membranes on the substrate. In Paper I we characterized the behavior of different molecular lipid species on variety of micro-fabricated solid supports with diverse characteristics. The variety included metals (Al, Au) and metal oxides (Al_2O_3 , SiO_2 , TiO_2), semiconductor materials (SiC), ceramics (ITO), minerals (Mica), graphene and highly hydrophobic polymers (Teflon AF, SU-8). Each of the substrates was fabricated in a controlled manner to understand the sole contribution of surface material to the membrane behavior. Microengineering of solid surfaces (*cf. 5.2 Surface fabrication*) ensures high degree of control of the material purity and surface roughness. Due to the precise control of the deposition, the engineered surfaces are usually of nanometer thickness and atomically flat. Glass is widely used in microscopy of biological samples and was used as a reference surface. TiO_2 surfaces are of importance in bone and tooth implants¹⁷¹, and graphene has interesting electronic properties. It is used in commercial applications, e.g. solar cells¹⁷² and anticorrosion paints¹⁷³.

Surfaces are subject to contamination from the ambient air, often referred to as *surface aging*¹⁷⁴,¹⁷⁵. As the surfaces tend to reduce their free energy, they react with the molecules present in the air such as airborne hydrocarbons, which can change the wetting properties of the surface^{176, 177}.

Therefore, prolonged storage of the surfaces should be avoided. Exposure of the surface to oxygen plasma is an efficient technique of eliminating hydrocarbon contamination and increasing surface free energy, thus restoring its wettability and hydrophilicity¹⁷⁸.

3.4 Natural mineral surfaces

The micro-engineered surfaces provided great insight into specific surface-membrane interactions and interfaces. However, they do not exactly represent natural surfaces e.g. minerals and rocks. Natural mineral surfaces are especially interesting in the context of Origin of Life and early Earth¹⁷⁹ Throughout the Earth's evolution, the mineral composition increased through approximately 60 mineral phases to over 4400 known minerals today¹⁸⁰. A mineral is a solid inorganic compound with well-defined chemical composition and crystal structure, occurring naturally in a pure form, or create aggregates in rocks with spatially distinct phases. Many surfaces utilized in Paper I have corresponding natural counterparts in form of minerals or rocks. Al₂O₃ in a crystalline form creates corundum¹⁸¹, a rock-forming mineral, the primary gem varieties of which include ruby and sapphire. TiO₂ minerals occur in various polymorphic forms including tetragonal anatase, rutile, and orthorhombic brookite¹⁸². Quartz, a hard crystalline mineral composite of SiO₂, is the second most abundant mineral in the Earth's continental crust. Al and Si elements are present in many mineral rocks dated to the Hadean Eon¹⁸³, such as plagioclase, feldspar, biotite and phengite, oxides of which make the phyllosilicate muscovite.

An interesting alternative to Earth's natural surfaces in the context of the origins of life are extraterrestrial materials. Among the planets in our solar system and the water based moons^{184, 185}, many investigations have been concentrating on Mars¹⁸⁶. Mars, based on the data from spectroscopic mineralogical work on meteorites¹⁸⁷, is thought to have once had an atmosphere, which would maintain liquid water. The composition of a Martian meteorite specimen (Northwest Africa NWA 7533) was analyzed and revealed the presence of feldspar and some oxides^{188, 189}. NWA 7533 is more than 4.4 billion years old, according to the zircon dating¹⁹⁰. This time period represents nearly the entire geologic history of Mars. The similarities of the natural surfaces and early environment on Mars and Earth inspired investigation of a thin sections of NWA 7533 meteorite and other natural surfaces as substrates for protocell formation and development in the prebiotic environment¹⁴⁴. Here I present preliminary findings on subcompartmentalization on a NWA 7533 sample. Upon reproducing the experiments in Paper II I observed adhesion of model protocells as well as subcompartmentalization on the Martian meteorite (**Figure 3.4.1**). The results encourage for the studies on subcompartments and prebiotic reactions to be performed also on the extraterrestrial surfaces.

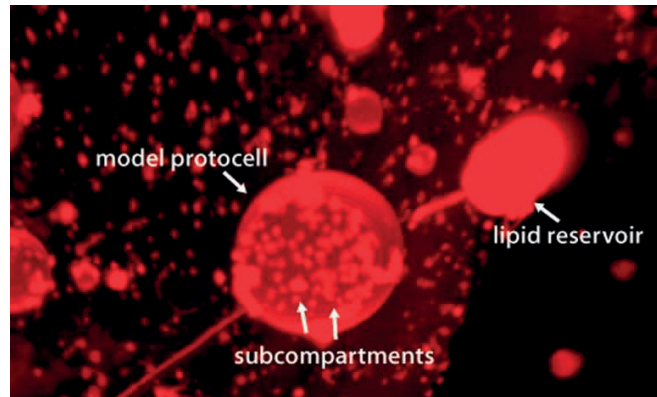


Figure 3.4.1 Confocal micrograph of subcompartmentalized model protocell on Martian meteorite NWA 7533 specimen. Several small subcompartments formed inside the surface-adhered model protocell in the same manner as on the microengineered surfaces shown in Paper II.

4 Membrane mechanics

Biological membranes have many important roles. The plasma membrane encloses the cell and defines its boundary, separating its contents from the external environment. The cell membrane consists of a phospholipid bilayer with embedded proteins and other lipid species, e.g. cholesterol and sphingolipids. Membranes are selectively permeable to critical nutrients and are able to efficiently remove waste to maintain the cell survival. Inside the cell, there exist organelles which are also membrane-bound⁴³ (cf. 2.4 Prebiotic subcompartmentalization). While ensuring cellular integrity, membranes must maintain physical flexibility to enable cellular growth, to respond to mechanical forces, support migration, and undergo division. These demands are balanced by the properties of membranes and their basic units, the lipids. In this chapter, I will describe lipid molecules and their self-assembly, and summarize some of the important parameters determining the free energy of lipid membranes.

4.1 Lipid molecules and lipid polymorphism

Lipid molecules, by definition, are amphipathic (or amphiphilic) molecules; their structure consists of a hydrophilic head group covalently bonded to a hydrophobic tail. The most common lipids in cell membranes are phospholipids (**Figure 4.1.1**). The phospholipid structure consists of a hydrophilic head group attached to the two long fatty acid chains via a glycerol molecule. The fatty acid chains are hydrocarbons with repeating series of CH₂ groups, mostly with 10-18 repeats. The structurally simplest head group belongs to phosphatidic acid which contains only of a phosphate. Any additional molecules attached to the phosphate, such as ethanolamine, choline or glycerol, may affect the charge of the head group and the overall charge of the membrane.

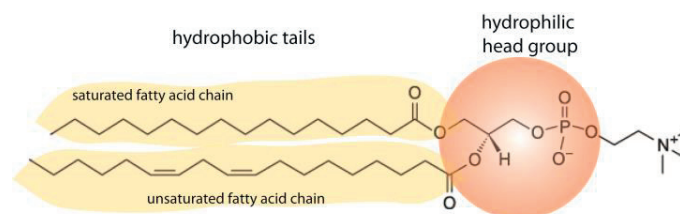


Figure 4.1.1 Chemical structure of phosphatidyl choline, a phospholipid molecule. It consists of a hydrophilic headgroup (orange) containing a phosphate and a choline and hydrophobic tails formed of fatty acid chains (yellow).

In addition to the phospholipids, cellular membranes contain structurally diverse lipid molecules¹⁹¹ (**Figure 4.1.2**). Sphingolipids are present in many eukaryotic cells where they create domains with essential functions, e.g. in brain development and maintenance¹⁹². Cholesterol is built from planar array of four fused aliphatic rings, and is known for significantly affecting membrane fluidity^{193, 194} (cf. 4.3 Lipid membrane fluidity).

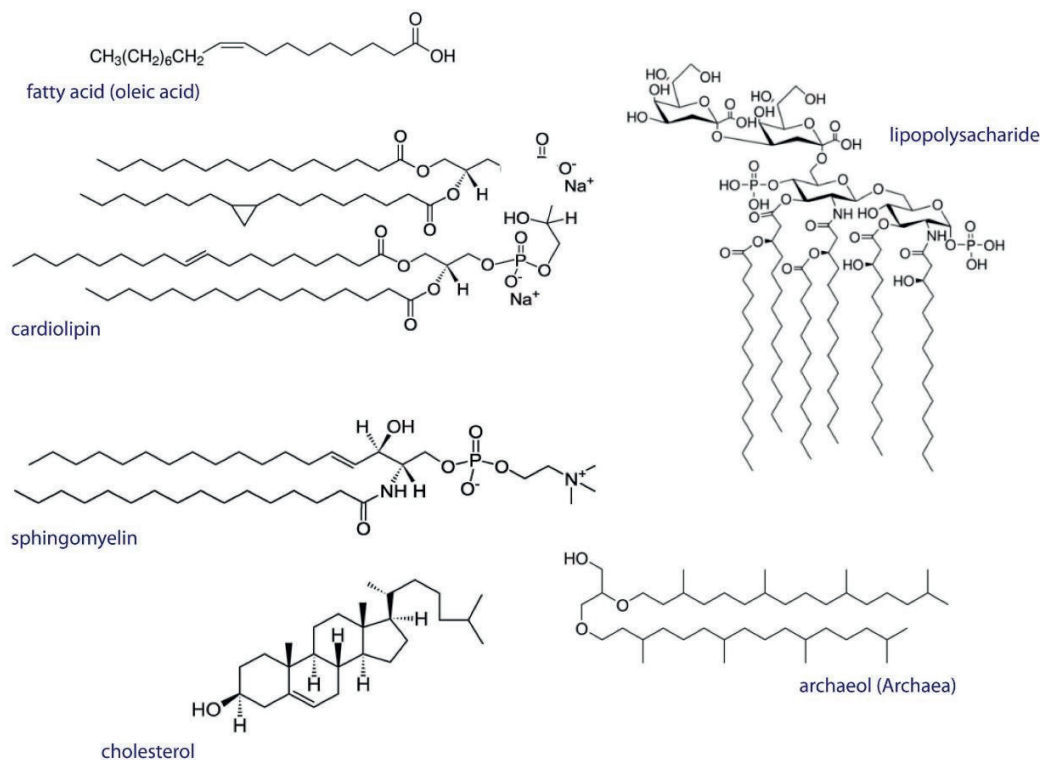


Figure 4.1.2 Chemical structures of various lipid molecules in cellular membranes.

Highly curved membrane regions in bacteria contain cardiolipin molecules, a dimeric structure composed of two phosphatidic acid moieties connected by a glycerol backbone¹⁹⁵. Gram negative bacteria such as *E. coli* have lipopolysaccharide present in outer leaflet the membrane¹⁹⁶. Evolutionary simpler archaea have a unique membrane composition which aids survival and adaptation to extreme environments. The main components are archaeols, lipids with isoprenoid moieties, which are also hypothesized to be present in membrane of LUCA¹⁹⁷.

In the context of the origins of life, different types of amphiphiles are thought to have been involved. Structurally simpler fatty acids with a single aliphatic chain have likely emerged before phospholipids (*cf.* 2.1 Hypotheses on the origins of life). Fatty acids are pH sensitive and require a comparatively higher molecular concentration for their assembly than phospholipids. Their dynamic nature is considered to be essential for permeability and growth of the prebiotic cell membranes^{72, 129}. The possible sources of fatty acids and phospholipids on the early Earth, and the experiments investigating their ability to form prebiotic compartments have been extensively discussed in chapter 2.2.1 *Membranous protocells*.

4.2 Self-assembly

Amphiphiles have the ability to ‘self-assemble’ into organized structures. When exposed to water, lipids seclude their hydrophobic parts from water, adapting an ordered arrangement. Self-assembly is an important aspect in the discussion on the origin of life, as it enables primitive membranous compartments to form spontaneously without the involvement of chemical reactions and bond formation.

When (polar) water molecules come in contact with a (non-polar) phospholipid molecule, the hydrogen bonds (H-bonds) between the water molecules are lost. Water molecules form new hydrogen bonds while positioning around the lipid molecule. The result is ‘hydrophobic hydration’¹⁹⁸; the formation of a clathrate-(cage) like structure of water molecules around the hydrophobic tail of the involved amphiphile (**Figure 4.2.1 a**). The organization of water molecule leads to an increase in order of the system, compared to the otherwise randomly dispersed water molecules in a bulk. High degree of order results in decrease in entropy and an increase in the Gibbs free energy (ΔG) of the system:

$$\Delta G = \Delta H - T\Delta S$$

where ΔH is change in enthalpy and $T\Delta S$ is change in entropy. The system aims to minimize its free energy via its entropy: as interaction of water molecules with individual lipid molecules leads to an increase in free energy, lipid molecules in aqueous environment self-assemble, excluding the water molecules from the vicinity of the tails and forming a hydrophobic core (**Figure 4.2.1 b-c**). By doing so, the water molecules restore hydrogen bonding which increases the system’s overall entropy and reduces the Gibbs free energy.

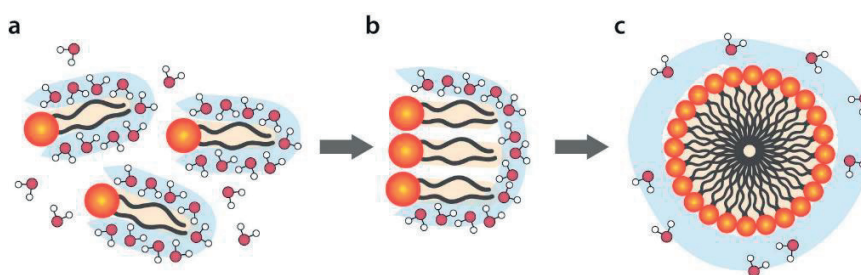


Figure 4.2.1 Self-assembly of lipid molecules. Exposure of hydrophobic moieties to water leads to a cage-like layer of water around lipid molecules, increasing order, thus decreasing entropy (a). This causes an increase in the surface free energy of the system. To minimize the surface free energy, lipids self-assemble, minimizing the exposure of their hydrophobic fractions to water (b-c).

The shape of the assembled structures depends on the geometrical parameters of the molecular lipid species. The shape of the hydrophilic tail is determined by the double bonds inducing a kink in the tail. The geometry of the lipid molecule can be characterized by its volume (v), the length (l) of the nonpolar hydrophobic tail and optimal surface area of the polar head group (a_0). The relation between these parameters is defined as critical packing parameter (p):

$$p = \frac{v}{la_0}$$

Many biomembrane lipids have a cylindrical shape with packing parameter 0,5-1, which entails them to organize as lipid bilayers (**Figure 4.2.2 a**). Molecules with bulky head group adapt a conical shape (packing parameter <0,5) and tend to form micellar structures (**Figure 4.2.2 b**), while inverted cone shaped lipids (packing parameter >1) form reversed crystal phases (**Figure 4.2.2 c**) e.g. inverse, hexagonal II phase. Other factors affecting the packing parameter are pH, ionic strength of the solvent, and temperature¹⁹⁹.

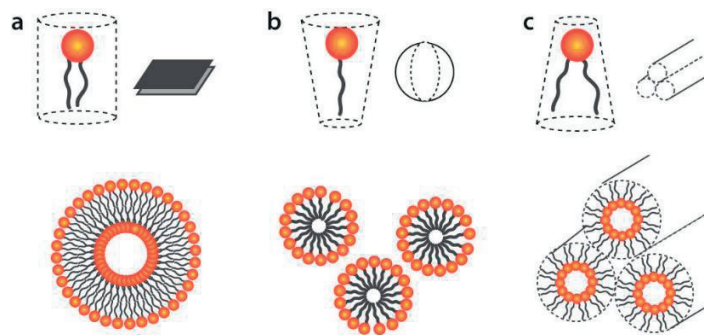


Figure 4.2.2 Shapes of lipid molecules and structures formed as a result of their self-assembly. (a) Lipid molecules with cylindrical shape form bilayers that can transform into spherical vesicle. (b) Lipid molecules with large head groups can be considered as conical, and aggregate as micelles. (c) Lipid molecules with small head group and branched fatty acid chains can assemble into inverse micelles or inverse hexagonal structures.

4.3 Lipid membrane fluidity

Lipid bilayers are dynamic; the lipid molecules within the bilayer are in constant motion and diffuse in 2D along the plane of the membrane. The lipid diffusion within the membrane was first described in *Fluid mosaic model*²⁰⁰. As the lipid molecules are held in the bilayer by a hydrophobic effect rather than strong chemical bonds, the membrane is considered fluid where the lipids and other embedded molecules can freely move and mix. The membrane fluidity is affected by the critical packing parameter, e.g. saturation of the fatty acid chains. The presence of double bonds increases the fluidity, making the membrane less viscous²⁰¹. Certain lipid species influence membrane fluidity. Cholesterol decreases membrane fluidity^{193, 194}, in contrast to the phospholipids with unsaturated hydrocarbon chains which disrupt the packing order of the membrane²⁰². Addition of sphingomyelin leads to a decrease in membrane fluidity²⁰³. Membrane fluidity can be also altered by changes in the local temperature. Increase in the temperature causes rise of kinetic energy, which helps lipids to overcome intermolecular forces holding the molecules together. The acquired thermal energy results in increased movement and more fluid membrane, and was shown to speed up membrane shape transformations¹⁴³ and promote vesicle fusion²⁰⁴.

4.4 Lipid membrane mechanics

Lipid membranes are ~5 nm thick and can extend along the membrane plane up to hundreds of micrometers. Due to their fluid nature and large aspect ratio, membranes can be treated as infinitely thin 2D elastic sheet, for which the elastic energy F is described as

$$F = \int dA \left[\frac{\kappa}{2} (c_1 + c_2 - c_0)^2 + \bar{\kappa} c_1 c_2 + \sigma \right]$$

This is the *Helfrich membrane curvature energy* ²⁰⁵. The first term inside the integral corresponds to the bending energy of a lipid membrane. dA is the surface area element, κ is the bending rigidity, i.e., the resistance of the membrane to change its curvature. c_1 and c_2 are the two principle curvatures of the membrane and c_0 is the spontaneous curvature^{202, 206}. The spontaneous curvature occurs due to structural differences between the two lipid monolayer leaflets²⁰⁶. In my work, this term is neglected, as the monolayers in the membranes are of identical composition. The second term in the integral $\bar{\kappa} c_1 c_2$ is the Gaussian curvature, where $\bar{\kappa}$ is the Gaussian modulus. For a flat lipid membrane, the Gaussian curvature is 0. For a spherical vesicle it is positive. For a saddle shape geometry, it is negative²⁰². In systems where the curvature of the membrane is alternating from flat membranes to nanoscale tubular structures, the bending term governs the membrane dynamics. In the studies included in this thesis, the Gaussian term therefore is neglected.

The third term σ represents the membrane tension. Under low tension the (relaxed) lipid membrane expands in the third dimension (perpendicular to the membrane plane) by thermal undulations²⁰⁵. Membrane tension increases due to stretching, resulting in an increased distance between the neighboring lipid molecules and decreasing number of lipid molecules per unit membrane area. The lipid membrane can stretch only up to 5% of its area²⁰⁷ before the membrane tension reaches lysis tension (~5-10 mN/m) and ruptures²⁰⁸.

4.5 Formation of vesicles from lipid bilayers

In an aqueous environment, lipid molecules initially self-assemble into a bilayer as a result of the hydrophobic effect (*cf.* 4.2 *Self-assembly*). If the concentration of lipid monomers in the solution is sufficient, the lipid bilayer initially adapts the form of a free-standing disc (**Figure 4.5.1 a**). At the edge of the disc, lipid molecules arrange in a micelle-like form (**Figure 4.5.1 a**, inset) where the distance between the lipid molecules is higher, as compared to the lipids in the plane of the membrane. This results in an edge tension. The edge energy cost of a lipid membrane is:

$$E_{edge} = 2\pi r \gamma$$

where r is the radius of the membrane disc and γ is the edge tension, experimentally determined to be 5-10 pN¹³⁴. The edge energy cost increases proportionally to the circumference of the patch²⁰⁹.

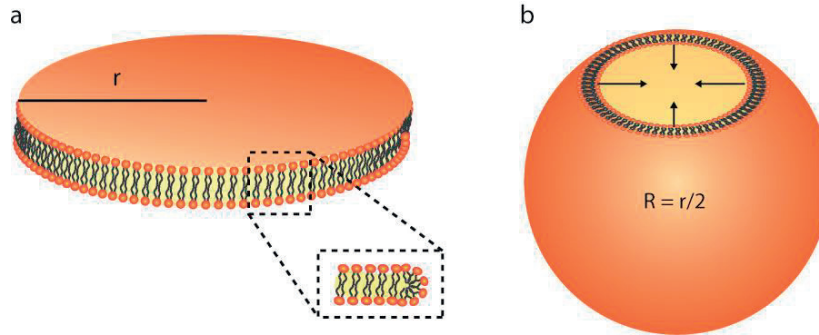


Figure 4.5.1 Formation of a lipid bilayer disc with a radius r to a vesicle with radius R . The lipids at the edge of the bilayer disc are curved (inset) causing an edge tension. To avoid the high edge energy cost the bilayer disc bends to form a spherical vesicle.

If the membrane disc continues to grow, e.g. due to increased lipid concentration, the circumference thus the edge energy cost of the system, increases. To avoid the cost of the edge energy, the disc-shaped bilayer bends and transforms into a spherical compartment (**Figure 4.5.1**).

For this transformation, the bending energy needs to be overcome. E_{bend} is based on the bending and Gaussian moduli (κ and $\bar{\kappa}$, respectively).

$$E_{bend} = 4\pi (2\kappa + \bar{\kappa})$$

A typical value for κ is $10 - 20 k_b T$ ($k_b T_{room} = 4 \times 10^{-21} J$)²⁰⁷. The Gaussian modulus $\bar{\kappa}$ is usually in the same order of magnitude, but contributes with a negative sign²¹⁰. As the lipid bilayer grows, the tension on the edge increases. At the point when the bending energy becomes smaller than the edge energy cost, the membrane favors bending and transforms into an energetically stable spherical shape.

$$\frac{E_{bend}}{E_{edge}} < 1 \rightarrow \frac{4\pi(2\kappa + \bar{\kappa})}{2\pi r\gamma} < 1 \rightarrow r > \frac{2(2\kappa + \bar{\kappa})}{\gamma}$$

The radius of the membrane disc (r) should be larger than $\frac{20 k_b T}{10 pN}$ for the bending to occur. This is the equivalent of several nanometers. This means, if the radius increases more than several nanometers, the lipid bilayer becomes unstable and spontaneously bends to form a closed vesicle (**Figure 4.5.1 b**).

4.6 Phospholipid vesicles

Lipid vesicles can exist as small ($d < 100$ nm), large ($d \approx 100$ -500 nm) or giant vesicles ($d > 1$ -100 μm)²¹¹ and can exhibit different lamellarity. Unilamellar vesicles consist of a single bilayer encapsulating an aqueous volume. Due to their ability to internalize compounds, liposomes are used as pharmaceutical carriers. Liposomes as drug carriers were first proposed in 1974 by Allison and Gregoriadis²¹². Since then the lipid vesicles have been widely used in drug^{211, 213-215} and vaccine delivery systems^{216, 217}. The liposomal membranes can be further functionalized with membrane-embedded polymers, peptides or antigen ligands for active targeting²¹⁸. Lipid vesicles are used to fabricate supported lipid bilayers for biosensors^{219, 220}, for membrane protein studies and as a bottom-up structural model for biological cells^{221, 222} and as models for protocells^{129, 157, 223}.

Multilamellar vesicles (MLVs) contain multiple bilayers densely packed together and can act as lipid reservoirs. The space between the lamellae is filled with a tiny volume of liquid, therefore MLVs are also employed as carrier liposomes^{224, 225}. In biological cells, lipid-protein complexes known as lamellar bodies contain multilamellar lipid membranes and serve as supply of lipid components²²⁶. Cells can also create temporary lipid storages by formation of invaginations and lipid-dense areas^{227, 228}. Formation of multilamellar outer vesicles has been reported in mutant bacteria²²⁹.

Multilamellar vesicles are schematically depicted as 'onion shell'-like structures, with perfectly aligned, defect-free bilayers (**Figure 4.6.1 a**) with no physical connections between the lamellae. Evidence indicates that the lamellae inside the MLVs are in reality connected to each other by nano-sized defects and fusion necks²³⁰ (**Figure 4.6.1 b**).

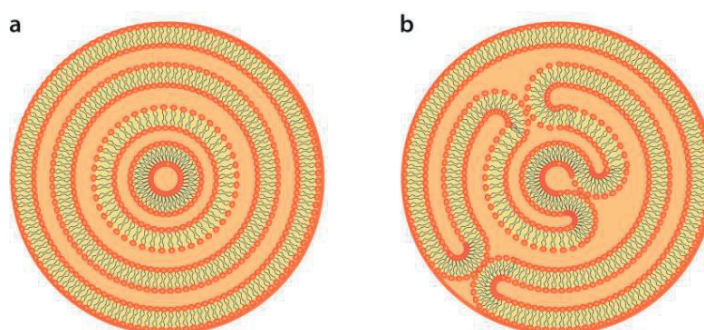


Figure 4.6.1 Schematic drawings of multilamellar vesicles. (a) Perfect concentric lamelles and (b) internal defects and fusion necks.

The interconnected bilayer structure of MLVs allows unfolding of the lipid bilayer, thus the membranes can spread on solid surfaces. In my work I utilized small unilamellar vesicles (liposomes) in Paper I for the formation of lipid films; giant unilamellar vesicles as model

protocells in Paper II and III; and multilamellar vesicles (lipid reservoirs) in Paper III and IV. The shape transformations observed following the deposition of lipid reservoirs on solid supports are explained in the following chapters.

4.7 Supported membranes

When lipid aggregates interact with a flat solid interface, they usually form lipid films of various architectures^{231, 232}. Lipid films can form by self-spreading of lipid reservoirs²³³, or by adhesion of several small unilamellar vesicles^{232, 234-236}. Supported membranes are often used as simplified models of biological cell membranes. Composition of these *biomimetic membranes* can be tuned and membrane proteins can be embedded, making them useful models for diverse studies and applications^{237, 238}.

One method to form supported membranes is the Langmuir-Blodgett/Langmuir-Schaefer^{232, 239} technique, where the substrate is first submerged into an aqueous medium containing lipids, and then pulled out, causing the lipid molecules at the air-water interface to form a thin lipid film on the substrate. Another method is small unilamellar vesicle adhesion and subsequent rupture^{232, 235, 240}. When SUVs are deposited onto a suitable solid surface, e.g. glass, each individual SUV adheres to the surface, wets an increasing surface area under growing tension in its membrane, and eventually ruptures forming a small lipid patch²³⁵. Deposition and rupturing of numerous SUVs eventually lead to merging of the individual small lipid patches and formation of a continuous lipid membrane film over time²³⁵. This is a convenient technique formation of supported bilayers as the protocol requires standard steps and equipment easily accessible in any wet lab.

Depending on the surface nature and the composition of the lipid vesicles, the membranes interact with solid supports in different ways, and form different morphologies. In Paper I we show the various behaviors of lipid films on a variety of technologically relevant surface materials, including metals, metal oxides, mica, borosilicate glass and plastics. On hydrophilic high energy surfaces vesicles form single lipid bilayers (borosilicate glass) or double bilayers (SiO₂, SiC). On hydrophobic surfaces, e.g. Teflon AF or SU-8, lipid membrane spreads as a monolayer with hydrophobic tails directly facing the substrate. In some cases, the SUVs adhere onto the substrate without rupturing and form a layer of adhered vesicles, e.g. neutrally charged membranes on TiO₂ or Mica.

Large lipid patches are formed by isotropic self-spreading of a lipid reservoir, e.g. MLV^{142, 208}. The bilayer spreads either as a single lipid bilayer or as a double bilayer onto the solid surface^{233, 241} depending on the type of surface: as single bilayer on glass, and as double bilayer on SiO₂. Self-spreading is a wetting phenomenon (*cf.* 3.2 *Wetting phenomena*) and is driven by the surface tension at the substrate interface. For the membrane to spread, the tension at the surface-

aqueous solution interface (σ_A) must be higher than the surface-lipid membrane interface (σ_L). The tension σ_S which drives the spreading is therefore defined as

$$\sigma_S = \sigma_A - \sigma_L$$

The lipid reservoir from which the lipids are drawn has an internal tension (σ_0), which oppose the spreading tension (σ_S). The difference between the energy gain by the wetting and the reservoir tension is defined as spreading power S

$$S = \sigma_S - \sigma_0 = \sigma_A - \sigma_L - \sigma_0$$

Spontaneous spreading of the lipid reservoir occurs when S has a positive value. The flow of lipids from lower to higher tension region is driven by the Marangoni effect²⁴². The spreading continues until the lipid reservoir is depleted, upon which the membranes rupture as the tension exceeds the membrane lysis tension (5-10 mN/m)²⁰⁸. Contact of giant unilamellar vesicles with solid surfaces of moderate surface energy leads to partial adhesion and formation of dome-like vesicles²⁴³. High surface tension leads to the rupture of vesicle and formation of a lipid patches on the solid substrate²⁴⁴⁻²⁴⁶, similar to the events following SUV deposition.

Supported membranes can also form by adhesion of giant vesicles onto solid substrates. The adhesion of vesicles can be facilitated by temporary pinning of lipid head groups to surface charges²⁴⁷, by complex organic molecules^{156, 248}, or by fusogenic agents. On hydrophilic, negatively charged surfaces, multivalent ions, e.g. Ca^{2+} , bridge the lipid molecules to the surface by binding to the negatively charged phosphate moiety in the lipid head group^{162, 249}. At the interface a thin lubricated layer of water remains between the lipid bilayer and the substrate²⁵⁰.

4.8 Nanotube formation and protocell nucleation

Lipid nanotubes are key structures in shape transformations described in Paper IV. During rupturing of the double bilayer, some regions of the distal membrane remain pinned to the proximal bilayer and immobilized. Due to the rapidly elongating membrane edges and the pinning points which cannot join the rupturing edge, thin, long membrane threads are formed between the rupturing front and pinned regions. The longer these threads become, the higher the edge energy cost of the membrane. To minimize the edge energy the elongating membrane regions bend and wrap into nanotubular structures¹⁴². The edge energy cost of a rectangular membrane, in principal similar to the lipid patch, is defined by its length (l) and the edge tension (γ).

$$E_{edge} = l\gamma$$

The bending energy of a lipid nanotube is derived from the *Helfrich bending energy equation*²⁰⁵,

$$E_{bend} = \frac{\pi l \kappa}{r}$$

for a nanotube with radius (r) and length (l). This shows that the bending energy cost increases with increasing length of the tubular structure. Previously, the relationship between edge tension and bending energy has been introduced (cf. 4.5 Formation of vesicles from lipid bilayers), which leads to:

$$\frac{E_{bend}}{E_{edge}} = \frac{\pi \kappa}{r \gamma} < 1$$

This shows that a distal membrane patch with a length of a few nanometers would necessarily bend to a nanotube to minimize its edge tension.

The total energy of a lipid nanotube, f , is given by:

$$f_{nanotube} = 2\pi \left(\frac{\kappa}{2r^2} + \sigma \right)$$

Assuming a minimum nanotube energy, the radius of a nanotube at the equilibrium can be obtained as:

$$r = \sqrt{\frac{\kappa}{2\sigma}}$$

At constant membrane tension, the radius of a nanotube is typically ~ 50 nm^{142, 242}. The nanotube structures therefore are highly curved bilayers, and therefore their bending energy cost is high. To reduce the curvature, nanotubes will tend to evolve to spherical vesicles^{5, 142}.

In cell biology, tunneling membrane nanotubes enhance cell-to-cell communication and allow transport of cellular compounds and organelles in mammalian cells²⁵¹. Only a decade ago, tunneling nanotubes have also been discovered within prokaryotes²⁵². In Paper IV we investigated the ability of lipid nanotubes to transport contents between protocells. Note that biological nanotubes are stabilized by membrane bending proteins, therefore typically have smaller dimensions than pure lipid membrane nanotubes.

4.9 Van der Waals Interactions

Van der Waals forces are short-range forces depending on the interaction between atoms or molecules. These forces may be repulsive or attractive and do not result in any form of chemical electronic bond, therefore are comparatively weak¹⁶⁴. Van der Waals forces have been studied in context of membrane-to-membrane adhesion in various ionic and pH conditions. Between cell membranes, the magnitude of van der Waals forces are influenced by membrane composition, specifically by the fractions of phospholipids, cholesterol, sugars and proteins²⁵³. The van der

Waals attraction between lipid bilayers is also dependent on the polarizability of solute molecules present in the aqueous space between the two membranes²⁵⁴. In Paper III, we investigated the influence of van der Waals interactions between the surface and membrane interface for the onset of formation of membrane instabilities/invaginations.

In the initial phase, the membrane adhesion onto a surface is mediated with pinning points. Upon their removal, the thermal energy results in fluctuations of the lipid bilayer, which can be further amplified by instabilities. Van der Waals forces at the membrane surface interface are attractive, and can destabilize a free interface that confines a liquid²⁵⁵. A longer distance between the membrane crest and surface due to the thermal fluctuations causes a decrease in strength of van der Waals interactions. This creates a pressure gradient on the neighboring troughs and causes influx of solvent, which further promote the process of crest growth.

Attractive van der Waals interactions (defined by the Hamaker constant A_H)²⁵⁵ and the membrane bending (bending modulus K , units Joules) set a critical wave number (q_c) below which the interface is unstable.

$$q_c = \frac{1}{h_0} \left(\frac{A_H}{2\pi K} \right)^{1/4}$$

The magnitude of A_H reflects the strength of the van der Waals force between the surface and the membrane molecules. The critical wave number sets the limit below which the van der Waals interactions dominate the membrane bending. Equal or higher wave numbers result in suppression of the crest, and the membrane remains stationary and flat. Results in Paper III show that the critical wave number corresponds to ~ 273 nm. The size of the membrane regions that are larger than ~ 273 nm can therefore result in growth of the crease into a spherical compartment.

4.10 Membrane permeability and transient pores

Internalization of complex molecules or genetic fragments inside a membranous compartment is considered a crucial step in the process of the emergence of living cells¹²². This can potentially occur by the spontaneous encapsulation of compounds during self-assembly - by forming a bilayer around the fragments⁷⁵, or via penetration through the membrane¹⁵⁷. A lipid cell membrane, however, especially if made from phospholipids, is limited by the size and the charge of the molecules. Generally, only small and uncharged molecules such as oxygen, can freely diffuse through the lipid bilayer. Larger and charged molecules are transported in living cells via active mechanisms using molecular pumps and proteins⁴³. One other means of encapsulation mechanism is the uptake via transient pores^{134, 256} (**Figure 4.10.1**). Pore opening in the lipid vesicles is driven by membrane tension. To reduce the tension, the membrane creates a pore

with a diameter of up to 5 nm²⁵⁷ in order to decrease the membrane area and distribute the lipid molecules to the areas with higher tension²⁵⁸. During the pore opening, the internal content of the vesicle leaks out, leading to a decrease in volume and therefore in the overall tension of the lipid membrane¹³⁵. Opening of pore creates an edge with its own size-dependent tension, which the membrane strives to reduce, thus the pore closes eventually¹³⁴ (**Figure 4.10.1**).

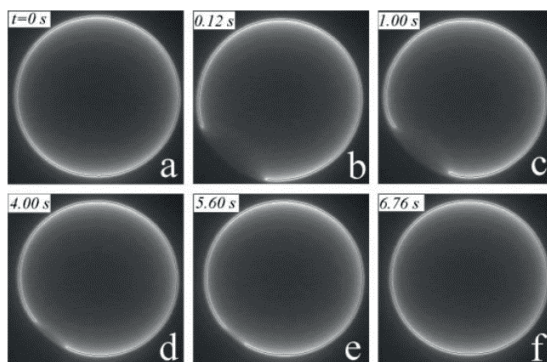


Figure 4.10.1 Transient pore in a giant unilamellar vesicle. When the lipid vesicle is under tension, it opens a pore through which internal content is released. The pore closes upon decrease of membrane tension. The experiments depicted here were performed in a solution with high viscosity to prolong the time scale and image the process. *Reprinted with permission from reference 134. Copyright ©2003 Society of Chemical Industry.*

In Papers II-IV we generated a hydrodynamic flow field to induce formation of transient pores on bilayers, and observed spontaneous encapsulation of fluorescein and single strand DNA molecules. The resulting high encapsulation efficiency indicated the presence of tension-induced pores. This hypothesis was also confirmed by finite element simulations in Paper II (*cf. 5.9 Analytical models*).

5 Methods

In this chapter I describe the main methods applied for the studies reported in this thesis. Preparation of lipid samples, surface fabrication and characterization, and confocal microscopy are the major methods. Other applied procedures such as application of microfluidic tools, and analytical computer modeling are also explained in brief.

5.1 Preparation of lipid vesicles

For the work included in this thesis, dehydration-rehydration method^{259, 260} was employed to form giant unilamellar- (GUVs) and multilamellar vesicles (MLVs). GUVs and MLVs were prepared from various lipid species including synthetic phospholipids or lipid extracts derived from plants and animals. Lipid vesicles are formed when hydrated thin lipid films detach during agitation and self-assemble in aqueous environment to form spherical compartments (**Figure 5.1.1**). The formation of a homogeneous lipid film of a uniform thickness is the most important requirement to obtain a suitable suspension of vesicles.

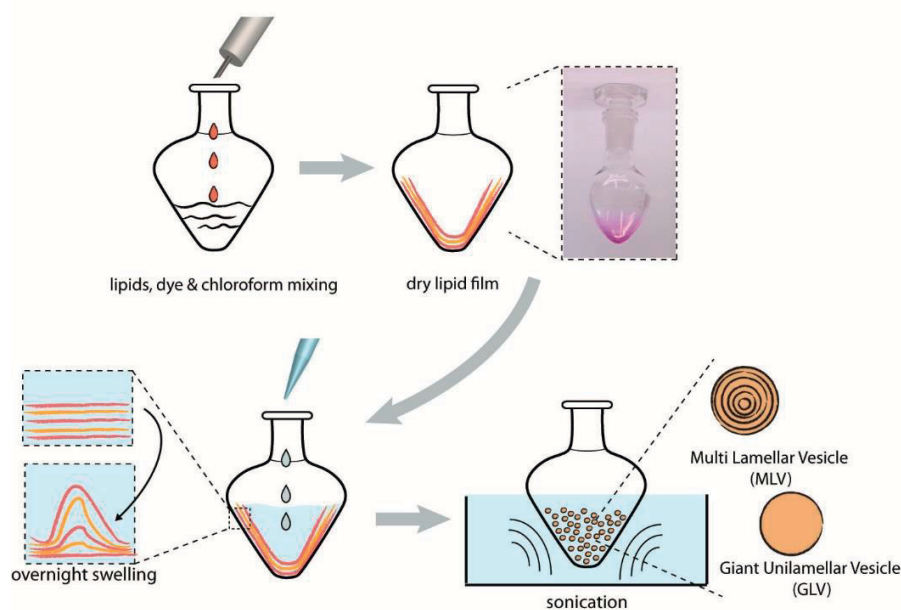


Figure 5.1.1 Preparation of lipid vesicles with the dehydration-rehydration method. Lipid molecules are initially dissolved in chloroform and the solvent is evaporated. As a result, a dry lipid cake forms on the walls of the flask. Upon rehydration, the lipid cake swells, and forms vesicles with varying lamellarity upon sonication.

During the preparation, the phospholipids and lipid-conjugated fluorophores are dissolved in desired ratios in chloroform, leading to a final concentration of 10 mg/ml. The solvent is evaporated under vacuum (20 kPa / 150 Torr) while slowly rotating the flask in a tilted position to ensure even formation of the lipid film on the walls of the flask. The dry lipid layers are rehydrated in aqueous buffer containing 1% glycerol overnight for swelling of the lipid film. Presence of the glycerol prevents complete dehydration of the lipid film and enable lipid

separation²⁶¹. The solution is then sonicated to decrease the size and lamellarity of lipid reservoirs and produce a homogeneous vesicle suspension. The exposure time should not exceed 30 s, as prolonged sonication leads to decrease in vesicle size and produce heat which may interfere with phase transition temperature of the dissolved lipids and negatively affect vesicle formation. The stock suspension can be stored at -20 °C.

For lipid vesicles sample preparation in Paper II, 4 µl from lipid stock solution is placed on clean glass coverslip and dehydrated using a vacuum desiccator for 20 min. The dry film is subsequently rehydrated using a buffer suitable for experiments.

5.1.1 Preparation of small unilamellar vesicles

For sample preparation in Paper I, small unilamellar vesicles (SUVs) were prepared by the extrusion method. Extrusion is a common technique where the size of the lipid vesicles of mixed lamellarity is reduced by mechanical energy²⁶².

The lipid vesicles in stock solution were diluted in buffer and initially disrupted by sonic energy (sonication) for several minutes. The solution was then filtered through polycarbonate filter using a syringe-based plunger system multiple times²⁶³. Due to defined pore size, and the deformation of the vesicles (elongation) due to shear stress at the pore walls, the extrusion yields vesicles with slightly larger diameter than the size of the filter pores, and the final size distribution depends on the number of extrusion cycles and extrusion temperature²⁶⁴. The SUVs suspension can be stored at +4 °C for up to 6 months without significant change in particle size²⁶⁴.

5.2 Surface fabrication

Solid surfaces in the work associated with this thesis have been fabricated in dedicated micro- and nanofabrication laboratories, i.e., 'cleanrooms'. Cleanroom facilities are specifically built for fabrication in a controlled environment with low to ultralow levels of particulates, required to obtain well defined, uncontaminated surfaces and structures. In urban areas, where the air is commonly more heavily polluted, there are approximately 300 million particles per cubic meter²⁶⁵. In cleanrooms the air is filtered to ensure much lower number of particles, for example down to 35 particles per cubic meter in Class 1 cleanrooms²⁶⁶.

In the work presented in this thesis, microscopy cover slips were used directly as substrate for material deposition. Different types of materials have been investigated in Paper I, including metals, metal oxides, semi-conductor oxide and polymers. In Paper II-IV aluminum, aluminum oxide and silicon dioxide were used. Generally, the materials are deposited as thin films using physical and chemical deposition methods, which are described in the following paragraphs to a

final thicknesses of 10-100 nm. Deposition thickness was selected such that the surfaces remained transparent and are therefore suitable for optical microscopy.

Silicon dioxide, aluminum, silicon carbide and titanium oxide: The films were fabricated using electron-beam (e-beam) evaporation (**Figure 5.2.1 a**), a physical vapor deposition technique²⁶⁷. Briefly, the material source is bombarded with an electron beam causing the atoms from the material to be dispelled into the gas phase. These atoms are directed onto the solid substrate, coating it with a thin layer of the evaporated material. E-beam evaporation is suitable for deposition of materials with higher melting temperature, such as metals and their oxides.

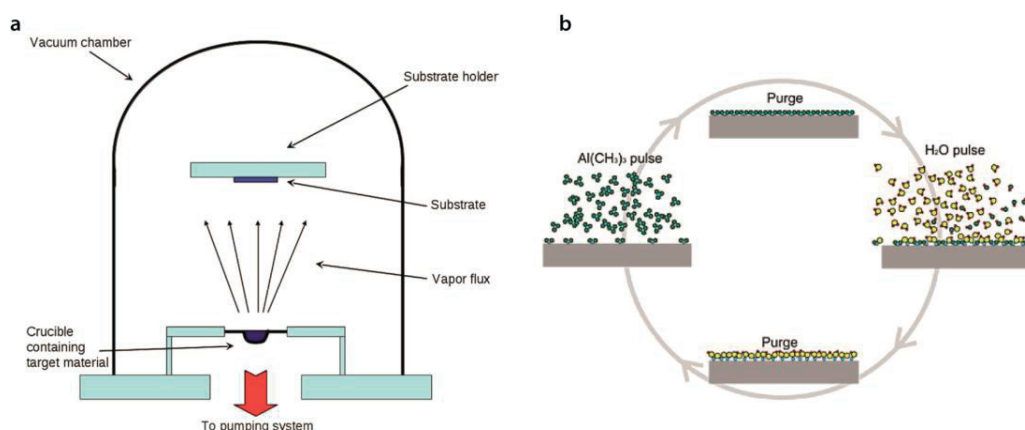


Figure 5.2.1 Schematic drawings depicting (a) e-beam evaporation and (b) atomic layer deposition. (a) Reprinted with permission from reference 267. Copyright ©2013 Elsevier. (b) Reprinted with permission from reference 269. Copyright ©2014 Elsevier.

Prior to deposition, the cover slides are loaded into the instrument chamber and the pressure is reduced to approximately 10^{-4} Torr. The filament inside the chamber is then heated until it starts emitting electrons. Under high voltage, typically from 5 to 20 kV, the electrons are accelerated and focused by a magnetic field onto a material source position at the bottom of the chamber (**Figure 5.2.1 a**). The material evaporates and vapor condenses on the glass slides. The focused beam only heats the material source, while the crucible is water cooled, allowing high purity deposition²⁶⁷. The thickness is monitored in real-time during deposition by means of a quartz crystal microbalance (QCM), and determined by monitoring the mass-dependent decrease in resonance frequency of the crystal resonator.

Aluminum oxide: The aluminum oxide films were fabricated using Atomic Layer Deposition (ALD)^{268, 269} (**Figure 5.2.1 b**). In this method the film is formed upon cycles of different precursor reactions on the surface, one at a time. The glass cover slips are loaded to the chamber and the pressure is reduced below to 2 mbar. The system relies on pulsing of the precursor gases into a chamber under vacuum (<1 Torr) to allow the precursor to react with the substrate surface. The process is self-limiting and forms only a single monolayer on the surface²⁶⁸. For Al₂O₃ deposition, the precursor tetra methyl aluminum (TMA) is pulsed to the chamber, releasing molecule of

methanol while forming a dense monolayer. Alternating purges with an inert gas (N_2) removes the byproduct and unbound precursor molecules. The second precursor H_2O is introduced and reacts with TMA monolayer, producing a solid aluminum oxide monolayer. Any residing byproduct is removed by a second purge with inert gas. The required thickness is obtained by several cycles. To create an approximately 10 nm thick layer, 70-100 cycles are required.

Polymers: Thin deposition of SU-8 and Teflon polymers was achieved with the spin coating procedure. The coating material is spread by centrifugal forces and tend toward uniformity in thickness due to self-leveling²⁷⁰. A small amount of polymer solution (1 mL) is pipetted on top of a circular glass substrate and rotated at high speed up to 10.000 rpm. The used solvent is usually volatile and simultaneously evaporates gradually. The final thickness depends on the speed of spinning and viscosity of the solution and the solvent. Following the deposition, fabricated films are baked on a hot plate.

Graphene: A monolayer of graphene was grown on a silicon carbide (SiC) substrate by thermal decomposition^{271, 272} (**Figure 5.2.2 a**). Graphene is an allotrope of carbon with atoms organized in two-dimensional hexagonal honeycomb lattice. A single layer can be grown by sublimating silicon atoms from SiC substrates at high temperature. The temperature above 1650 °C leads to desorption of the silicon atoms from the surface (**Figure 5.2.2 a**), while the carbon atoms with lower vapor pressure remain and naturally form a layer of graphene²⁷².

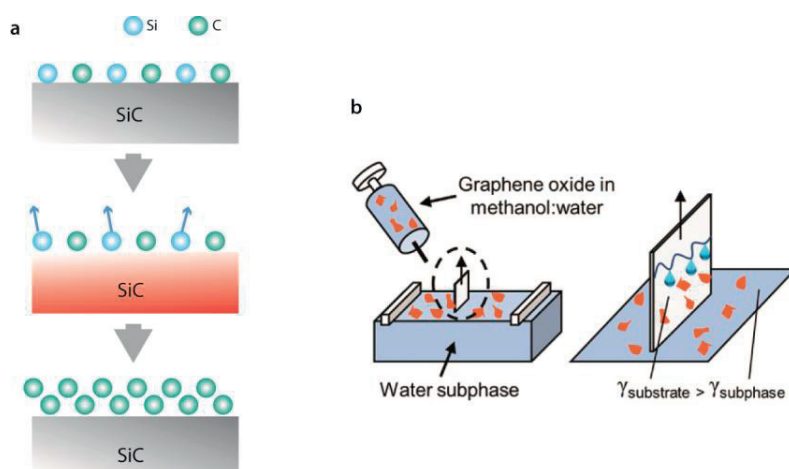


Figure 5.2.2 Schematic drawings depicting the fabrication of graphene. (a) Growth of graphene monolayer from SiC substrate by desorption of Si due to increase in temperature. (b) Graphene flake deposition with the Langmuir-Blodgett method. (b) is reprinted with permission from reference 239. Copyright ©2018 American Chemical Society.

Graphene oxide: The graphene oxide (flakes) substrates, were prepared using the Langmuir-Blodgett method²³⁹ (**Figure 5.2.2 b**). This method is based on the transfer of graphene flakes in methanol as a monolayer adsorbed on the solid interface during vertical dipping. The material is deposited onto dust-free 1:1 water:methanol solution, forming a molecular amphiphilic layer on the air-water interface. To transfer the film to a solid support, the glass slides are immersed in

the solution and then extracted with the surface film adsorbed onto it. The process can be repeated to obtain various consecutive layers.

5.3 Characterization of surfaces

Zeta potential is the electrokinetic potential established on interfaces of any material in contact with a liquid medium. The zeta potential measurements provide information on the charge-based interaction of dissolved compounds with the solid surface, which is indicative of surface functionality. Zeta potential of nanofabricated surfaces in Paper I was measured with the streaming potential technique²⁷³, suitable for measurements of macroscopic planar solid surfaces.

When a solid material comes in contact with a liquid, the functional groups on its surface react with the surrounding medium and the surface charge attracts and accumulates oppositely charged ions¹⁶³ (**Figure 5.3.1**).

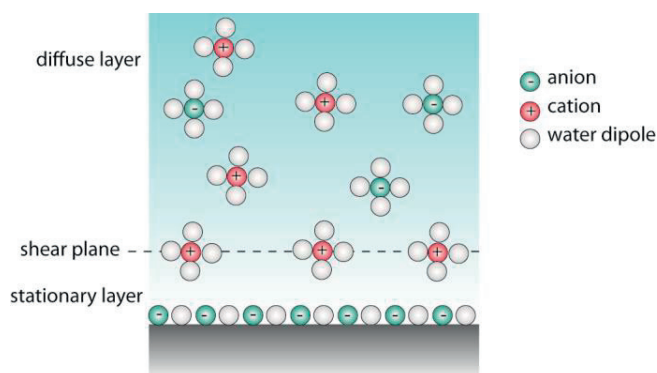


Figure 5.3.1 Schematic drawing of the electrochemical double layer. The negatively charged surface attracts counterions from the liquid medium, which form a stationary layer. Free ions in solution above the shear plane form a diffuse layer.

This creates a surface potential. Acidic groups on the surface dissociate upon contact with water and become negatively charged, while basic groups become protonated leading to a final positive charge. The equilibrium of dissociation and protonation is strongly dependent on the pH of the liquid medium and has strong influence on the surface charge of a material²⁷⁴. The counter ions present in the medium then arrange spontaneously into an electrochemical double bilayer (ELD)²⁷⁵. Ions in the closest proximity of the surface are immobilized due to strong interactions with the surface, and create a stationary layer. The diffuse layer consists of ions which are at located at a distance from the stationary layer, less attracted to the surface, and mobile. The zeta potential is defined at this hydrodynamic interface, and is measured in millivolt (mV) units.

For measurements of larger surfaces, the sample is mounted onto a holder in order to form a capillary flow channel. The liquid medium, an electrolyte, moves with respect to the solid sample

and the ions forms ELD. The resulting charge separation creates electrochemical effects, among them streaming potential²⁷⁶. The zeta potential (ζ) of the surface is then calculated using the Helmholtz-Smoluchowski equation:

$$\zeta = \frac{dl}{d\Delta p} \times \frac{\eta}{\varepsilon \times \varepsilon_0} \times \frac{L}{A}$$

where dl/dp defines the slope of the plot showing streaming current versus differential pressure, η is electrolyte's viscosity, ε and ε_0 are the dielectric coefficient and permittivity of the electrolyte, and the L/A is the ratio of the length and cross-section of the streaming channel.

5.4 Epifluorescence and confocal fluorescence microscopy

The most frequently employed instrumental technique in the experimental work leading to this thesis was light microscopy, specifically confocal fluorescence microscopy²⁷⁷. Fluorescence microscopy requires fluorescent labeling of the lipid membrane structures, which can be achieved via incorporation of fluorophore-conjugated lipid molecules into the membrane. Fluorophores are chemical moieties which absorb light of specific wavelength (excitation) and emit the light (emission) at a longer wavelength²⁷⁸. These fluorescent molecules typically contain several annulated aromatic rings. When the fluorophore absorbs a photon, the energy of the electronic states of the molecule at the ground state (S_0) elevates to an excited state (S_1) (*cf.* simple Jablonski diagram in **Figure 5.4.2**)²⁷⁹. This is followed by rapid vibrational relaxation (**Figure 5.4.2**) during which a fraction of the energy dissipates (non-radiative transition, red arrows in **Figure 5.4.2**). The remaining energy is released by emitting a photon and the electrons return to the low energy ground state. This is a radiative transition leading to the fluorescence signal (green arrow in **Figure 5.4.2**). The time scale of the radiative transition is 10^{-10} to 10^{-8} s²⁷⁷. Fluorophores can be added to biological samples²⁷⁸ to perform imaging of selected structures and processes at the nano- and microscale. Since they absorb and emit light at specific wavelengths, combinations of fluorophores allow for visualization of different structures simultaneously. The experimental work frequently required visualization of fluorescently labeled membranes together with water-soluble fluorescent dyes or genetic fragments chemically conjugated to fluorophores (Paper II-IV). Accordingly, the absorption and emission spectrum of each fluorophore needed to be carefully considered, as spectral overlap can lead to energy transfer between the different fluorophore species, resulting in cross-talk and related imaging errors.

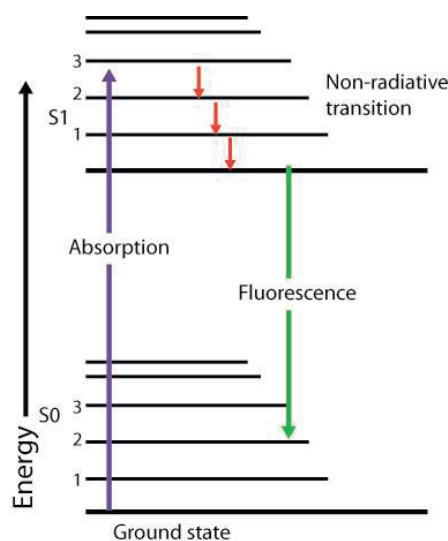


Figure 5.4.1 Simplified Jablonski diagram showing the electronic states of a fluorophore molecule.

Another related aspect of importance is the photobleaching phenomenon²⁸⁰. Photobleaching occurs due to a fluorophore's irreversible decomposition. Generally, long-term or intense light exposure of a fluorescent molecule results in photobleaching. It can be intentionally utilized in several microscopy techniques, including fluorescence recovery after photobleaching (FRAP)^{281, 282} which is discussed below.

The thickness of the lipid bilayer is approximately 4-5 nm, and the sample chamber including solid support is optically transparent. If the sample, e.g. lipid membrane, is doped with a fluorophore, the specimen can be illuminated with a selected wavelength in order to visualize it under the microscope. In a standard fluorescence microscope (**Figure 5.4.3 a**), the excitation light passes through an entrance filter, reflects from the surface of a semipermeable (dichroic) mirror, and reaches the specimen through the objective lens. The labeled sample component subsequently emits light of slightly decreased energy (Stokes shift) isotropically. Parts of this emitted light is collected by the objective and passed back through the dichromatic mirror and an emission filter to the detector, e.g. a camera or, in case of the confocal microscope (**Figure 5.4.3.b**), a photomultiplier tube (PMT) detector. The wavelength difference between excitation and emission light allows the dichroic mirror to discriminate between incident light and sample response, and the emission filter removes unwanted contributions from scattered and ambient light. The matching combination of filters and dichroic mirror in an exchangeable frame is commonly referred to as filter cube.

The micrographs in this thesis have been obtained with an inverted confocal microscope, where the objective is positioned under the sample, facing upwards (**Figure 5.4.3 b**). This makes it possible, in contrast to an upright microscope (**Figure 5.4.3 a**), that the specimen remains accessible from the top, e.g. for liquid exchange or micromanipulation.

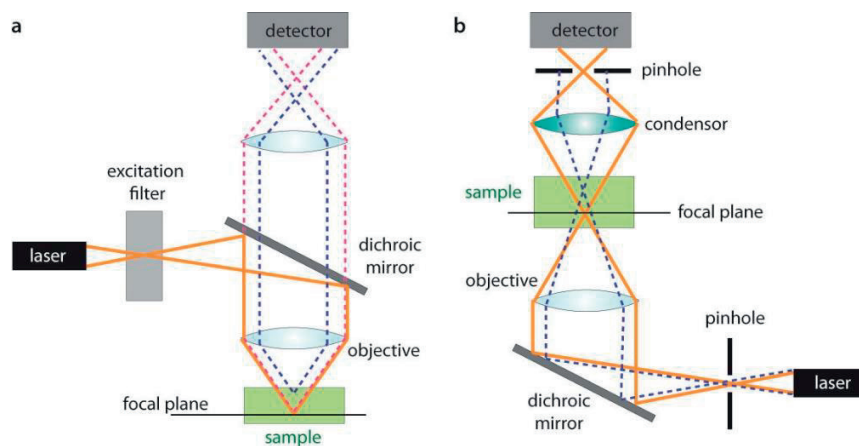


Figure 5.4.2 Schematic drawings showing (a) an upright epi-fluorescence and (b) an inverted confocal microscope. In epi-fluorescence mode, all emitted light reaches the detector. In confocal microscopy, light that is emitted out of focus is blocked by a pinhole before reaching the detector.

In contrast to wide field fluorescence microscopy, where the entire field of view is evenly illuminated by the incident light, and an image is obtained as a snap shot, the confocal microscope is a scanning technique, where a narrow focal volume is moved across a selected region, and the image is constructed from intensity values obtained from the PMT detector. Confocal microscopes provide high optical resolution and enable 2D sectioning of 3D samples due to the employment of a pinhole for screening of unwanted light. The experiments in this thesis were performed with a laser confocal scanning microscopy (LCSM), mostly using a 40x magnification immersion oil objective with NA of 1.3. In an LCSM, a focused beam scans the sample in a line pattern, and the pinhole aperture (**Figure 5.4.3 b**) blocks out-of-focus light in the image collection path, therefore allows for nearly exclusively collecting light from the focal plane with a thickness from 0.5 to 1.5 μm . Through scanning two-dimensional images while elevating the focal plane stepwise, sets of thin sections can be obtained and rendered to three-dimensional fluorescence images. In epifluorescence microscopy, which does not contain a pinhole, the signal is collected from the whole body of the sample (**Figure 5.4.3 a**), with the disadvantage that fine details of the sample structure are convoluted, limiting the resolution.

All optical microscope objectives gather and focus light to the detector through a system of lenses, which besides providing magnification also ensure aberration- and distortion-free, color-correct images over a large wavelength range. They are divided into several categories: magnification (4-100x), working distance and dry or immersion objectives. In general, dry objectives have longer working distances but a lower numerical aperture (NA). The NA value shows the ability of an objective lens to capture diffracted light arriving from the specimen. The NA of a lens is defined as

$$NA = n \sin \alpha_0$$

where n is the refractive index of the medium between the lens and the specimen (≈ 1 for air) and α_0 is half the angle spanned by the objective. With increasing NA the resolution in the observed sample improves. A measure of the resolving power is given as

$$\delta = \frac{\lambda}{2NA}$$

where λ is the wavelength of light. Immersion objectives operate with a liquid medium of defined refractive index between the lens and the sample carrier, which restricts their working distance, but provides higher NA. The immersion liquid increases the NA of the objective lens due to its higher refractive index, e.g. 1.3 for water and 1.51 for immersion oil.

5.5 Fluorescence recovery after photobleaching

Fluorescence recovery after photobleaching (FRAP)^{281, 282} is a method for characterizing the mobility and kinetics of molecules. FRAP can be conducted with laser scanning confocal microscopy where a selected region on a sample that is homogeneously labeled, e.g. lipid membrane, is photobleached with high intensity laser and monitored over time.

If the sample is fluid and the molecules in the sample are mobile, the photobleached molecules will diffuse out of the laser exposed area⁴, and the fluorescent molecules in the sample that were not photobleached repopulate the laser-exposed spot. The diffusion is driven by Brownian motion, and its speed depends on the fluidity of the membrane⁴. Eventually, the photobleached molecules will evenly distribute across the membrane resulting in recovery of the fluorescence intensity in the initially photobleached region. If the sample is rigid, and the molecules are immobile, diffusion will not take place and no recovery will be observed²⁸³.

In Paper I the fluidity of lipid membranes on different microengineering surfaces was investigated using FRAP. In Paper IV it was employed to examine the diffusion of fluorescent molecules between nanotube connected protocells. In the latter paper, the fluorescent content in the aqueous volume inside the model protocells was photobleached, whereas in Paper I it was the membrane.

5.6 Near infrared laser heating

To increase the temperature locally around the lipid membranes, infrared laser heating has been employed. Water strongly absorbs light around 1470 nm, corresponding to the short-wavelength infrared B (IR-B) that is used in common communication lasers. In Papers II and III we employed 1470 nm infrared semiconductor diode laser coupled to an optical fiber with a core diameter of 50 μm (**Figure 5.6.1** inset). The optical fiber is submerged into the sample by using 3-axis hydraulic micromanipulator (**Figure 5.6.1**). The fiber tip is located near the model protocell (~ 30 -

50 μm above the surface) and through it the IR-B laser is projected onto the sample resulting in a local temperature increase in the region of interest^{284, 285}. The heating can be applied to an area of approximately 400 μm^2 .

The temperature can be measured with reasonable accuracy using a microthermocouple²⁸⁵. In Paper II we established temperatures of 40-70 $^{\circ}\text{C}$ to facilitate the dewetting and subcompartmentalization of adherent protocells. Similarly, in Paper III, IR-B laser heating was used to enhance growth and fusion of subcompartment colonies.

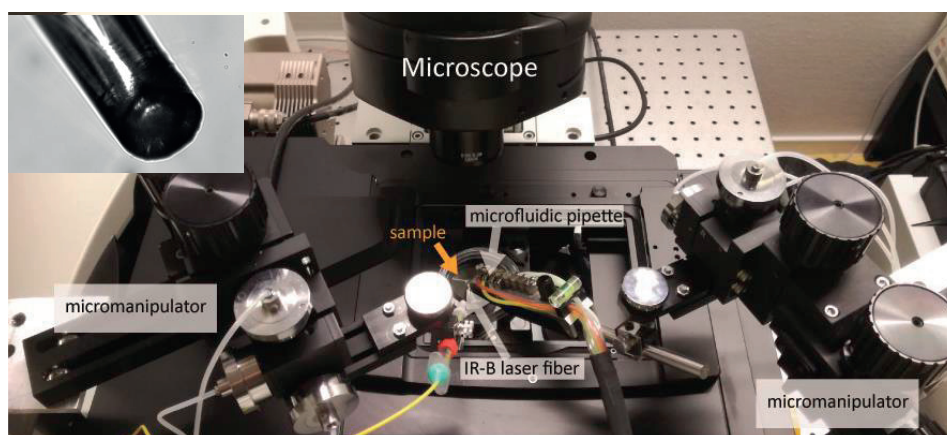


Figure 5.6.1 Photograph showing an overview of the experimental setup. IR-B laser and microfluidic pipette are both attached to micromanipulators. The sample is mounted on an inverted confocal microscope.

5.7 Microfluidics

Microfluidics is a technique of precise manipulation of small volume of liquids (fL to μL) in channels of tens to a few hundred micrometers in size²⁸⁶. The microfluidic methods and devices provide an advantage of low consumption and controlled manipulation of liquids.

Liquids in small channels flow in form of smooth lines, termed as laminar flow. In contrast to turbulent flow, laminar flow allows two or more fluids to co-flow side by side without mixing. This is a result of the microscale dimensions, characterized by low Reynolds number (Re).

$$\text{Re} = \frac{\rho v_0 L_0}{\eta}$$

The Reynolds number is a non-dimensional number defined as a ratio of inertial forces such as liquid density (ρ), velocity (v_0) and channel length (L_0) to viscous forces (η). Considering water as a working fluid, typical values in the microfluidics such as velocities of 1 $\mu\text{m/s}$ -1 cm/s , and channel radii of 1-100 μm , the Reynolds numbers range between 10^{-6} to 10^{287} . Fluids defined by a Re in this range exhibit laminar flow where they continuously exchange molecules only through diffusion. The complete transition to turbulent flow occurs in a regime where Re is between 2000-3000²⁸⁷. Microfluidics is not only a technology in the laboratory, but an important principle

of biology. For example, capillary blood vessels accommodate laminar flow whereas major arteries exhibit turbulent flow features²⁸⁸.

Conventional on-chip applications involve manipulation of fluids inside the microfluidic channels²⁸⁹. In the experiments we used an open space microfluidic device, specifically a microfluidic pipette²⁹⁰ (**Figure 5.7.1**), fabricated from an optically transparent soft elastomer poly-(dimethylsiloxane) (PDMS). In open space microfluidics at least one boundary of the system is removed, allowing the exposure of the fluid to another fluid interface. The microfluidic pipette creates a controlled hydrodynamic flow zone²⁹¹ consisting of a small volume of liquid at the tip of device (**Figure 5.7.1**). The diameter of the recirculation zone can be less than 10 μm in diameter, making it extraordinarily convenient to work on a single cell in a culture plate or a surface-adhered single vesicle in a population²⁹². The device tip consists of three adjacent channels: the one in the center injects the fluid and the two side channels aspirate it (**Figure 5.7.1**). A “re-circulating” volume is maintained by controlling the ratio of the outflow of the fluid to the inflow at the tip of the device. When the microfluidic device is submerged to a sample, the recirculation zone comes in contact with the aqueous solution around it, where the fluid boundary between the two liquids is diffusive, but flow velocity-to-diffusion ratio is high, dispersion across the boundary can be neglected²⁹⁰ (**Figure 5.7.1**).

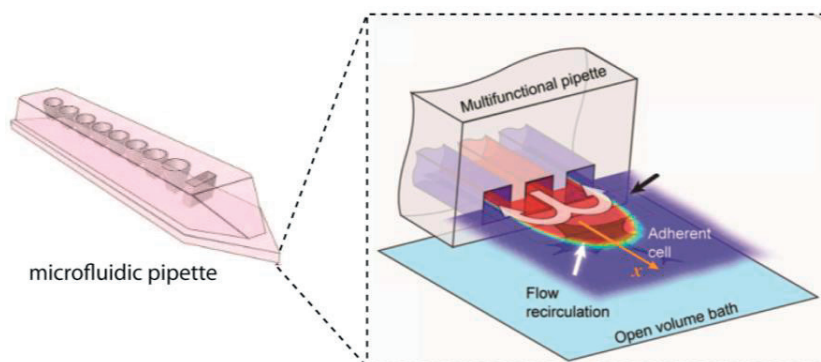


Figure 5.7.1 The microfluidic pipette. A hydrodynamic flow zone at the tip of the pipette (red zone) does not mix with the ambient solution (blue zone) due to confinement. *Image on the right is reprinted with permission from reference 291. Copyright ©2012 MDPI.*

Each reservoir well in the microfluidic pipette (**Figure 5.7.1**) is loaded with 30 μl of sample prior to the experiment. In Paper I, this small volume of liquid contained SUVs in buffered suspension. The device was positioned approximately 10 μm above a liquid submerged surface, and the SUVs were recirculated. Recirculation for a minute led to the adsorption and rupture of SUVs, and formation of a lipid film.

Controlled exposure of protocells to fluorescent dyes and fluorescently labeled genetic fragments via microfluidic pipette was used in Paper II-IV. The water-soluble compounds were delivered to the exterior of the protocell and the encapsulation was recorded in real-time. This

is similar to the superfusion in physiology^{293, 294} where a stream of liquid is run over the surface of a section of suspended tissue, keeping it viable and allowing observation of the interchange of substances.

5.8 DNA strand displacement reactions

In Paper III we employed a non-enzymatic, entropy driven reaction²⁹⁵ (**Figure 5.8.1**). One of the reactants is a double stranded DNA (dsDNA). One of the strands contain 20 base pairs and is conjugated to a fluorophore (blue colored strand in **Figure 5.8.1**). The complementary strand has an extending toehold on one end and a quencher on the other end (magenta colored strand in **Figure 5.8.1**). The toehold is complementary to a single stranded DNA (ssDNA), which acts as an 'invading strand' (orange colored strand in **Figure 5.8.1**). When the invading strand is introduced, it initiates strand displacement by hybridizing with the toehold. This initially creates a DNA complex composed of three strands of DNA, but the invading strand eventually displaces the single strand with the fluorophore. While the fluorophore was initially quenched by the dimerization, upon release it starts to emit fluorescence (**Figure 5.8.1**).

Prior to the DNA displacement experiment, the protocell structures were grown in a medium containing quenched dsDNA. The ambient solution was removed in several washing cycles to eliminate the non-encapsulated dimers. The compartments were subsequently exposed to the invading ssDNA via the microfluidic pipette. The increasing fluorescent signal inside the compartments indicated that the invading strand was spontaneously encapsulated, leading to a successful displacement reaction.

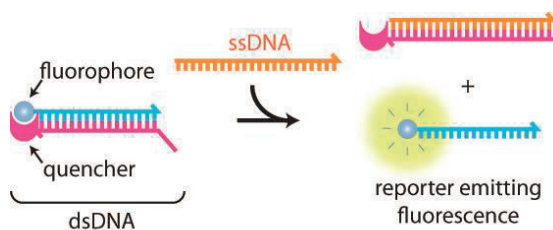


Figure 5.8.1 Schematic drawing summarizing the DNA strand displacement reaction. Addition of an invading strand (orange) leads to the displacement of one of the strands (blue) of a double stranded DNA. The strand released due to the displacement exhibits fluorescence.

5.9 Analytical models

Computational models overcome limitations of the experimental methods, such as resolving power of optical instruments, and can complement experimental data²⁹⁶. Computer models can provide detailed insight about the interactions of individual components in an experimental system at the molecular or mesoscale.

Analytical models addressing dynamic biomembrane systems can be categorized depending on the time scale and the length scale of an analyzed system. Quantum mechanics (QM) and molecular mechanics (MM) simulations are used to model formation and breaking of chemical bonds, hydration effects and conformational changes of the molecules at the nanoscale²⁹⁶. Atomistic membrane models, such as molecular dynamics simulations (MD), focus on physical movement of individual atoms and molecules (\approx ns- μ s). The MD models are commonly employed to investigate lipid membranes and identify their structural and dynamic properties^{296, 297}.

Coarse-grained models simplify the molecules by describing group of atoms as a single vector. This allows studying a system over a longer period of time. In coarse-grained models detailed chemical structure of molecules is not important. The materials are treated as a continuous mass in contrast to the previously mentioned methods analyzing individual particles²⁹⁸.

5.9.1 Finite element model for uptake through transient pores

To understand the dynamics of diffusion of molecules through the membrane pores, the finite element method (FEM) was used. FEM analysis subdivides the studied domain into a mesh of small discrete elements, calculates the governing equations for each element and then assembles them to provide system equations to be solved in order to model the entire structure^{299, 300}. Equations for each element, which are parts of the virtual network (mesh), are solved simultaneously.

In Paper II the COMSOL Multiphysics software was used for FEM analysis. The simulations focused on the diffusion of fluorescent molecules through a single membrane nanopore into a lipid vesicle (**Figure 5.9.1**), varying a set of parameters such as vesicle diameter, pore radius and diffusion coefficient. Due to the small size of the assumed pore, this is experimentally not feasible with confocal microscopy. As an initial condition the concentration of solutes outside the lipid vesicles has set to be high and inside the vesicle, low. The concentration gradient was depicted with a heat map (red for high concentration, blue for low concentration) (**Figure 5.9.1**). Assuming constant concentration in the external volume and taking into account the diffusion coefficient of the molecule, the change in the concentration inside the lipid vesicle was calculated in time steps. This was iterated through different pore and vesicle sizes

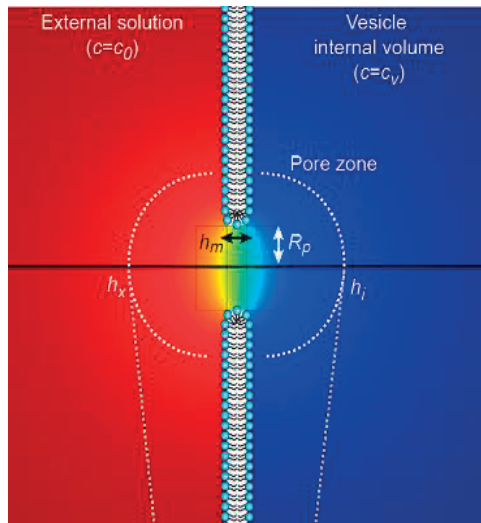


Figure 5.9.1 Schematic representation of the finite element model. Diffusion of fluorescent molecule through a single nanopore into the lipid compartment was analyzed. The red color shows the highest concentration of solutes in the external solution. The blue color represents the concentration of the solutes inside the compartment. The green zone inside the pore represents a concentration gradient formed due to molecular diffusion. Reprinted with permission from reference 5. Copyright ©2021 John Wiley and sons.

In Paper III a continuum elastohydrodynamic model was employed to characterize the formation of instabilities leading to superstructures. The model was established using the open source finite element analysis (FEA) library FEniCS on Python 3.6³⁰¹. The time evolution of the height between membrane and surface, the liquid pressure and the flow speed were determined for different wave numbers at different time points. As a result, a critical length scale for the membrane invaginations was obtained above which leads to the superstructures (cf 4.9 *Van der Waals Interactions*).

6 Summary of the main findings

Paper I. Molecular Lipid Films on Microengineering Materials

The formation and development of phospholipid films on a variety of microengineered solid substrates was investigated, including borosilicate glass, Al (native oxide), Al₂O₃, TiO₂, ITO, SiO₂, Au, Teflon AF, SU-8 and graphene. The surfaces were characterized by their electrical (zeta) potential, which for graphene monolayer it was reported for the first time. The membrane-surface interactions were analyzed by laser confocal microscopy and FRAP. Various membrane-surface interactions were observed including single- and double bilayer film formation, vesicle adhesion as well as several non-trivial adhesion phenomena, such as reverse rolling of spreading bilayers and spontaneous nucleation of multilamellar vesicles. A diagram depicting different behaviors based on lipid membrane compositions and corresponding surface charges was established, supporting the development of membrane-interface devices and models. The findings provided detailed insight into membrane-surface interactions and thus allow for more accurate prediction of lipid film behavior.

Paper II. Subcompartmentalization and Pseudo-Division of Model Protocells

The spontaneous subcompartmentalization of model surface-adhered protocells was observed as the result of physicochemical interactions at the surface-membrane interface. Several small dynamic unilamellar subcompartments were formed at the basal membrane of the protocells, resembling intra-cellular organelles. The subcompartments were able to uptake ambient compounds via openings on the surface, and segregate it. We showed the spontaneous encapsulation of the same compounds as in the main protocell volume, and hypothesized that it occurs via nano-sized transient pores. We supported the transient pore hypothesis by a finite element model which predicts uptake rates similar to those observed in the experiments. Moreover, a primitive division mechanism was reported where the enveloping protocell membrane disintegrated, leaving individual subcompartments to become individual daughter protocells.

Paper III. Colony-like Protocell Superstructures

A prebiotically feasible pathway for formation and growth of large protocell superstructures, reminiscent of microbial colonies, was shown. An analytical model anticipated the onset of membrane instabilities in the basal membrane, which can later grow into microcontainers, based on the contribution of the van der Waals forces. The model protocell colonies exhibited higher mechanical stability compared to the individual compartments, and were able to encapsulate molecules from the ambient, such as DNA, and accommodate non-enzymatic DNA displacement reactions. A new pathway of uptake was observed, via exo-compartments, which spontaneously extended out of the colonies as individual compartments. The exo-compartments encapsulated ambient molecules and fused with the colony delivering the cargo to the protocell colony. Upon disintegration of the enveloping (outer) membrane, the individual compartments were able to transform into daughter cells and migrate to remote locations, still carrying the encapsulated cargo.

Paper IV. Transport among Protocells via Tunneling Nanotubes

Molecular transport through the lipid nanotubes connecting surface-adhered protocells was shown for the first time. Different fluorescent cargo, e.g. ATTO 488, RNA, DNA, was encapsulated in the protocell volume, its diffusive transport through the connecting nanotubes was induced and analyzed via FRAP. The internal fluorescence of the photobleached protocells within the networks recovered over time, confirming the transport of the cargo between neighboring protocells through the nanotubes. An analytical model was established in order to estimate the most influential physical parameters of the system. The most effective parameter for recovery of contents was determined to be the diameter of the nanotubes, compared to nanotube length, protocell size and the diffusion properties of the fluorescent cargo. Nanotube-mediated transport in protocell networks was shown to be a feasible way of chemical communication among primitive cells.

7 Conclusion and future outlook

In this thesis I showed new, feasible, and consistent solid surface-based routes to sophisticated membranous protocell morphologies. One of these routes involved a previously unknown subcompartmentalization phenomenon, where surface-adhered lipid compartments produced multiple internal membranous compartments. Spatial separation of the internal volume into membrane-enveloped compartments is an apparent key feature of the living cells, since the presence of separate organelles has been reported across all domains of life. Much like their biological counterparts, internal subcompartments in the protocell models can take up ambient compounds and create distinct, secluded spaces. The availability of excess lipid material in the experimental model enables the spontaneous formation bacterial colony-like superstructures, which were earlier suggested as a possible step in development of protocells, but have never been shown before to occur under prebiotically relevant experimental conditions.

One of the novel observations in these systems is an alternative pathway to primitive cell division, which occurs when the enveloping protocell membrane disintegrates, and exposes the internal compartments, i.e., daughter cells. This introduces a new angle to the protocell division problem which is conventionally viewed as the splitting of a spherical compartment into two smaller compartments.

Colony-like protocell populations have great potential to accommodate prebiotic reactions and reaction networks, and can be further explored in this context in the future. Their unique architecture can allow chemical information sharing among individual subcompartments while protecting them from unwanted interferences.

Acknowledgments

First and foremost, I want to thank my supervisor Irep for accepting me as a PhD student and giving me this amazing opportunity. Thank you for always fighting for me, for your endless support, for your advices and lessons for life. These past 3 years have been a journey and I am grateful I was able to complete my PhD under your supervision.

To my co-supervisors Reidar and Andreas, thank you for your support, all discussion and valuable advices.

To my colleagues, all current and former; Elif, Aysu, Inga, Lin, Ingrid, Maivizhi, Gizem, Annie and Thomas, thank you for all the memories in the work and outside. Your friendship made my PhD journey full of laughter and great memories. All the trips, group dinners, board game nights and coffee breaks will remain among my favorite parts of these past years.

To Aldo, thank you for always bringing new ideas and solutions to problems, for very valuable feedback on my work, and especially for proof-reading my thesis. Thanks to you our laboratory is equipped with things we never knew we needed.

To all my co-authors, thank you for your contributions and help. To Silver, Alar, Ruslan, Esteban, Chinmay and Nadir, the co-authors I had the pleasure to meet outside of emails, thank you for discussions, new perspectives and ideas, which made my work better.

To my colleagues and friends in NCMM, thank you for creating nice working environment. I enjoyed our squash sessions, potlucks and meeting you in and outside of the lab. To members of Bio3 section in Department of Chemistry, thank you for all the helpful discussions during our section meetings and fun at the section beers.

To Jakub, thank you for your support right from the beginning. You encouraged me to apply for my very first research position, and helped me all along the way till now. Thank you for always being just a call away with an advice I need to hear.

To Renáta and Dominika, thank you for being my 'PhD' buddies. Our late night talks about life as a PhD student and shared laughs always lifted my spirit.

Last but not least, I want to thank my family and friends for their love and support. To my Oslo family, thank you for welcoming me and being there for me, for celebrating with me every little achievement.

To my family back home: Tato, Mama, Saša a Peťo, ďakujem za Vašu podporu a pomoc. Nikdy som nebola príliš ďaleko aby ste nenašli spôsob ako so mnou osláviť malé či veľké veci, poradiť, či ma rozosmiať.

Thank you. Takk. Ďakujem.

References

1. Trifonov, E. N., Vocabulary of Definitions of Life Suggests a Definition. *Journal of Biomolecular Structure and Dynamics* **2011**, *29* (2), 259-266.
2. Ganti, T., *The Principles of Life*. Oxford University Press UK: 2003.
3. Lunine, J. I., Physical conditions on the early Earth. *Philos Trans R Soc Lond B Biol Sci* **2006**, *361* (1474), 1721-1731.
4. Jõemetsa, S.; Spustova, K.; Kustanovich, K.; Ainla, A.; Schindler, S.; Eigler, S.; Lobovkina, T.; Lara-Avila, S.; Jesorka, A.; Gözen, I., Molecular Lipid Films on Microengineering Materials. *Langmuir* **2019**, *35* (32), 10286-10298.
5. Spustova, K.; Köksal, E. S.; Ainla, A.; Gözen, I., Subcompartmentalization and Pseudo-Division of Model Protocells. *Small* **2021**, *17* (2), 2005320.
6. Serafino, L., Abiogenesis as a theoretical challenge: Some reflections. *Journal of Theoretical Biology* **2016**, *402*, 18-20.
7. National Aeronautics and Space Administration, N. About Life Detection. <https://astrobiology.nasa.gov/research/life-detection/about/> (accessed 10. September).
8. Darwin, C., *On the Origin of Species*. London, 1859.
9. Monnard, P.-A.; Deamer, D. W., Membrane self-assembly processes: Steps toward the first cellular life. **2002**, *268* (3), 196-207.
10. Manhes, G.; Allègre, C. J.; Dupré, B.; Hamelin, B., Lead isotope study of basic-ultrabasic layered complexes: Speculations about the age of the earth and primitive mantle characteristics. *Earth and Planetary Science Letters* **1980**, *47* (3), 370-382.
11. Patterson, C., Age of meteorites and the earth. *Geochimica et Cosmochimica Acta* **1956**, *10* (4), 230-237.
12. Mojzsis, S. J.; Harrison, T. M.; Pidgeon, R. T., Oxygen-isotope evidence from ancient zircons for liquid water at the Earth's surface 4,300 Myr ago. *Nature* **2001**, *409* (6817), 178-181.
13. Piani, L.; Marrocchi, Y.; Rigaudier, T.; Vacher Lionel, G.; Thomassin, D.; Marty, B., Earth's water may have been inherited from material similar to enstatite chondrite meteorites. *Science* **2020**, *369* (6507), 1110-1113.
14. Hassenkam, T.; Rosing, M. T., 3.7 billion year old biogenic remains. *Communicative & Integrative Biology* **2017**, *10* (5-6), e1380759.
15. Djokic, T.; Van Kranendonk, M. J.; Campbell, K. A.; Walter, M. R.; Ward, C. R., Earliest signs of life on land preserved in ca. 3.5 Ga hot spring deposits. *Nature Communications* **2017**, *8* (1), 15263.
16. Duda, J.-P.; Van Kranendonk, M. J.; Thiel, V.; Ionescu, D.; Strauss, H.; Schäfer, N.; Reitner, J., A Rare Glimpse of Paleoarchean Life: Geobiology of an Exceptionally Preserved Microbial Mat Facies from the 3.4 Ga Strelley Pool Formation, Western Australia. *PloS one* **2016**, *11* (1), e0147629-e0147629.
17. Weiss, M. C.; Sousa, F. L.; Mrnjavac, N.; Neukirchen, S.; Roettger, M.; Nelson-Sathi, S.; Martin, W. F., The physiology and habitat of the last universal common ancestor. *Nature Microbiology* **2016**, *1* (9), 16116.
18. Kawaguchi, Y., Panspermia Hypothesis: History of a Hypothesis and a Review of the Past, Present, and Future Planned Missions to Test This Hypothesis. In *Astrobiology: From the Origins of Life to the Search for Extraterrestrial Intelligence*, Yamagishi, A.; Kakegawa, T.; Usui, T., Eds. Springer Singapore: Singapore, 2019; pp 419-428.
19. Furukawa, Y.; Chikaraishi, Y.; Ohkouchi, N.; Ogawa, N. O.; Glavin, D. P.; Dworkin, J. P.; Abe, C.; Nakamura, T., Extraterrestrial ribose and other sugars in primitive meteorites. *Proceedings of the National Academy of Sciences* **2019**, *116* (49), 24440-24445.

20. Oba, Y.; Takano, Y.; Naraoka, H.; Furukawa, Y.; Glavin, D. P.; Dworkin, J. P.; Tachibana, S., Extraterrestrial hexamethylenetetramine in meteorites—a precursor of prebiotic chemistry in the inner solar system. *Nature Communications* **2020**, *11* (1), 6243.
21. Oparin, A. I., *The Origin of Life*. Dover Publications, Inc.: 1965.
22. Haldane, J. B. S., *The Origin of Life, Rationnalist Annual*. Oxford University Press: Oxford, 1985.
23. Miller, S. L., A Production of Amino Acids Under Possible Primitive Earth Conditions. *Science* **1953**, *117* (3046), 528.
24. Abelson, P. H., Chemical events on the primitive Earth. *Proc Natl Acad Sci U S A* **1966**, *55* (6), 1365-72.
25. Kasting James, F., Earth's Early Atmosphere. *Science* **1993**, *259* (5097), 920-926.
26. Cleaves, H. J.; Chalmers, J. H.; Lazcano, A.; Miller, S. L.; Bada, J. L., A Reassessment of Prebiotic Organic Synthesis in Neutral Planetary Atmospheres. *Origins of Life and Evolution of Biospheres* **2008**, *38* (2), 105-115.
27. Spiess, F. N.; Macdonald Ken, C.; Atwater, T.; Ballard, R.; Carranza, A.; Cordoba, D.; Cox, C.; Garcia, V. M. D.; Francheteau, J.; Guerrero, J.; Hawkins, J.; Haymon, R.; Hessler, R.; Juteau, T.; Kastner, M.; Larson, R.; Luyendyk, B.; Macdougall, J. D.; Miller, S.; Normark, W.; Orcutt, J.; Rangin, C., East Pacific Rise: Hot Springs and Geophysical Experiments. *Science* **1980**, *207* (4438), 1421-1433.
28. Martin, W.; Baross, J.; Kelley, D.; Russell, M. J., Hydrothermal vents and the origin of life. *Nature Reviews Microbiology* **2008**, *6* (11), 805-814.
29. Von Damm, K. L.; Lilley, M. D.; Shanks, W. C.; Brockington, M.; Bray, A. M.; O'Grady, K. M.; Olson, E.; Graham, A.; Proskurowski, G., Extraordinary phase separation and segregation in vent fluids from the southern East Pacific Rise. *Earth and Planetary Science Letters* **2003**, *206* (3-4), 365-378.
30. Kelley Deborah, S.; Karson Jeffrey, A.; Früh-Green Gretchen, L.; Yoerger Dana, R.; Shank Timothy, M.; Butterfield David, A.; Hayes John, M.; Schrenk Matthew, O.; Olson Eric, J.; Proskurowski, G.; Jakuba, M.; Bradley, A.; Larson, B.; Ludwig, K.; Glickson, D.; Buckman, K.; Bradley Alexander, S.; Brazelton William, J.; Roe, K.; Elend Mitch, J.; Delacour, A.; Bernasconi Stefano, M.; Lilley Marvin, D.; Baross John, A.; Summons Roger, E.; Sylva Sean, P., A Serpentinite-Hosted Ecosystem: The Lost City Hydrothermal Field. *Science* **2005**, *307* (5714), 1428-1434.
31. Brazelton, W. J.; Ludwig, K. A.; Sogin, M. L.; Andreishcheva, E. N.; Kelley, D. S.; Shen, C.-C.; Edwards, R. L.; Baross, J. A., Archaea and bacteria with surprising microdiversity show shifts in dominance over 1,000-year time scales in hydrothermal chimneys. *Proceedings of the National Academy of Sciences* **2010**, *107* (4), 1612-1617.
32. Wirth, R., Colonization of Black Smokers by Hyperthermophilic Microorganisms. *Trends in Microbiology* **2017**, *25* (2), 92-99.
33. Holland, H. D., *The Chemical Evolution of the Atmosphere and Oceans*. Princeton University Press: 1984.
34. Petersen, S.; Krätschell, A.; Augustin, N.; Jamieson, J.; Hein, J. R.; Hannington, M. D., News from the seabed – Geological characteristics and resource potential of deep-sea mineral resources. *Marine Policy* **2016**, *70*, 175-187.
35. Mulkidjanian, A. Y.; Galperin, M. Y., On the origin of life in the zinc world. 2. Validation of the hypothesis on the photosynthesizing zinc sulfide edifices as cradles of life on Earth. *Biology direct* **2009**, *4*, 27-27.
36. Wächtershäuser, G., Groundworks for an evolutionary biochemistry: The iron-sulphur world. *Progress in Biophysics and Molecular Biology* **1992**, *58* (2), 85-201.
37. Follmann, H.; Brownson, C., Darwin's warm little pond revisited: from molecules to the origin of life. *Naturwissenschaften* **2009**, *96* (11), 1265-1292.
38. Darwin, C. "Letter no. 7471". <https://www.darwinproject.ac.uk/letter/DCP-LETT-7471.xml> (accessed 2021).

39. Becker, S.; Feldmann, J.; Wiedemann, S.; Okamura, H.; Schneider, C.; Iwan, K.; Crisp, A.; Rossa, M.; Amatov, T.; Carell, T., Unified prebiotically plausible synthesis of pyrimidine and purine RNA ribonucleotides. *Science* **2019**, *366* (6461), 76-82.
40. Segré, D.; Ben-Eli, D.; Deamer, D. W.; Lancet, D., The lipid world. *Orig Life Evol Biosph* **2001**, *31* (1-2), 119-45.
41. Gilbert, W., Origin of life: The RNA world. *Nature* **1986**, *319* (6055), 618-618.
42. Pearce, B. K. D.; Pudritz, R. E.; Semenov, D. A.; Henning, T. K., Origin of the RNA world: The fate of nucleobases in warm little ponds. *Proc Natl Acad Sci U S A* **2017**, *114* (43), 11327-11332.
43. Alberts, B. B., D.; Lewis, J.; Raff, M.; Roberts, K. and Watson, J. D., *Molecular Biology of the Cell*. Garland Science: New York, 1994.
44. Pressman, A.; Blanco, C.; Chen, Irene A., The RNA World as a Model System to Study the Origin of Life. *Current Biology* **2015**, *25* (19), R953-R963.
45. Martin, W. F., Older Than Genes: The Acetyl CoA Pathway and Origins. *Front Microbiol* **2020**, *11*, 817-817.
46. Varma, S. J.; Muchowska, K. B.; Chatelain, P.; Moran, J., Native iron reduces CO₂ to intermediates and end-products of the acetyl-CoA pathway. *Nature Ecology & Evolution* **2018**, *2* (6), 1019-1024.
47. Bernhardt, H. S., The RNA world hypothesis: the worst theory of the early evolution of life (except for all the others)(a). *Biology direct* **2012**, *7*, 23-23.
48. Caetano-Anollés, G.; Seufferheld, M. J., The Coevolutionary Roots of Biochemistry and Cellular Organization Challenge the RNA World Paradigm. *Microbial Physiology* **2013**, *23* (1-2), 152-177.
49. Powner, M. W.; Gerland, B.; Sutherland, J. D., Synthesis of activated pyrimidine ribonucleotides in prebiotically plausible conditions. *Nature* **2009**, *459* (7244), 239-242.
50. Banfalvi, G., Prebiotic Pathway from Ribose to RNA Formation. *International Journal of Molecular Sciences* **2021**, *22* (8), 3857.
51. Paul, N.; Joyce, G. F., A self-replicating ligase ribozyme. *Proceedings of the National Academy of Sciences* **2002**, *99* (20), 12733-12740.
52. Lincoln, T. A.; Joyce, G. F., Self-Sustained Replication of an RNA Enzyme. *Science* **2009**, *323* (5918), 1229-1232.
53. Tjhung, K. F.; Shokhirev, M. N.; Horning, D. P.; Joyce, G. F., An RNA polymerase ribozyme that synthesizes its own ancestor. *Proceedings of the National Academy of Sciences* **2020**, *117* (6), 2906-2913.
54. Horning, D. P.; Joyce, G. F., Amplification of RNA by an RNA polymerase ribozyme. *Proceedings of the National Academy of Sciences* **2016**, *113* (35), 9786-9791.
55. Janzen, E.; Blanco, C.; Peng, H.; Kenchel, J.; Chen, I. A., Promiscuous Ribozymes and Their Proposed Role in Prebiotic Evolution. *Chemical Reviews* **2020**, *120* (11), 4879-4897.
56. Jash, B.; Tremmel, P.; Jovanovic, D.; Richert, C., Single nucleotide translation without ribosomes. *Nature Chemistry* **2021**, *13* (8), 751-757.
57. Deamer, D., The Role of Lipid Membranes in Life's Origin. *Life* **2017**, *7* (1), 5.
58. Saha, R.; Pohorille, A.; Chen, I. A., Molecular Crowding and Early Evolution. *Origins of Life and Evolution of Biospheres* **2014**, *44* (4), 319-324.
59. Grochmal, A.; Prout, L.; Makin-Taylor, R.; Prohens, R.; Tomas, S., Modulation of Reactivity in the Cavity of Liposomes Promotes the Formation of Peptide Bonds. *Journal of the American Chemical Society* **2015**, *137* (38), 12269-12275.
60. Saha, R.; Verbanic, S.; Chen, I. A., Lipid vesicles chaperone an encapsulated RNA aptamer. *Nature Communications* **2018**, *9* (1), 2313.
61. Blocher, M.; Liu, D.; Walde, P.; Luisi, P. L., Liposome-Assisted Selective Polycondensation of α -Amino Acids and Peptides. *Macromolecules* **1999**, *32* (21), 7332-7334.
62. Luisi, P. L.; Walde, P.; Oberholzer, T., Lipid vesicles as possible intermediates in the origin of life. *Current Opinion in Colloid & Interface Science* **1999**, *4* (1), 33-39.

63. Cornell, C. E.; Black, R. A.; Xue, M.; Litz, H. E.; Ramsay, A.; Gordon, M.; Mileant, A.; Cohen, Z. R.; Williams, J. A.; Lee, K. K.; Drobny, G. P.; Keller, S. L., Prebiotic amino acids bind to and stabilize prebiotic fatty acid membranes. *Proceedings of the National Academy of Sciences* **2019**, *116* (35), 17239-17244.
64. Cuccovia, I. M.; Quina, F. H.; Chaimovich, H., A remarkable enhancement of the rate of ester thiolysis by synthetic amphiphile vesicles. *Tetrahedron* **1982**, *38* (7), 917-920.
65. Fendler, J. H. F., E. J., *Catalysis in Micellar and Macromolecular Systems*. Elsevier, Inc.: 1975.
66. Lai, Y.-C.; Liu, Z.; Chen, I. A., Encapsulation of ribozymes inside model protocells leads to faster evolutionary adaptation. *Proceedings of the National Academy of Sciences* **2021**, *118* (21), e2025054118.
67. Lancet, D.; Zidovetzki, R.; Markovitch, O., Systems protobiology: origin of life in lipid catalytic networks. *Journal of The Royal Society Interface* **2018**, *15* (144), 20180159.
68. Luisi, P. L.; Varela, F. J., Self-replicating micelles — A chemical version of a minimal autopoietic system. *Origins of life and evolution of the biosphere* **1989**, *19* (6), 633-643.
69. Luisi, P. L., Autopoiesis: a review and a reappraisal. *Naturwissenschaften* **2003**, *90* (2), 49-59.
70. Bachmann, P. A.; Luisi, P. L.; Lang, J., Autocatalytic self-replicating micelles as models for prebiotic structures. *Nature* **1992**, *357* (6373), 57-59.
71. Segré, D.; Ben-Eli, D.; Lancet, D., Compositional genomes: prebiotic information transfer in mutually catalytic noncovalent assemblies. *Proc Natl Acad Sci U S A* **2000**, *97* (8), 4112-4117.
72. Chen, I. A.; Szostak, J. W., A Kinetic Study of the Growth of Fatty Acid Vesicles. *Biophys J* **2004**, *87* (2), 988-998.
73. Zhu, T. F.; Szostak, J. W., Coupled growth and division of model protocell membranes. *J Am Chem Soc* **2009**, *131* (15), 5705-13.
74. Chen, I. A.; Roberts, R. W.; Szostak, J. W., The emergence of competition between model protocells. *Science (New York, N.Y.)* **2004**, *305* (5689), 1474-1476.
75. Walde, P.; Wick, R.; Fresta, M.; Mangone, A.; Luisi, P. L., Autopoietic Self-Reproduction of Fatty Acid Vesicles. *Journal of the American Chemical Society* **1994**, *116* (26), 11649-11654.
76. Le Vay, K.; Mutschler, H., The difficult case of an RNA-only origin of life. *Emerg Top Life Sci* **2019**, *3* (5), 469-475.
77. Patel, B. H.; Percivalle, C.; Ritson, D. J.; Duffy, C. D.; Sutherland, J. D., Common origins of RNA, protein and lipid precursors in a cyanosulfidic protometabolism. *Nature chemistry* **2015**, *7* (4), 301-307.
78. Sprunt, E. S.; Brace, W. F., Direct observation of microcavities in crystalline rocks. *International Journal of Rock Mechanics and Mining Sciences & Geomechanics Abstracts* **1974**, *11* (4), 139-150.
79. Viennet, J.-C.; Bernard, S.; Le Guillou, C.; Sautter, V.; Grégoire, B.; Jambon, A.; Pont, S.; Beyssac, O.; Zanda, B.; Hewins, R.; Remusat, L., Martian Magmatic Clay Minerals Forming Vesicles: Perfect Niches for Emerging Life? *Astrobiology* **2021**, *21* (5), 605-612.
80. Erastova, V.; Degiacomi, M. T.; Fraser, D. G.; Greenwell, H. C., Mineral surface chemistry control for origin of prebiotic peptides. *Nature Communications* **2017**, *8* (1).
81. Bernal, J. D., The Physical Basis of Life. *Proceedings of the Physical Society. Section B* **1949**, *62* (10), 597-618.
82. Huang, W.; Ferris, J. P., Synthesis of 35–40 mers of RNA oligomers from unblocked monomers. A simple approach to the RNA world. *Chemical Communications* **2003**, (12), 1458-1459.
83. Huang, W.; Ferris, J. P., One-Step, Regioselective Synthesis of up to 50-mers of RNA Oligomers by Montmorillonite Catalysis. *Journal of the American Chemical Society* **2006**, *128* (27), 8914-8919.
84. Jheeta, S.; Joshi, P. C., Prebiotic RNA synthesis by montmorillonite catalysis. *Life (Basel)* **2014**, *4* (3), 318-330.
85. Lambert, J. F., Adsorption and polymerization of amino acids on mineral surfaces: A review. *Origins of Life and Evolution of Biospheres* **2008**, *38* (3), 211-242.

86. Hashizume, H., Role of Clay Minerals in Chemical Evolution and the Origins of Life. In *Clay Minerals in Nature*, Intech Open: 2012.
87. Aumiller, W. M., Jr.; Keating, C. D., Experimental models for dynamic compartmentalization of biomolecules in liquid organelles: Reversible formation and partitioning in aqueous biphasic systems. *Adv Colloid Interface Sci* **2017**, *239*, 75-87.
88. Love, C.; Steinkühler, J.; Gonzales, D. T.; Yandrapalli, N.; Robinson, T.; Dimova, R.; Tang, T.-Y. D., Reversible pH-Responsive Coacervate Formation in Lipid Vesicles Activates Dormant Enzymatic Reactions. *Angewandte Chemie International Edition* **2020**, *59* (15), 5950-5957.
89. Nakashima, K. K.; Vibhute, M. A.; Spruijt, E., Biomolecular Chemistry in Liquid Phase Separated Compartments. *Front Mol Biosci* **2019**, *6*, 21-21.
90. Jia, T. Z.; Hentrich, C.; Szostak, J. W., Rapid RNA Exchange in Aqueous Two-Phase System and Coacervate Droplets. *Origins of Life and Evolution of Biospheres* **2014**, *44* (1), 1-12.
91. Drobot, B.; Iglesias-Artola, J. M.; Le Vay, K.; Mayr, V.; Kar, M.; Kreysing, M.; Mutschler, H.; Tang, T. Y. D., Compartmentalised RNA catalysis in membrane-free coacervate protocells. *Nature Communications* **2018**, *9* (1), 3643.
92. Cakmak, F. P.; Choi, S.; Meyer, M. O.; Bevilacqua, P. C.; Keating, C. D., Prebiotically-relevant low polyion multivalency can improve functionality of membraneless compartments. *Nature Communications* **2020**, *11* (1), 5949.
93. Poudyal, R. R.; Keating, C. D.; Bevilacqua, P. C., Polyanion-Assisted Ribozyme Catalysis Inside Complex Coacervates. *ACS Chemical Biology* **2019**, *14* (6), 1243-1248.
94. Subramaniam, A. B.; Wan, J.; Gopinath, A.; Stone, H. A., Semi-permeable vesicles composed of natural clay. *Soft Matter* **2011**, *7* (6), 2600-2612.
95. Thompson, K. L.; Williams, M.; Armes, S. P., Colloidosomes: Synthesis, properties and applications. *Journal of Colloid and Interface Science* **2015**, *447*, 217-228.
96. Li, M.; Harbron, R. L.; Weaver, J. V. M.; Binks, B. P.; Mann, S., Electrostatically gated membrane permeability in inorganic protocells. *Nature Chemistry* **2013**, *5* (6), 529-536.
97. Cakmak, F. P.; Marianelli, A. M.; Keating, C. D., Phospholipid membrane formation templated by coacervate droplets. *bioRxiv* **2021**, 2021.02.17.431720.
98. Dora Tang, T. Y.; Rohaida Che Hak, C.; Thompson, A. J.; Kuimova, M. K.; Williams, D. S.; Perriman, A. W.; Mann, S., Fatty acid membrane assembly on coacervate microdroplets as a step towards a hybrid protocell model. *Nature Chemistry* **2014**, *6* (6), 527-533.
99. Bernardino de la Serna, J.; Schütz, G. J.; Eggeling, C.; Cebecauer, M., There Is No Simple Model of the Plasma Membrane Organization. *Frontiers in Cell and Developmental Biology* **2016**, *4* (106).
100. Chan, Y.-H. M.; Boxer, S. G., Model membrane systems and their applications. *Curr Opin Chem Biol* **2007**, *11* (6), 581-587.
101. Claey's, P.; Morbidelli, A., Late Heavy Bombardment. In *Encyclopedia of Astrobiology*, Gargaud, M.; Amils, R.; Quintanilla, J. C.; Cleaves, H. J.; Irvine, W. M.; Pinti, D. L.; Viso, M., Eds. Springer Berlin Heidelberg: Berlin, Heidelberg, 2011; pp 909-912.
102. Pizzarello, S.; Shock, E., The organic composition of carbonaceous meteorites: the evolutionary story ahead of biochemistry. *Cold Spring Harb Perspect Biol* **2010**, *2* (3), a002105.
103. Sephton, M. A., Organic compounds in carbonaceous meteorites. *Nat Prod Rep* **2002**, *19* (3), 292-311.
104. Lai, J. C. Y.; Pearce, B. K. D.; Pudritz, R. E.; Lee, D., Meteoritic abundances of fatty acids and potential reaction pathways in planetesimals. *Icarus* **2019**, *319*, 685-700.
105. Hargreaves, W. R.; Deamer, D. W., Liposomes from ionic, single-chain amphiphiles. *Biochemistry* **1978**, *17* (18), 3759-3768.
106. Deamer, D. W., Boundary structures are formed by organic components of the Murchison carbonaceous chondrite. *Nature* **1985**, *317* (6040), 792-794.

107. Rivilla, V. M.; Jiménez-Serra, I.; Martín-Pintado, J.; Briones, C.; Rodríguez-Almeida, L. F.; Rico-Villas, F.; Tercero, B.; Zeng, S.; Colzi, L.; de Vicente, P.; Martín, S.; Requena-Torres, M. A., Discovery in space of ethanolamine, the simplest phospholipid head group. *Proceedings of the National Academy of Sciences* **2021**, *118* (22), e2101314118.
108. Rojas, J.; Duprat, J.; Engrand, C.; Dartois, E.; Delauche, L.; Godard, M.; Gounelle, M.; Carrillo-Sánchez, J. D.; Pokorný, P.; Plane, J. M. C., The micrometeorite flux at Dome C (Antarctica), monitoring the accretion of extraterrestrial dust on Earth. *Earth and Planetary Science Letters* **2021**, *560*, 116794.
109. Flynn, G. J.; Keller, L. P.; Feser, M.; Wirick, S.; Jacobsen, C., The origin of organic matter in the solar system: evidence from the interplanetary dust particles. *Geochimica et Cosmochimica Acta* **2003**, *67* (24), 4791-4806.
110. Sabbah, H.; Morrow, A. L.; Jenniskens, P.; Shaddad, M. H.; Zare, R. N., Polycyclic aromatic hydrocarbons in asteroid 2008 TC3: Dispersion of organic compounds inside asteroids. *Meteoritics & Planetary Science* **2010**, *45* (10-11), 1710-1717.
111. Botta, O.; Bada, J. L., Extraterrestrial Organic Compounds in Meteorites. *Surveys in Geophysics* **2002**, *23* (5), 411-467.
112. Dalai, P.; Kaddour, H.; Sahai, N., Incubating Life: Prebiotic Sources of Organics for the Origin of Life. *Elements* **2016**, *12* (6), 401-406.
113. Sahai, N.; Kaddour, H.; Dalai, P., The Transition from Geochemistry to Biogeochemistry. *Elements* **2016**, *12* (6), 389-394.
114. Chyba, C.; Sagan, C., Endogenous production, exogenous delivery and impact-shock synthesis of organic molecules: an inventory for the origins of life. *Nature* **1992**, *355*, 125-32.
115. Genge, M. J.; Larsen, J.; Van Ginneken, M.; Suttle, M. D., An urban collection of modern-day large micrometeorites: Evidence for variations in the extraterrestrial dust flux through the Quaternary. *Geology* **2017**, *45* (2), 119-122.
116. Fiore, M., The synthesis of mono-alkyl phosphates and their derivatives: an overview of their nature, preparation and use, including synthesis under plausible prebiotic conditions. *Org Biomol Chem* **2018**, *16* (17), 3068-3086.
117. Fiore, M.; Strazewski, P., Prebiotic Lipidic Amphiphiles and Condensing Agents on the Early Earth. *Life* **2016**, *6* (2), 17.
118. Hargreaves, W. R.; Mulvihill, S. J.; Deamer, D. W., Synthesis of phospholipids and membranes in prebiotic conditions [27]. *Nature* **1977**, *266* (5597), 78-80.
119. Rao, M.; Eichberg, J.; Oró, J., Synthesis of phosphatidylcholine under possible primitive Earth conditions. *Journal of Molecular Evolution* **1982**, *18* (3), 196-202.
120. Rao, M.; Eichberg, J.; Oró, J., Synthesis of phosphatidylethanolamine under possible primitive earth conditions. *Journal of Molecular Evolution* **1987**, *25* (1), 1-6.
121. Liu, L.; Zou, Y.; Bhattacharya, A.; Zhang, D.; Lang, S. Q.; Houk, K. N.; Devaraj, N. K., Enzyme-free synthesis of natural phospholipids in water. *Nature Chemistry* **2020**, *12* (11), 1029-1034.
122. Monnard, P.-A.; Walde, P., Current Ideas about Prebiological Compartmentalization. *Life (Basel)* **2015**, *5* (2), 1239-1263.
123. Sakashita, A.; Urakami, N.; Zihler, P.; Imai, M., Three-dimensional analysis of lipid vesicle transformations. *Soft Matter* **2012**, *8* (33), 8569-8581.
124. Zhu, T. F.; Budin, I.; Szostak, J. W., Preparation of fatty acid micelles. *Methods Enzymol* **2013**, *533*, 283-288.
125. Pöldsalu, I.; Köksal, E. S.; Gözen, I., Mixed fatty acid-phospholipid protocell networks. *bioRxiv* **2021**, 2021.03.08.434432.
126. Zhu, T. F.; Adamala, K.; Zhang, N.; Szostak, J. W., Photochemically driven redox chemistry induces protocell membrane pearling and division. *Proceedings of the National Academy of Sciences* **2012**, *109* (25), 9828-9832.

127. Wick, R.; Walde, P.; Luisi, P. L., Light microscopic investigations of the autocatalytic self-reproduction of giant vesicles. *Journal of the American Chemical Society* **1995**, *117* (4), 1435-1436.
128. Kindt, J. T.; Szostak, J. W.; Wang, A., Bulk Self-Assembly of Giant, Unilamellar Vesicles. *ACS Nano* **2020**, *14* (11), 14627-14634.
129. Budin, I.; Szostak, J. W., Physical effects underlying the transition from primitive to modern cell membranes. *Proceedings of the National Academy of Sciences* **2011**, *108* (13), 5249-5254.
130. Kanavarioti, A.; Bernasconi, C. F.; Doodokyan, D. L.; Alberas, D. J., Magnesium ion catalyzed phosphorus-nitrogen bond hydrolysis in imidazolide-activated nucleotides. Relevance to template-directed synthesis of polynucleotides. *Journal of the American Chemical Society* **1989**, *111* (18), 7247-7257.
131. Rasi, S.; Mavelli, F.; Luisi, P. L., Matrix Effect in Oleate Micelles-Vesicles Transformation. *Origins of life and evolution of the biosphere* **2004**, *34* (1), 215-224.
132. Berclaz, N.; Blöchliger, E.; Müller, M.; Luisi, P. L., Matrix Effect of Vesicle Formation As Investigated by Cryotransmission Electron Microscopy. *The Journal of Physical Chemistry B* **2001**, *105* (5), 1065-1071.
133. Markvoort, A. J.; Pflieger, N.; Staffhorst, R.; Hilbers, P. A.; van Santen, R. A.; Killian, J. A.; de Kruijff, B., Self-reproduction of fatty acid vesicles: a combined experimental and simulation study. *Biophys J* **2010**, *99* (5), 1520-8.
134. Karatekin, E.; Sandre, O.; Brochard-Wyart, F., Transient pores in vesicles. **2003**, *52* (4), 486-493.
135. Chabanon, M.; Ho, J. C. S.; Liedberg, B.; Parikh, A. N.; Rangamani, P., Pulsatile Lipid Vesicles under Osmotic Stress. *Biophys J* **2017**, *112* (8), 1682-1691.
136. Steinkühler, J.; Knorr, R. L.; Zhao, Z.; Bhatia, T.; Bartelt, S. M.; Wegner, S.; Dimova, R.; Lipowsky, R., Controlled division of cell-sized vesicles by low densities of membrane-bound proteins. *Nature Communications* **2020**, *11* (1), 905.
137. Dreher, Y.; Jahnke, K.; Bobkova, E.; Spatz, J. P.; Göpfrich, K., Division and Regrowth of Phase-Separated Giant Unilamellar Vesicles**. *Angewandte Chemie International Edition* **2021**, *60* (19), 10661-10669.
138. Gözen, İ., Did Solid Surfaces Enable the Origin of Life? *Life* **2021**, *11* (8).
139. Dalai, P.; Sahai, N., Mineral-Lipid Interactions in the Origins of Life. *Trends in Biochemical Sciences* **2019**, *44* (4), 331-341.
140. Hanczyc, M. M.; Fujikawa, S. M.; Szostak, J. W., Experimental Models of Primitive Cellular Compartments: Encapsulation, Growth, and Division. **2003**, *302* (5645), 618-622.
141. Hanczyc, M. M.; Mansy, S. S.; Szostak, J. W., Mineral Surface Directed Membrane Assembly. *Origins of Life and Evolution of Biospheres* **2007**, *37* (1), 67-82.
142. Köksal, E. S.; Liese, S.; Kantarci, I.; Olsson, R.; Carlson, A.; Gözen, I., Nanotube-Mediated Path to Protocell Formation. *ACS Nano* **2019**, *13* (6), 6867-6878.
143. Köksal, E. S.; Liese, S.; Xue, L.; Ryskulov, R.; Viitala, L.; Carlson, A.; Gözen, I., Rapid growth and fusion of protocells in surface-adhered membrane networks. **2020**, 2020.03.10.980417.
144. Köksal, E. S.; Pöldsalu, I.; Friis, H.; Mojszis, S.; Bizzarro, M.; Gözen, I., Spontaneous formation of prebiotic compartment colonies on Hadean Earth and pre-Noachian Mars. *bioRxiv* **2021**, 2021.05.11.443509.
145. Gözen, İ., A Hypothesis for Protocell Division on the Early Earth. *ACS Nano* **2019**, *13* (10), 10869-10871.
146. Zhang, Y.; Liu, Y.; Liu, H.; Tang, W. H., Exosomes: biogenesis, biologic function and clinical potential. *Cell & Bioscience* **2019**, *9* (1), 19.
147. Ma, L.; Li, Y.; Peng, J.; Wu, D.; Zhao, X.; Cui, Y.; Chen, L.; Yan, X.; Du, Y.; Yu, L., Discovery of the migrasome, an organelle mediating release of cytoplasmic contents during cell migration. *Cell Research* **2015**, *25* (1), 24-38.

148. Mitrea, D. M.; Kriwacki, R. W., Phase separation in biology; functional organization of a higher order. *Cell Communication and Signaling* **2016**, *14* (1), 1.
149. Dominak, L. M.; Gundermann, E. L.; Keating, C. D., Microcompartmentation in artificial cells: PH-induced conformational changes alter protein localization. *Langmuir* **2010**, *26* (8), 5697-5705.
150. Deshpande, S.; Brandenburg, F.; Lau, A.; Last, M. G. F.; Spoelstra, W. K.; Reese, L.; Wunnava, S.; Dogterom, M.; Dekker, C., Spatiotemporal control of coacervate formation within liposomes. *Nature Communications* **2019**, *10* (1), 1800.
151. Long, M. S.; Jones, C. D.; Helfrich, M. R.; Mangeney-Slavin, L. K.; Keating, C. D., Dynamic microcompartmentation in synthetic cells. *Proc Natl Acad Sci U S A* **2005**, *102* (17), 5920-5925.
152. Diekmann, Y.; Pereira-Leal, J. B., Evolution of intracellular compartmentalization. *Biochemical Journal* **2013**, *449* (2), 319-331.
153. Cornejo, E.; Abreu, N.; Komeili, A., Compartmentalization and organelle formation in bacteria. *Current Opinion in Cell Biology* **2014**, *26*, 132-138.
154. Giuliano, C. B.; Cvjetan, N.; Ayache, J.; Walde, P., Multivesicular Vesicles: Preparation and Applications. *ChemSystemsChem* **2021**, *3* (2), e2000049.
155. Bernard, A.-L.; Guedeau-Boudeville, M.-A.; Jullien, L.; di Meglio, J.-M., Raspberry vesicles. *Biochimica et Biophysica Acta (BBA) - Biomembranes* **2002**, *1567*, 1-5.
156. Moreno-Flores, S., Inward multivesiculation at the basal membrane of adherent giant phospholipid vesicles. *Biochimica et Biophysica Acta (BBA) - Biomembranes* **2016**, *1858* (4), 793-799.
157. Wang, X.; Tian, L.; Du, H.; Li, M.; Mu, W.; Drinkwater, B. W.; Han, X.; Mann, S., Chemical communication in spatially organized protocell colonies and protocell/living cell micro-arrays. *Chemical Science* **2019**, *10* (41), 9446-9453.
158. Casas-Ferrer, L.; Brisson, A.; Massiera, G.; Casanellas, L., Design of vesicle prototissues as a model for cellular tissues. *Soft Matter* **2021**, *17* (19), 5061-5072.
159. Carrara, P.; Stano, P.; Luisi, P. L., Giant Vesicles "Colonies": A Model for Primitive Cell Communities. **2012**, *13* (10), 1497-1502.
160. de Souza, T. P.; Bossa, G. V.; Stano, P.; Steiniger, F.; May, S.; Luisi, P. L.; Fahr, A., Vesicle aggregates as a model for primitive cellular assemblies. *Physical Chemistry Chemical Physics* **2017**, *19* (30), 20082-20092.
161. Li, Q.; Li, S.; Zhang, X.; Xu, W.; Han, X., Programmed magnetic manipulation of vesicles into spatially coded prototissue architectures arrays. *Nature Communications* **2020**, *11* (1), 232.
162. Bilal, T.; Gözen, I., Formation and dynamics of endoplasmic reticulum-like lipid nanotube networks. *Biomaterials Science* **2017**, *5* (7), 1256-1264.
163. Israelachvili, J. N., 17 - Adhesion and Wetting Phenomena. In *Intermolecular and Surface Forces (Third Edition)*, Israelachvili, J. N., Ed. Academic Press: San Diego, 2011; pp 415-467.
164. Israelachvili, J. N., Chapter 13 - Van der Waals Forces between Particles and Surfaces. In *Intermolecular and Surface Forces (Third Edition)*, Israelachvili, J. N., Ed. Academic Press: San Diego, 2011; pp 253-289.
165. Harper, A. *Plastics Materials and Processes* **2003**, 1-48.
166. Butt, H.-J. G., Karlheinz; Kappl, Michael, Contact Angle Phenomena and Wetting. In *Physics and Chemistry of Interfaces*, 2003; pp 118-144.
167. Emami, F. S.; Puddu, V.; Berry, R. J.; Varshney, V.; Patwardhan, S. V.; Perry, C. C.; Heinz, H., Force Field and a Surface Model Database for Silica to Simulate Interfacial Properties in Atomic Resolution. *Chemistry of Materials* **2014**, *26* (8), 2647-2658.
168. Bollen, C. M.; Papaioanno, W.; Van Eldere, J.; Schepers, E.; Quiryne, M.; van Steenberghe, D., The influence of abutment surface roughness on plaque accumulation and peri-implant mucositis. *Clin Oral Implants Res* **1996**, *7* (3), 201-11.

169. Parvate, S.; Dixit, P.; Chattopadhyay, S., Superhydrophobic Surfaces: Insights from Theory and Experiment. *The Journal of Physical Chemistry B* **2020**, *124* (8), 1323-1360.
170. Manoharan, K.; Bhattacharya, S., Superhydrophobic surfaces review: Functional application, fabrication techniques and limitations. *Journal of Micromanufacturing* **2019**, *2* (1), 59-78.
171. Ahn, T. K.; Lee, D. H.; Kim, T. S.; Jang, G. C.; Choi, S.; Oh, J. B.; Ye, G.; Lee, S., Modification of Titanium Implant and Titanium Dioxide for Bone Tissue Engineering. *Adv Exp Med Biol* **2018**, *1077*, 355-368.
172. Adil, S. F.; Khan, M.; Kalpana, D., 7 - Graphene-based nanomaterials for solar cells. In *Multifunctional Photocatalytic Materials for Energy*, Lin, Z.; Ye, M.; Wang, M., Eds. Woodhead Publishing: 2018; pp 127-152.
173. Kyhl, L.; Nielsen, S. F.; Čabo, A. G.; Cassidy, A.; Miwa, J. A.; Hornekær, L., Graphene as an anti-corrosion coating layer. *Faraday Discussions* **2015**, *180* (0), 495-509.
174. Chiesa, M.; Lai, C.-Y., Surface aging investigation by means of an AFM-based methodology and the evolution of conservative nanoscale interactions. *Physical Chemistry Chemical Physics* **2018**, *20* (29), 19664-19671.
175. Zhang, W.; Chen, X.; Ma, Y.; Xu, Z.; Wu, L.; Yang, Y.; Tsang, S.-W.; Chen, S., Positive Aging Effect of ZnO Nanoparticles Induced by Surface Stabilization. *The Journal of Physical Chemistry Letters* **2020**, *11* (15), 5863-5870.
176. Bennett, M. K.; Zisman, W. A., Confirmation of spontaneous spreading by water on pure gold. *The Journal of Physical Chemistry* **1970**, *74* (11), 2309-2312.
177. Shinozaki, A.; Arima, K.; Morita, M.; Kojima, I.; Azuma, Y., FTIR-ATR Evaluation of Organic Contaminant Cleaning Methods for SiO₂ Surfaces. *Analytical Sciences* **2003**, *19* (11), 1557-1559.
178. Li, Z.; Wang, Y.; Kozbial, A.; Shenoy, G.; Zhou, F.; McGinley, R.; Ireland, P.; Morganstein, B.; Kunkel, A.; Surwade, S. P.; Li, L.; Liu, H., Effect of airborne contaminants on the wettability of supported graphene and graphite. *Nature Materials* **2013**, *12* (10), 925-931.
179. Hazen, R. M.; Sverjensky, D. A., Mineral surfaces, geochemical complexities, and the origins of life. *Cold Spring Harb Perspect Biol* **2010**, *2* (5), a002162-a002162.
180. Hazen, R. M.; Ferry, J. M., Mineral Evolution: Mineralogy in the Fourth Dimension. *Elements* **2010**, *6* (1), 9-12.
181. Cynn, H.; Isaak, D. G.; E., C. R.; Nicol, M. F.; Anderson, O. L., A high-pressure phase transition of corundum predicted by the potential induced breathing model. *American Mineralogist* **1990**, *75* (3-4), 439-442.
182. Yang, M.-H.; Chen, P.-C.; Tsai, M.-C.; Chen, T.-T.; Chang, I. C.; Chiu, H.-T.; Lee, C.-Y., Anatase and brookite TiO₂ with various morphologies and their proposed building block. *CrystEngComm* **2014**, *16* (3), 441-447.
183. Papineau, D., Mineral Environments on the Earliest Earth. *Elements* **2010**, *6* (1), 25-30.
184. Chyba, C. F.; Phillips, C. B., Possible ecosystems and the search for life on Europa. *Proceedings of the National Academy of Sciences* **2001**, *98* (3), 801-804.
185. Neveu, M.; Anbar, A. D.; Davila, A. F.; Glavin, D. P.; MacKenzie, S. M.; Phillips-Lander, C. M.; Sherwood, B.; Takano, Y.; Williams, P.; Yano, H., Returning Samples From Enceladus for Life Detection. *Frontiers in Astronomy and Space Sciences* **2020**, *7* (26).
186. Clark, B. C.; Kolb, V. M.; Steele, A.; House, C. H.; Lanza, N. L.; Gasda, P. J.; VanBommel, S. J.; Newsom, H. E.; Martínez-Frías, J., Origin of Life on Mars: Suitability and Opportunities. *Life* **2021**, *11* (6), 539.
187. Bandfield, J. L., Global mineral distributions on Mars. *Journal of Geophysical Research: Planets* **2002**, *107* (E6), 9-1-9-20.

188. Humayun, M.; Nemchin, A.; Zanda, B.; Hewins, R. H.; Grange, M.; Kennedy, A.; Lorand, J. P.; Göpel, C.; Fieni, C.; Pont, S.; Deldicque, D., Origin and age of the earliest Martian crust from meteorite NWA 7533. *Nature* **2013**, *503* (7477), 513-516.
189. Santos, A. R.; Agee, C. B.; McCubbin, F. M.; Shearer, C. K.; Burger, P. V.; Tartèse, R.; Anand, M., Petrology of igneous clasts in Northwest Africa 7034: Implications for the petrologic diversity of the martian crust. *Geochimica et Cosmochimica Acta* **2015**, *157*, 56-85.
190. Costa, M. M.; Jensen, N. K.; Bouvier, L. C.; Connelly, J. N.; Mikouchi, T.; Horstwood, M. S. A.; Suuronen, J.-P.; Moynier, F.; Deng, Z.; Agranier, A.; Martin, L. A. J.; Johnson, T. E.; Nemchin, A. A.; Bizzarro, M., The internal structure and geodynamics of Mars inferred from a 4.2-Gyr zircon record. *Proceedings of the National Academy of Sciences* **2020**, *117* (49), 30973-30979.
191. van Meer, G.; Voelker, D. R.; Feigenson, G. W., Membrane lipids: where they are and how they behave. *Nature Reviews Molecular Cell Biology* **2008**, *9* (2), 112-124.
192. Olsen, A. S. B.; Færgeman, N. J., Sphingolipids: membrane microdomains in brain development, function and neurological diseases. *Open Biology* **2017**, *7* (5), 170069.
193. Cooper, R. A., Influence of increased membrane cholesterol on membrane fluidity and cell function in human red blood cells. *J Supramol Struct* **1978**, *8* (4), 413-30.
194. de Meyer, F.; Smit, B., Effect of cholesterol on the structure of a phospholipid bilayer. *Proceedings of the National Academy of Sciences* **2009**, *106* (10), 3654-3658.
195. El Khoury, M.; Swain, J.; Sautrey, G.; Zimmermann, L.; Van Der Smissen, P.; Décout, J.-L.; Mingeot-Leclercq, M.-P., Targeting Bacterial Cardiolipin Enriched Microdomains: An Antimicrobial Strategy Used by Amphiphilic Aminoglycoside Antibiotics. *Scientific Reports* **2017**, *7* (1), 10697.
196. Polissi, A.; Sperandio, P., The lipopolysaccharide export pathway in *Escherichia coli*: structure, organization and regulated assembly of the Lpt machinery. *Mar Drugs* **2014**, *12* (2), 1023-1042.
197. Jain, S.; Caforio, A.; Driessen, A. J. M., Biosynthesis of archaeal membrane ether lipids. *Front Microbiol* **2014**, *5*, 641-641.
198. Head-Gordon, T., Is water structure around hydrophobic groups clathrate-like? *Proc Natl Acad Sci U S A* **1995**, *92* (18), 8308-8312.
199. Marsh, D., Thermodynamics of phospholipid self-assembly. *Biophys J* **2012**, *102* (5), 1079-1087.
200. Singer, S. J.; Nicolson, G. L., The fluid mosaic model of the structure of cell membranes. *Science* **1972**, *175* (4023), 720-31.
201. Marsh, D., Structural and thermodynamic determinants of chain-melting transition temperatures for phospholipid and glycolipids membranes. *Biochimica et Biophysica Acta (BBA) - Biomembranes* **2010**, *1798* (1), 40-51.
202. Phillips, R.; Kondev, J.; Theriot, J.; Garcia, H. G.; Orme, N., *Physical biology of the cell*. 2013.
203. Shinitzky, M.; Barenholz, Y., Dynamics of the Hydrocarbon Layer in Liposomes of Lecithin and Sphingomyelin Containing Dicetylphosphate. *Journal of Biological Chemistry* **1974**, *249* (8), 2652-2657.
204. Bolognesi, G.; Friddin, M. S.; Salehi-Reyhani, A.; Barlow, N. E.; Brooks, N. J.; Ces, O.; Elani, Y., Sculpting and fusing biomimetic vesicle networks using optical tweezers. *Nature Communications* **2018**, *9* (1).
205. Helfrich, W., Effect of thermal undulations on the rigidity of fluid membranes and interfaces. *J. Phys. France* **1985**, *46* (7), 1263-1268.
206. Różycki, B.; Lipowsky, R., Spontaneous curvature of bilayer membranes from molecular simulations: Asymmetric lipid densities and asymmetric adsorption. *The Journal of Chemical Physics* **2015**, *142* (5), 054101.
207. Rawicz, W.; Olbrich, K. C.; McIntosh, T.; Needham, D.; Evans, E., Effect of chain length and unsaturation on elasticity of lipid bilayers. *Biophys J* **2000**, *79* (1), 328-339.
208. Gözen, I.; Dommersnes, P.; Czolkos, I.; Jesorka, A.; Lobovkina, T.; Orwar, O., Fractal avalanche ruptures in biological membranes. *Nature Materials* **2010**, *9* (11), 908-912.

209. Huang, C.; Quinn, D.; Sadovsky, Y.; Suresh, S.; Hsia, K. J., Formation and size distribution of self-assembled vesicles. *Proc Natl Acad Sci U S A* **2017**, *114* (11), 2910-2915.
210. Hu, M.; Briguglio, J. J.; Deserno, M., Determining the Gaussian Curvature Modulus of Lipid Membranes in Simulations. *Biophys J* **2012**, *102* (6), 1403-1410.
211. Pinheiro, M.; Lúcio, M.; Lima, J. L.; Reis, S., Liposomes as drug delivery systems for the treatment of TB. *Nanomedicine* **2011**, *6* (8), 1413-1428.
212. Allison, A. G.; Gregoriadis, G., Liposomes as immunological adjuvants. *Nature* **1974**, *252* (5480), 252.
213. Chacko, I. A.; Ghate, V. M.; Dsouza, L.; Lewis, S. A., Lipid vesicles: A versatile drug delivery platform for dermal and transdermal applications. *Colloids and Surfaces B: Biointerfaces* **2020**, *195*, 111262.
214. Sercombe, L.; Veerati, T.; Moheimani, F.; Wu, S. Y.; Sood, A. K.; Hua, S., Advances and Challenges of Liposome Assisted Drug Delivery. *Frontiers in Pharmacology* **2015**, *6* (286).
215. Guimarães, D.; Cavaco-Paulo, A.; Nogueira, E., Design of liposomes as drug delivery system for therapeutic applications. *International Journal of Pharmaceutics* **2021**, *601*, 120571.
216. Wang, N.; Chen, M.; Wang, T., Liposomes used as a vaccine adjuvant-delivery system: From basics to clinical immunization. *J Control Release* **2019**, *303*, 130-150.
217. Gregoriadis, G.; McCormack, B.; Obrenovic, M.; Saffie, R.; Zadi, B.; Perrie, Y., Vaccine entrapment in liposomes. *Methods* **1999**, *19* (1), 156-62.
218. Riaz, M. K.; Riaz, M. A.; Zhang, X.; Lin, C.; Wong, K. H.; Chen, X.; Zhang, G.; Lu, A.; Yang, Z., Surface Functionalization and Targeting Strategies of Liposomes in Solid Tumor Therapy: A Review. *International journal of molecular sciences* **2018**, *19* (1), 195.
219. Liu, Q.; Boyd, B. J., Liposomes in biosensors. *Analyst* **2013**, *138* (2), 391-409.
220. Mazur, F.; Bally, M.; Städler, B.; Chandrawati, R., Liposomes and lipid bilayers in biosensors. *Advances in Colloid and Interface Science* **2017**, *249*, 88-99.
221. Zepik, H. H.; Walde, P.; Kostoryz, E. L.; Code, J.; Yourtee, D. M., Lipid Vesicles as Membrane Models for Toxicological Assessment of Xenobiotics. *Critical Reviews in Toxicology* **2008**, *38* (1), 1-11.
222. Xu, C.; Hu, S.; Chen, X., Artificial cells: from basic science to applications. *Materials Today* **2016**, *19* (9), 516-532.
223. Mansy, S. S.; Szostak, J. W., Thermostability of model protocell membranes. *Proceedings of the National Academy of Sciences* **2008**, *105* (36), 13351-13355.
224. Liu, Y.; Kim, Y. J.; Siriwon, N.; Rohrs, J. A.; Yu, Z.; Wanga, P., Combination drug delivery via multilamellar vesicles enables targeting of tumor cells and tumor vasculature. *Biotechnology and Bioengineering* **2018**, *115* (6), 1403-1415.
225. Moon, J. J.; Suh, H.; Bershteyn, A.; Stephan, M. T.; Liu, H.; Huang, B.; Sohail, M.; Luo, S.; Um, S. H.; Khant, H.; Goodwin, J. T.; Ramos, J.; Chiu, W.; Irvine, D. J., Interbilayer-crosslinked multilamellar vesicles as synthetic vaccines for potent humoral and cellular immune responses. *Nature materials* **2011**, *10* (3), 243-251.
226. Schmitz, G.; Müller, G., Structure and function of lamellar bodies, lipid-protein complexes involved in storage and secretion of cellular lipids. *J Lipid Res* **1991**, *32* (10), 1539-70.
227. Kosmalska, A. J.; Casares, L.; Elosegui-Artola, A.; Thottacherry, J. J.; Moreno-Vicente, R.; González-Tarragó, V.; Del Pozo, M.; Mayor, S.; Arroyo, M.; Navajas, D.; Trepach, X.; Gauthier, N. C.; Roca-Cusachs, P., Physical principles of membrane remodelling during cell mechanoadaptation. *Nat Commun* **2015**, *6*, 7292.
228. Staykova, M.; Holmes, D. P.; Read, C.; Stone, H. A., Mechanics of surface area regulation in cells examined with confined lipid membranes. *Proceedings of the National Academy of Sciences* **2011**, *108* (22), 9084-9088.

229. Takaki, K.; Tahara, Y. O.; Nakamichi, N.; Hasegawa, Y.; Shintani, M.; Ohkuma, M.; Miyata, M.; Futamata, H.; Tashiro, Y., Multilamellar and Multivesicular Outer Membrane Vesicles Produced by a *Buttiauxella agrestis* tolB Mutant. *Appl Environ Microbiol* **2020**, *86* (20), e01131-20.
230. Gozen, I.; Dommersnes, P.; Orwar, O.; Jesorka, A., Evidence for membrane flow through pores in stacked phospholipid membranes. *Soft Matter* **2012**, *8* (23), 6220-6225.
231. Czolkos, I.; Jesorka, A.; Orwar, O., Molecular phospholipid films on solid supports. *Soft Matter* **2011**, *7* (10), 4562-4576.
232. Richter, R. P.; Him, J. L. K.; Brisson, A., Supported lipid membranes. *Materials Today* **2003**, *6* (11), 32-37.
233. Raedler, J.; Strey, H.; Sackmann, E., Phenomenology and Kinetics of Lipid Bilayer Spreading on Hydrophilic Surfaces. *Langmuir* **1995**, *11* (11), 4539-4548.
234. Keller, C. A.; Kasemo, B., Surface specific kinetics of lipid vesicle adsorption measured with a quartz crystal microbalance. *Biophys J* **1998**, *75* (3), 1397-1402.
235. Richter, R.; Mukhopadhyay, A.; Brisson, A., Pathways of lipid vesicle deposition on solid surfaces: a combined QCM-D and AFM study. *Biophys J* **2003**, *85* (5), 3035-3047.
236. Richter, R. P.; Bérat, R.; Brisson, A. R., Formation of solid-supported lipid bilayers: an integrated view. *Langmuir* **2006**, *22* (8), 3497-505.
237. Grupi, A.; Ashur, I.; Degani-Katzav, N.; Yudovich, S.; Shapira, Z.; Marzouq, A.; Morgenstein, L.; Mandel, Y.; Weiss, S., Interfacing the Cell with "Biomimetic Membrane Proteins". *Small* **2019**, *15* (52), 1903006.
238. Sarkis, J.; Vié, V., Biomimetic Models to Investigate Membrane Biophysics Affecting Lipid-Protein Interaction. *Front Bioeng Biotechnol* **2020**, *8*, 270-270.
239. Holm, A.; Wrasman, C. J.; Kao, K.-C.; Riscoe, A. R.; Cargnello, M.; Frank, C. W., Langmuir–Blodgett Deposition of Graphene Oxide—Identifying Marangoni Flow as a Process that Fundamentally Limits Deposition Control. *Langmuir* **2018**, *34* (33), 9683-9691.
240. Kalb, E.; Frey, S.; Tamm, L. K., Formation of supported planar bilayers by fusion of vesicles to supported phospholipid monolayers. *Biochimica et Biophysica Acta (BBA) - Biomembranes* **1992**, *1103* (2), 307-316.
241. Sackmann, E., Supported membranes: scientific and practical applications. *Science* **1996**, *271* (5245), 43-8.
242. Lobovkina, T.; Gözen, I.; Erkan, Y.; Olofsson, J.; Weber, S. G.; Orwar, O., Protrusive growth and periodic contractile motion in surface-adhered vesicles induced by Ca²⁺-gradients. *Soft Matter* **2010**, *6* (2), 268-272.
243. Aoki, P. H. B.; Schroder, A. P.; Constantino, C. J. L.; Marques, C. M., Bioadhesive giant vesicles for monitoring hydroperoxidation in lipid membranes. *Soft Matter* **2015**, *11* (30), 5995-5998.
244. Leng, J.; Nallet, F.; Roux, D., Swelling kinetics of a compressed lamellar phase. *European Physical Journal E: Soft matter and biological physics* **2001**, *4*, 77.
245. Hamai, C.; Cremer, P. S.; Musser, S. M., Single Giant Vesicle Rupture Events Reveal Multiple Mechanisms of Glass-Supported Bilayer Formation. *Biophys J* **2007**, *92* (6), 1988-1999.
246. Ngassam, V. N.; Su, W.-C.; Gettel, D. L.; Deng, Y.; Yang, Z.; Wang-Tomic, N.; Sharma, V. P.; Purushothaman, S.; Parikh, A. N., Recurrent dynamics of rupture transitions of giant lipid vesicles at solid surfaces. *Biophys J* **2021**, *120* (4), 586-597.
247. Klacar, S.; Dimitrievski, K.; Kasemo, B., Influence of Surface Pinning Points on Diffusion of Adsorbed Lipid Vesicles. *The Journal of Physical Chemistry B* **2009**, *113* (17), 5681-5685.
248. Limozin, L.; Sengupta, K., Modulation of vesicle adhesion and spreading kinetics by hyaluronan cushions. *Biophys J* **2007**, *93* (9), 3300-3313.

249. Melcrová, A.; Pokorna, S.; Pullanchery, S.; Kohagen, M.; Jurkiewicz, P.; Hof, M.; Jungwirth, P.; Cremer, P. S.; Cwiklik, L., The complex nature of calcium cation interactions with phospholipid bilayers. *Scientific Reports* **2016**, *6* (1), 38035.
250. Tamm, L. K.; McConnell, H. M., Supported phospholipid bilayers. *Biophys J* **1985**, *47* (1), 105-13.
251. Gerdes, H. H.; Carvalho, R. N., Intercellular transfer mediated by tunneling nanotubes. *Curr Opin Cell Biol* **2008**, *20* (4), 470-5.
252. Dubey, G. P.; Ben-Yehuda, S., Intercellular Nanotubes Mediate Bacterial Communication. *Cell* **2011**, *144* (4), 590-600.
253. Nir, S.; Andersen, M., Van der Waals interactions between cell surfaces. *J Membr Biol* **1977**, *31* (1-2), 1-18.
254. Lybarger, R. Z.; Petrache, H. I., Van Der Waals Interactions of Lipid Membranes in Highly Polarizable Solutions. *Biophys J* **2015**, *108* (2), 85a.
255. Israelachvili, J. N., 6 - Van der Waals Forces. In *Intermolecular and Surface Forces (Third Edition)*, Israelachvili, J. N., Ed. Academic Press: San Diego, 2011; pp 107-132.
256. Sandre, O.; Moreaux, L.; Brochard-Wyart, F., Dynamics of transient pores in stretched vesicles. **1999**, *96* (19), 10591-10596.
257. Levadny, V.; Tsuboi, T. A.; Belaya, M.; Yamazaki, M., Rate constant of tension-induced pore formation in lipid membranes. *Langmuir* **2013**, *29* (12), 3848-52.
258. Gozen, I.; Dommersnes, P., Pore dynamics in lipid membranes. *The European Physical Journal Special Topics* **2014**, *223* (9), 1813-1829.
259. Kirby, C.; Gregoriadis, G., Dehydration-Rehydration Vesicles: A Simple Method for High Yield Drug Entrapment in Liposomes. *Bio/Technology* **1984**, *2* (11), 979-984.
260. Köksal, E. S.; Belletati, P. F.; Reint, G.; Olsson, R.; Leitl, K. D.; Kantarci, I.; Gözen, I., Spontaneous Formation and Rearrangement of Artificial Lipid Nanotube Networks as a Bottom-Up Model for Endoplasmic Reticulum. *JoVE* **2019**, (143), e58923.
261. Schrader, A. M.; Cheng, C.-Y.; Israelachvili, J. N.; Han, S., Communication: Contrasting effects of glycerol and DMSO on lipid membrane surface hydration dynamics and forces. *The Journal of chemical physics* **2016**, *145* (4), 041101-041101.
262. Hunter, D. G.; Frisken, B. J., Effect of Extrusion Pressure and Lipid Properties on the Size and Polydispersity of Lipid Vesicles. *Biophys J* **1998**, *74* (6), 2996-3002.
263. Hope, M. J.; Bally, M. B.; Webb, G.; Cullis, P. R., Production of large unilamellar vesicles by a rapid extrusion procedure. Characterization of size distribution, trapped volume and ability to maintain a membrane potential. *Biochimica et Biophysica Acta (BBA) - Biomembranes* **1985**, *812* (1), 55-65.
264. Ong, S. G. M.; Chitneni, M.; Lee, K. S.; Ming, L. C.; Yuen, K. H., Evaluation of Extrusion Technique for Nanosizing Liposomes. *Pharmaceutics* **2016**, *8* (4), 36.
265. Grobéty, B.; Gieré, R.; Dietze, V.; Stille, P., Airborne Particles in the Urban Environment. *Elements* **2010**, *6* (4), 229-234.
266. Cleanrooms, M. ISO CLEAN ROOM STANDARDS. <https://www.mecart-cleanrooms.com/learning-center/cleanroom-classifications-iso-8-iso-7-iso-6-iso-5/>.
267. Martín-Palma, R. J.; Lakhtakia, A., Chapter 15 - Vapor-Deposition Techniques. In *Engineered Biomimicry*, Lakhtakia, A.; Martín-Palma, R. J., Eds. Elsevier: Boston, 2013; pp 383-398.
268. Johnson, R. W.; Hultqvist, A.; Bent, S. F., A brief review of atomic layer deposition: from fundamentals to applications. *Materials Today* **2014**, *17* (5), 236-246.
269. Leskelä, M.; Niinistö, J.; Ritala, M., 4.05 - Atomic Layer Deposition. In *Comprehensive Materials Processing*, Hashmi, S.; Batalha, G. F.; Van Tyne, C. J.; Yilbas, B., Eds. Elsevier: Oxford, 2014; pp 101-123.
270. Emslie, A. G.; Bonner, F. T.; Peck, L. G., Flow of a Viscous Liquid on a Rotating Disk. *Journal of Applied Physics* **1958**, *29* (5), 858-862.

271. Virojanadara, C.; Syväjarvi, M.; Yakimova, R.; Johansson, L. I.; Zakharov, A. A.; Balasubramanian, T., Homogeneous large-area graphene layer growth on ζ -SiC(0001). *Physical Review B* **2008**, *78* (24), 245403.
272. Emtsev, K. V.; Bostwick, A.; Horn, K.; Jobst, J.; Kellogg, G. L.; Ley, L.; McChesney, J. L.; Ohta, T.; Reshanov, S. A.; Röhrl, J.; Rotenberg, E.; Schmid, A. K.; Waldmann, D.; Weber, H. B.; Seyller, T., Towards wafer-size graphene layers by atmospheric pressure graphitization of silicon carbide. *Nature Materials* **2009**, *8* (3), 203-207.
273. Erickson, D.; Li, D.; Werner, C., An Improved Method of Determining the ζ -Potential and Surface Conductance. *Journal of Colloid and Interface Science* **2000**, *232* (1), 186-197.
274. Li, H.; Qing, C. L.; Wei, S. Q.; Jiang, X. J., An approach to the method for determination of surface potential on solid/liquid interface: theory. *Journal of Colloid and Interface Science* **2004**, *275* (1), 172-176.
275. Butt, H.-J. G., Karlheinz; Kappl, Michael, The Electric Double Layer. In *Physics and Chemistry of Interfaces*, 2003; pp 42-56.
276. Butt, H.-J.; Graf, K.; Kappl, M., The Electric Double Layer. In *Physics and Chemistry of Interfaces*, 2003; pp 42-56.
277. Jerome, W. G., Price, Robert L., Basic Confocal Microscopy. Springer International Publishing: 2018.
278. Martynov, V. I.; Pakhomov, A. A.; Popova, N. V.; Deyev, I. E.; Petrenko, A. G., Synthetic Fluorophores for Visualizing Biomolecules in Living Systems. *Acta Naturae* **2016**, *8* (4), 33-46.
279. Jablonski, A., Efficiency of Anti-Stokes Fluorescence in Dyes. *Nature* **1933**, *131* (3319), 839-840.
280. Demchenko, A. P., Photobleaching of organic fluorophores: quantitative characterization, mechanisms, protection. *Methods Appl Fluoresc* **2020**, *8* (2), 022001.
281. Ishikawa-Ankerhold, H.; Ankerhold, R.; Drummen, G., Fluorescence Recovery After Photobleaching (FRAP). *eLS* **2014**.
282. Lorén, N.; Hagman, J.; Jonasson, J. K.; Deschout, H.; Bernin, D.; Cella-Zanacchi, F.; Diaspro, A.; McNally, J. G.; Ameloot, M.; Smisdom, N.; Nydén, M.; Hermansson, A.-M.; Rudemo, M.; Braeckmans, K., Fluorescence recovery after photobleaching in material and life sciences: putting theory into practice. *Quarterly Reviews of Biophysics* **2015**, *48* (3), 323-387.
283. Orwick Rydmark, M.; Christensen, M. K.; Köksal, E. S.; Kantarci, I.; Kustanovich, K.; Yantchev, V.; Jesorka, A.; Gözen, I., Styrene maleic acid copolymer induces pores in biomembranes. *Soft Matter* **2019**, *15* (39), 7934-7944.
284. Gözen, I.; Shaali, M.; Ainla, A.; Örtmen, B.; Pöldsalu, I.; Kustanovich, K.; Jeffries, G. D. M.; Konkoli, Z.; Dommersnes, P.; Jesorka, A., Thermal migration of molecular lipid films as a contactless fabrication strategy for lipid nanotube networks. *Lab on a Chip* **2013**, *13* (19), 3822-3826.
285. Spustova, K.; Xue, L.; Ryskulov, R. J., A.; S.; Gözen, I, *Manipulation of Lipid Membranes with Thermal Stimuli*. in press.
286. Whitesides, G. M., The origins and the future of microfluidics. *Nature* **2006**, *442* (7101), 368-373.
287. Squires, T. M.; Quake, S. R., Microfluidics: Fluid physics at the nanoliter scale. *Reviews of Modern Physics* **2005**, *77* (3), 977-1026.
288. Stepanchuk, A. P., Blood motion: turbulent or laminar? *Wiad Lek* **2017**, *70* (2 pt 2), 331-334.
289. Niculescu, A.-G.; Chircov, C.; Bîrcă, A. C.; Grumezescu, A. M., Fabrication and Applications of Microfluidic Devices: A Review. *International Journal of Molecular Sciences* **2021**, *22* (4).
290. Ainla, A.; Jeffries, G. D. M.; Brune, R.; Orwar, O.; Jesorka, A., A multifunctional pipette. *Lab on a Chip* **2012**, *12* (7), 1255-1261.
291. Ainla, A.; Jeffries, G.; Jesorka, A., Hydrodynamic Flow Confinement Technology in Microfluidic Perfusion Devices. *Micromachines (Basel)* **2012**, *3* (2).
292. Ainla, A.; Jansson, E. T.; Stepanyants, N.; Orwar, O.; Jesorka, A., A Microfluidic Pipette for Single-Cell Pharmacology. *Analytical Chemistry* **2010**, *82* (11), 4529-4536.

293. Dittert, I.; Benedikt, J.; Vyklický, L.; Zimmermann, K.; Reeh, P. W.; Vlachová, V., Improved superfusion technique for rapid cooling or heating of cultured cells under patch-clamp conditions. *J Neurosci Methods* **2006**, *151* (2), 178-85.
294. Veselovsky, N. S.; Engert, F.; Lux, H. D., Fast local superfusion technique. *Pflugers Arch* **1996**, *432* (2), 351-4.
295. Zhang, D. Y.; Winfree, E., Control of DNA Strand Displacement Kinetics Using Toehold Exchange. *Journal of the American Chemical Society* **2009**, *131* (47), 17303-17314.
296. Ryazantsev, M. N.; Nikolaev, D. M.; Struts, A. V.; Brown, M. F., Quantum Mechanical and Molecular Mechanics Modeling of Membrane-Embedded Rhodopsins. *The Journal of Membrane Biology* **2019**, *252* (4), 425-449.
297. Yesylevskyy, S.; Rivel, T.; Ramseyer, C., Curvature increases permeability of the plasma membrane for ions, water and the anti-cancer drugs cisplatin and gemcitabine. *Scientific Reports* **2019**, *9* (1), 17214.
298. Simunovic M., V. G. A., Simulating Protein-Mediated Membrane Remodeling at Multiple Scales. In *Physics of Biological Membranes*, Springer, Cham: 2018.
299. Seshu, P., *Textbook of Finite Element Analysis*. Prentice-Hall of India Pvt.Ltd: 2004.
300. Thompson, J. M. T.; Kolston, P. J., Finite-element modelling: a new tool for the biologist. *Philosophical Transactions of the Royal Society of London. Series A: Mathematical, Physical and Engineering Sciences* **2000**, *358* (1766), 611-631.
301. Alnæs, M. S.; Blechta, J.; Hake, J.; Johansson, A.; Kehlet, B.; Logg, A.; Richardson, C.; Ring, J.; Rognes, M. E.; Wells, G. N., The FEniCS project version 1.5. *Archive of Numerical Software* **2015**, (Vol. 3, No. 100).

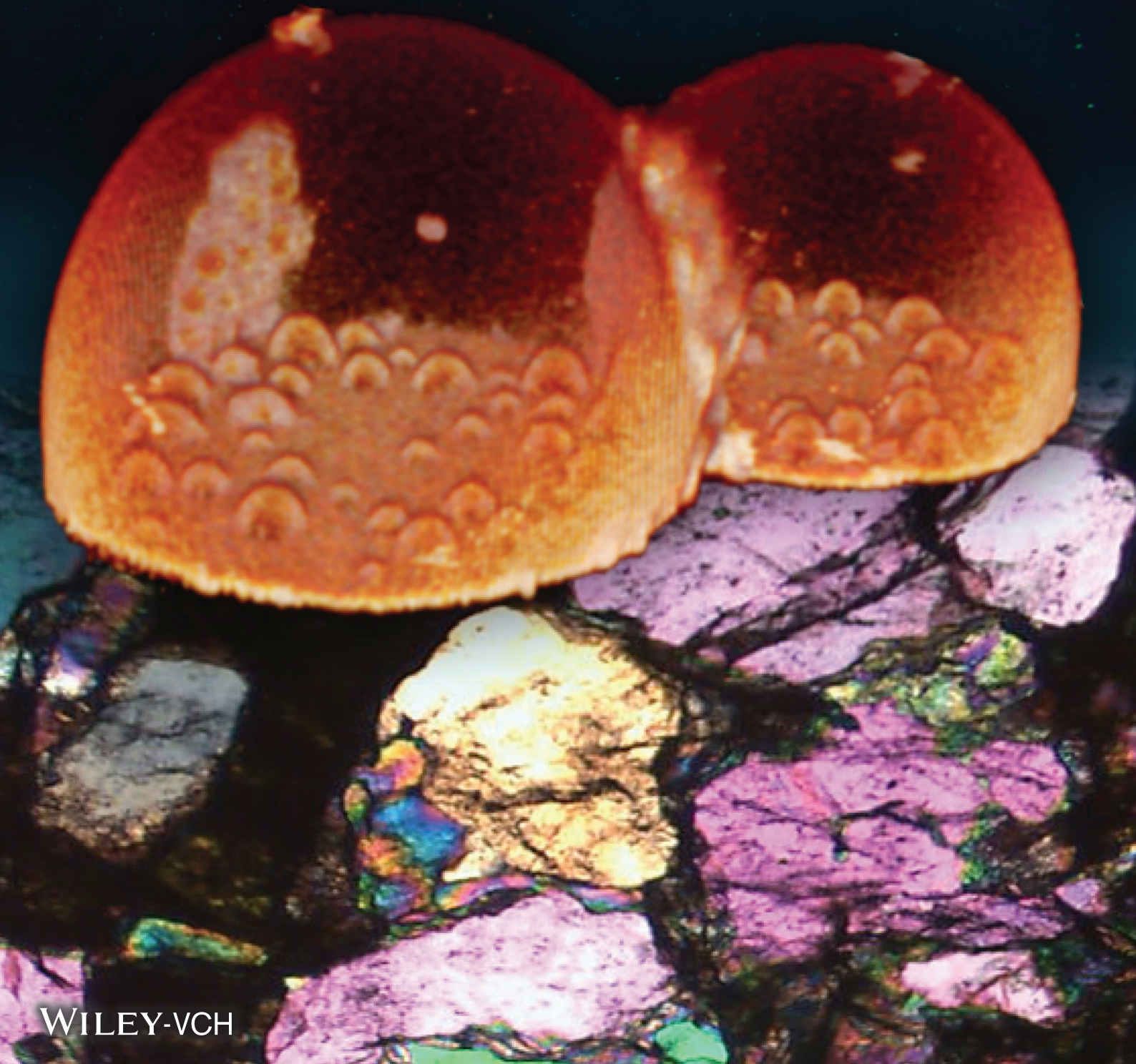
Appendix

Paper II

Vol. 17 • No. 2 • January 14 • 2021

www.small-journal.com

NANO • MICRO small



WILEY-VCH

Subcompartmentalization and Pseudo-Division of Model Protocells

Karolina Spustova, Elif Senem Köksal, Alar Ainla, and Irep Gözen*

Membrane enclosed intracellular compartments have been exclusively associated with the eukaryotes, represented by the highly compartmentalized last eukaryotic common ancestor. Recent evidence showing the presence of membranous compartments with specific functions in archaea and bacteria makes it conceivable that the last universal common ancestor and its hypothetical precursor, the protocell, may have exhibited compartmentalization. To the authors' knowledge, there are no experimental studies yet that have tested this hypothesis. They report on an autonomous subcompartmentalization mechanism for protocells which results in the transformation of initial subcompartments to daughter protocells. The process is solely determined by the fundamental materials properties and interfacial events, and does not require biological machinery or chemical energy supply. In the light of the authors' findings, it is proposed that similar events may have taken place under early Earth conditions, leading to the development of compartmentalized cells and potentially, primitive division.

exist in other domains of life, such as in archaea and bacteria.^[1,2] Archaea, for example, have acidocalcisomes, the membrane enclosed electron-dense granular organelles rich in calcium and phosphate, which is crucial for osmoregulation and Ca^{2+} homeostasis.^[3] In cyanobacteria, membrane-bound thylakoids^[4] have been identified as compartments in which the light-dependent reactions of photosynthesis take place.

Despite the differences between eukaryotic and prokaryotic compartments in terms of structural and functional complexity, the presence of membranous compartments in prokaryota^[1] establishes a possibility of compartments having existed in protocells, and being evolutionarily conserved. There is essentially no experimental material, however, on how compartments could have consistently

emerged from membranes in a prebiotic environment lacking membrane-shaping and -stabilizing proteins.

Membrane-less laboratory models of cytoplasmic suborganization have been developed inside synthetic cells, that is, giant unilamellar vesicles.^[5] These models require moderately elaborate chemical systems. A few examples of the utilized materials and mechanisms to induce compartment formation involve thermo-responsive hydrogels,^[6] pH driven protein (human serum albumin) localization^[7] or a poly(ethylene glycol)-dextran aqueous two-phase system.^[8] One study which report on the membrane-based multi-vesiculation inside amphiphilic compartments, has employed protein–ligand couples to induce this behavior, that is, biotin–avidin conjugates.^[9] Membrane-enveloped subcompartment formation in biological systems is therefore considered to be ultimately dependent on the genetic make-up of the cells.^[10]

In this study, we have investigated a protocell subcompartmentalization model on solid surfaces. The reported mechanism relies on the self-assembly and shape transformation abilities of biosurfactant bilayer membranes, and is largely governed by changes in the membrane-surface adhesion. Model protocells in form of giant unilamellar compartments are initially adhered to a solid substrate via Ca^{2+} anchors, but the adhesion is subsequently reversed upon depletion of Ca^{2+} . Small membrane regions released from the surface transform into small unilamellar subcompartments inside the model protocell. They remain partially adhered to the surface and continue growing, consuming the membrane material of the primary container. The subcompartments can take up solutes

1. Introduction


The origin of the eukaryotic cell is closely associated with the development of subcompartments, which create specific microenvironments to spatially or temporally regulate biochemical reactions, simultaneously. Until recently, cellular compartmentalization was associated solely with eukaryotic systems. Recent evidence shows that membrane-enclosed compartments also

K. Spustova, E. S. Köksal, Dr. I. Gözen
Centre for Molecular Medicine Norway
Faculty of Medicine
University of Oslo
Oslo 0318, Norway
E-mail: irep@uio.no

Dr. A. Ainla
International Iberian Nanotechnology Laboratory
Braga 4715-330, Portugal

Dr. I. Gözen
Department of Chemistry
Faculty of Mathematics and Natural Sciences
University of Oslo
Oslo 0315, Norway

Dr. I. Gözen
Department of Chemistry and Chemical Engineering
Chalmers University of Technology
Göteborg SE-412 96, Sweden

 The ORCID identification number(s) for the author(s) of this article can be found under <https://doi.org/10.1002/smll.202005320>.

DOI: 10.1002/smll.202005320

from the external environment and exchange them with the primary volume. Our experiments and finite element simulations point to a parallel uptake mechanism of solutes via transient pores in the protocell membrane. The enveloping membrane can eventually rupture to release the subcompartments as independent daughter vesicles.

Previous studies indicate that surfaces might have played a role in catalysis and synthesis of compounds relevant to prebiotic chemistry, for example, enhanced polymerization of aminoacids on mineral surfaces,^[11] or the synthesis of prebiotic peptides^[12] and RNA.^[13] Our work shows that the surface-assisted subcompartmentalization of protocells is a feasible recurring process and, due to the minimal requirements, could have potentially occurred under early Earth conditions. The newly established pathway to daughter vesicles, although relatively unsophisticated, indicates that the role of materials properties-driven transformation processes of surfactant membranes in

the development of primitive protocells, as well as the enabling function of surfaces, might have been underestimated.

2. Results

2.1. Spontaneous Compartmentalization

Figure 1a is a 3D reconstruction of the subcompartments that have spontaneously formed inside a substrate-adherent model protocell. The dome-shaped lipid container of approximately 50 μm in diameter is adhered on an Al_2O_3 surface where its distal membrane envelopes tens of subcompartments of an average size of 5 μm formed on the surface. Figure 1b shows an xy cross-sectional view recorded 4 μm above the surface. Figure 1c–f contains confocal micrographs of the compartmentalization process each step of which is explained in schematics in Figure 1g–j.

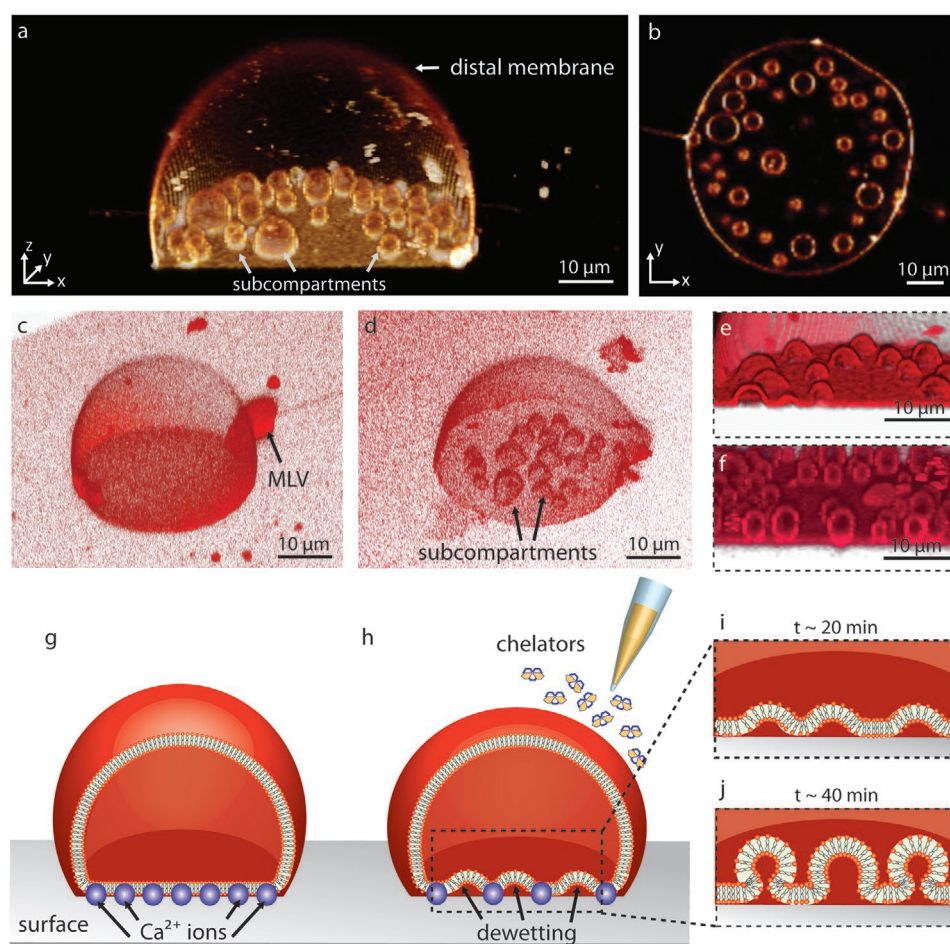


Figure 1. Subcompartmentalization in surface-adherent model protocells. a) Confocal micrograph, reconstructed in 3D, showing a model protocell enveloping several subcompartments. b) model protocell in (a) in xy cross-sectional view. Confocal micrograph of c) a model protocell adhered on a solid surface in presence of Ca^{2+} , d) a model protocell with subcompartments after chelator exposure, e) emerging subcompartments ≈ 20 min after chelator exposure, f) mature subcompartments ≈ 40 min after chelator exposure. Schematic representation of the subcompartmentalization process: g) A single model protocell consisting of a single lipid membrane, adheres onto the surface in presence of Ca^{2+} . h) Chelators are brought into the vicinity of the compartment, leading to removal of Ca^{2+} followed by subcompartmentalization. The initially surface-adhered bilayer of the model protocell transforms into i) semi-spherical, and later to j) spherical subcompartments. Micrographs in (c)–(f) are from different experiments. Membrane composition of model protocells shown in (a)–(f) is PC-DOPE. The surfaces used in (a) and (b) and (e) and (f) is Al_2O_3 , and in (c) and (d) is Al. All other experimental conditions for (a–f) were identical. Background fluorescence in (c) and (d) is due to reflection from the Al surface.

The model protocells were generated by the dehydration–rehydration method;^[14] and transferred onto the solid substrates in presence of Ca^{2+} as adhesion promoter^[15,16] (Figure 1c,g). Subsequently, by means of an automatic pipette, the ambient buffer was exchanged with a Ca^{2+} chelator-containing buffer, leading to the gradual removal of Ca^{2+} from the membrane–surface interface (Figure 1d,h). The basal membrane, that is, the adhered portion of the giant lipid container to the surface, de-wets the surface, bulges at various locations (Figure 1e,i) and transform within ≈ 40 min into spherical subcompartments (Figure 1f,j). The model protocells in Figure 1c,d are isolated. The elevated background intensity should not be mistaken for a lipid film. The substrate is composed of Al which reflects light during the imaging. A lipid reservoir, that is, multilamellar vesicle (MLV), is attached to the model protocell in Figure 1c.

2.2. Temperature-Enhanced Subcompartmentalization

Temperature has a strong influence on membrane viscosity and membrane–surface adhesion.^[17] When the temperature was

locally increased from 20 °C (room temperature) to 40 °C, the basal membrane started to de-wet the surface, forming subcompartments twice as rapidly. **Figure 2a–f** shows an experiment, during which the subcompartments inside a surface-adhered model protocell form at increased temperature (Movie S1, Supporting Information). The subcompartments fuse upon contact and grow in size (Movie S1, Supporting Information). For example, the three compartments which are initially distinct (yellow symbols in panel d), merge at $t = 33$ min to form a single subcompartment (yellow symbols in panel f). A similar experiment is depicted in Figure 2g–l (Movie S1, Supporting Information). Both experiments shown in Figure 2 have been performed on Al_2O_3 . The green plot in Figure 2m shows the circumference of the basal membrane depicted in Figure 2a–f, over time. The periphery of the surface-adhered portion of the lipid membrane is not retracting, as the circumference remains constant (Figure 2m, green line). The blue plot in Figure 2m represents the total membrane area utilized by the formation of subcompartments over time. The geometry of the emerging subcompartments has been assumed to be half-spheres in

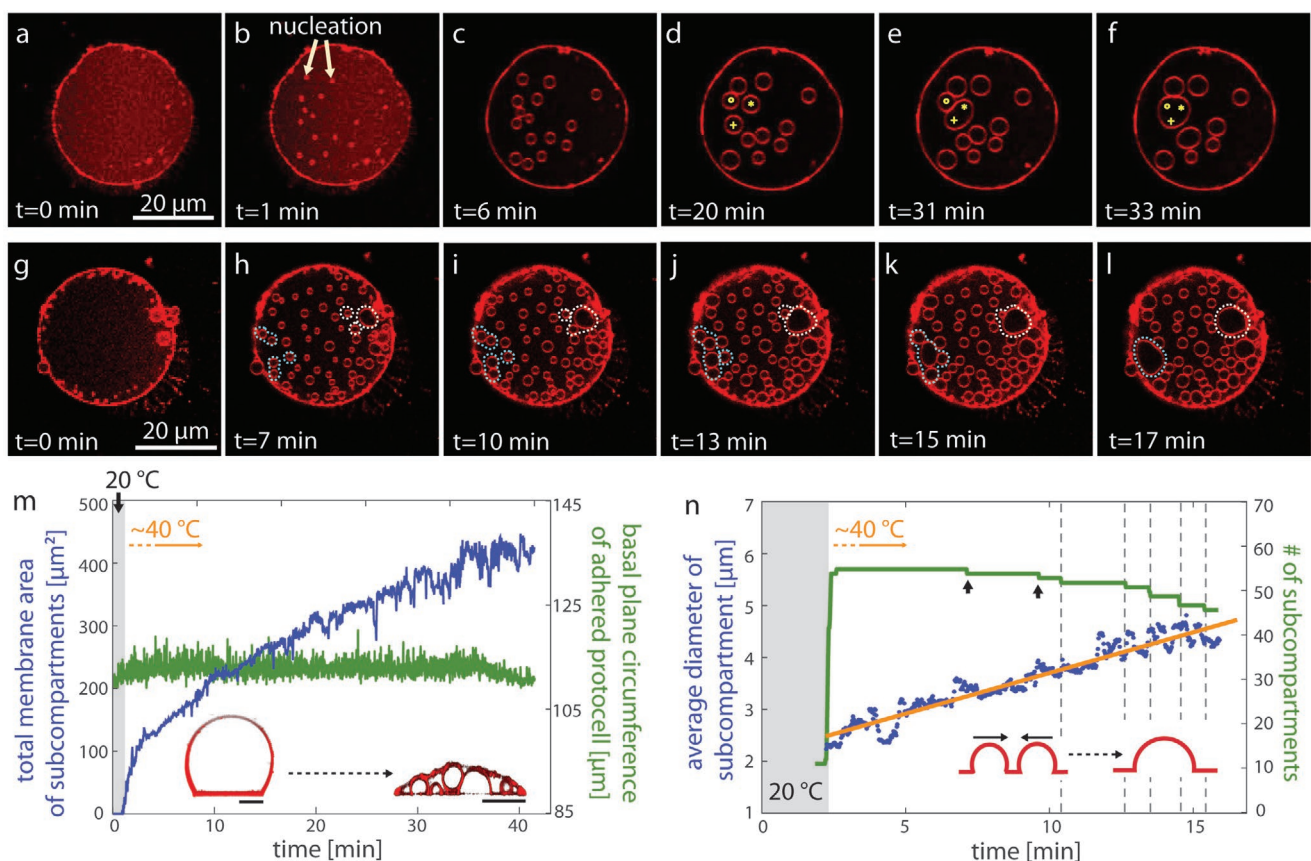


Figure 2. Enhanced subcompartmentalization at increased temperature. a–l) Confocal fluorescence micrographs showing two different experiments ((a)–(f), (g)–(l)) of temperature-enhanced subcompartmentalization (xy cross-sectional view). m) Plots showing the increase in subcompartment membrane area (blue), and the circumference of the protocell (green), versus time, for the experiment shown in (a)–(f). The inset shows the xz cross-sectional view of two protocells from different experiments before and after temperature increase. Scale bars (inset): 10 μm . n) The average diameter and number of subcompartments during the experiment shown in (g)–(l). The number of subcompartments (green plot) increases instantly with temperature increase, and decreases during fusion or, rarely, due to the sudden collapse of the subcompartments (black arrows). The inset in (n) is the schematic drawing of fusion of the subcompartments. The time point of each fusion event is marked with a dashed vertical line. The average diameter (orange line fitted to data points in blue, $d = 0.0032 \times t + 2.5$) gradually increases during subcompartment growth. The membrane of the model protocells shown in this figure is composed of PC-DOPE, and the surface is Al_2O_3 .

order to estimate the minimally required membrane area. The insets in Figure 2m shows cross sections of model protocells from two different experiments in the xz plane (side view), one at the beginning of an experiment (left) and the other after the subcompartmentalization has occurred (right). The distal membrane of the giant lipid container has decreased in area, indicating that this fraction of the membrane is partially consumed during formation. The plots in Figure 2n show the number (green) and the average diameter (blue points, orange line) of the new compartments in Figure 2g–l. With the emergence and growth of many small subcompartments, the diameter gradually increases over time. Some eventually fuse (inset), intermittently causing sudden drops in the total number (dashed vertical lines in Figure 2n). Subcompartments occasionally collapse (black arrows in Figure 2n and Movie S1, Supporting Information), presumably due to the consumption of their membrane by the competing growth of other containers in their vicinity.

2.3. Encapsulation and Isolation of Contents

The purpose of subcompartments in a biological cell is the segregation of chemical compounds and processes within individual boundaries inside the main volume of the cell (primary volume). In order to investigate the ability of the subcompartments to encapsulate molecules from the ambient environment and to maintain them, we delivered a water-soluble fluorescent compound to the exterior of each protocell (*cf.* Section S2 and S3, Supporting Information, for the details of the setup) and monitored the transmembrane transfer. Figure 3a shows a 3D micrograph (x - y - z) of a protocell on Al_2O_3 with several subcompartments, one of which maintains the encapsulated fluorescein solution. In order to achieve encapsulation in a selected model protocell, the fluorescein buffer (25 μM) was delivered with an open-space microfluidic device^[18] (Figure 3b). The presence of the compound can be switched on and off on demand, and the fluorescence signal during the cycles of exposure and removal can be monitored in real time inside the protocell and the subcompartments. We observe that during fluorescein exposure, the subcompartments rapidly encapsulate the compound, and immediately release it upon removal from the surrounding. This indicates that the compartments are not fully closed and have access to the surrounding solution through the space between the surface and the model protocell (Figure 3c). After a certain time point, some subcompartments hold the content and can maintain it during a long period of time, indicating that the size of the opening of the subcompartment is reduced, or completely sealed (Figure 3d). Upon temperature increase, the compartments appear to maintain the content longer.

Figure 3e–g depicts the time series of an encapsulation experiment at room temperature (*cf.* Movie S2, Supporting Information), with the corresponding fluorescein intensity plots of selected regions during multiple exposure cycles (Figure 3h). The fluorescence intensity of three different regions was monitored: the solution outside the protocell (region circled in white dashed lines in Figure 3f), the primary volume of the protocell (Figure 3f, yellow dashed circle) and the intensity of all of the subcompartments, which later was averaged. The plots

show an instant encapsulation of fluorescein within the subcompartments with the initiation of the exposure, and immediate release of the contents once the exposure is terminated (Figure 3h). The model protocell, on the other hand, encapsulates the fluorescence molecule gradually and maintains it.

At elevated temperatures (Figure 3i–p and Movie S2, Supporting Information), the leakage of fluorescein from the subcompartments decreases (Figure 3l), compared to the leakage in the experiment depicted in Figure 3e–g, which indicates a reduction of the size of their opening (Figures 3k,l and 3o,p). The concentration of the fluorescein inside the contracted subcompartment can eventually be slightly higher than in the internal medium of the primary volume (Figure 3l,p).

2.4. Pore-Mediated Uptake

We then examined the role of transient pores in the uptake of material from the ambient solution. As showed in Figure 3, the fluorescein molecules are encapsulated by the primary volume. To analyze the mechanism of the uptake, we exposed individual surface-adhered protocells without internal compartments to a fluorescein buffer, using an open volume microfluidic device (Figure 4 and Section S2–S3, Supporting Information). Figure 4a shows the fluorescence intensity inside 5 different protocells of similar size versus time upon exposure to fluorescein. Uptake rates varying from less than 20% of the stock solution (Figure 4a, plot in pink color) to almost 90% (plot in blue color) were observed. These uptake rates imply that it is not via simple diffusion through the membrane. We attribute this behavior to the presence of transient membrane pores, which has been previously observed and characterized in similar systems.^[19] We then compared the experimental values depicted in Figure 4a to the results of finite element model (FEM) simulations shown in Figure 4b–d. The FEM here assumes a single container of size 5 μm with membrane thickness of 1 nm. The model vesicle is exposed to the fluorescein present in the external solution. Figure 4c shows the magnified view of the pore marked with a white frame in Figure 4b.

In the model, the passage of molecules is assumed to occur through a single membrane pore (Figure 4c), $\varnothing = 5$ nm, while the diffusion through the membrane otherwise is prevented. The uptake rates of fluorescein are calculated as the fluorescein diffuses from the external solution into the model protocell through the membrane pore. The diffusion coefficient of fluorescein in water at room temperature, $D = 4.25 \times 10^{-10} \text{ m}^2 \text{ s}^{-1}$,^[20] is taken into consideration. Each plot in Figure 4d represents a different time point upon exposure changing from 0.1. to 600 s. The concentration of the fluorescein in the external medium is considered to be 100%. The plots in Figure 4d show final concentrations inside the cell at different time-points, with a steep concentration gradient inside the pore zone (green region). The pore zone is almost symmetrical in both external and internal side of the membrane interface, and reaches a distance of approximately twice the pore radius. The size of the pore zone varies with the changing pore radius (inset to Figure 4d). Further away from the pore, the concentration of the solutes can be considered homogeneous on either side (Figure 4d, red and blue area). The model protocell

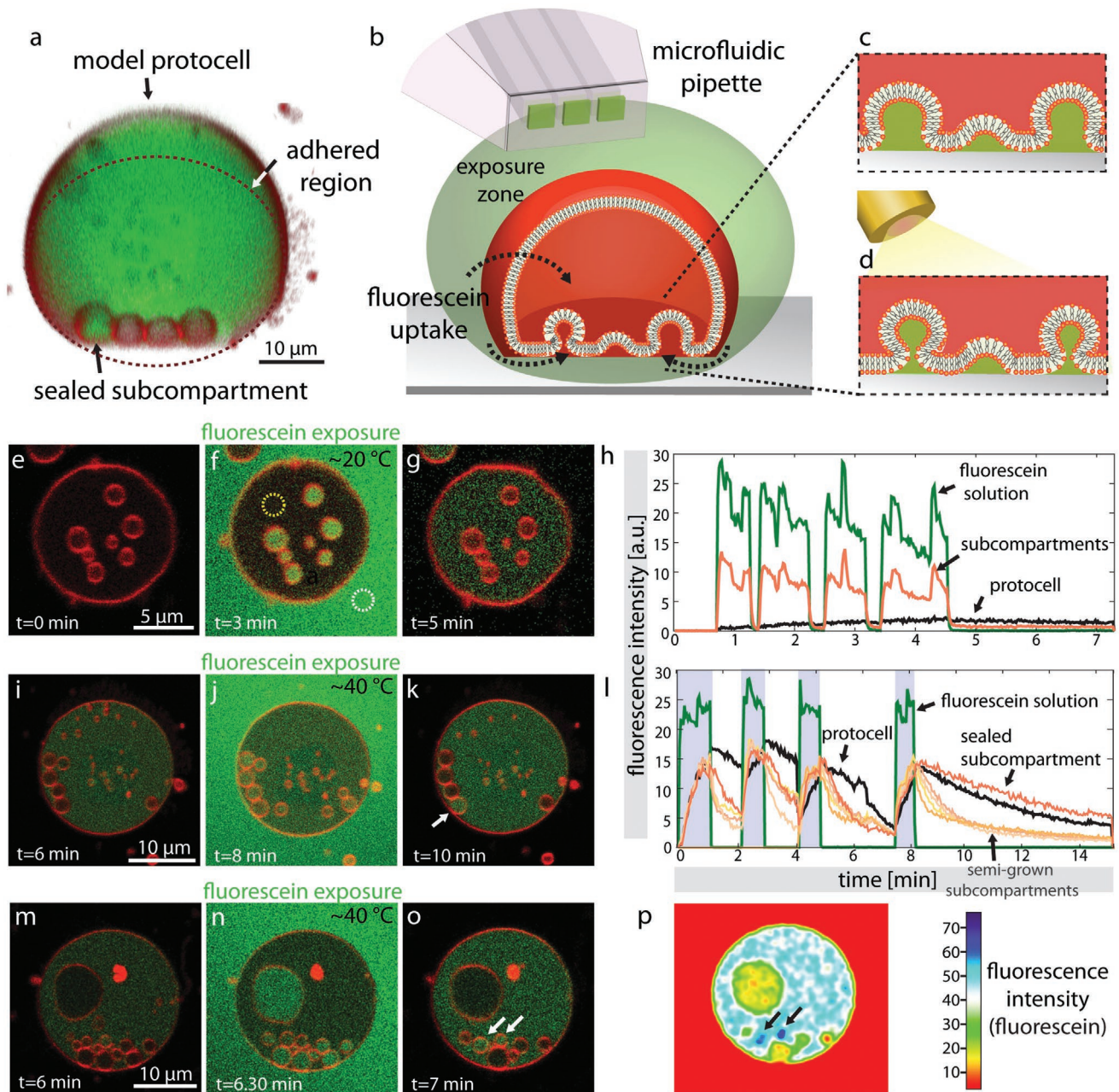
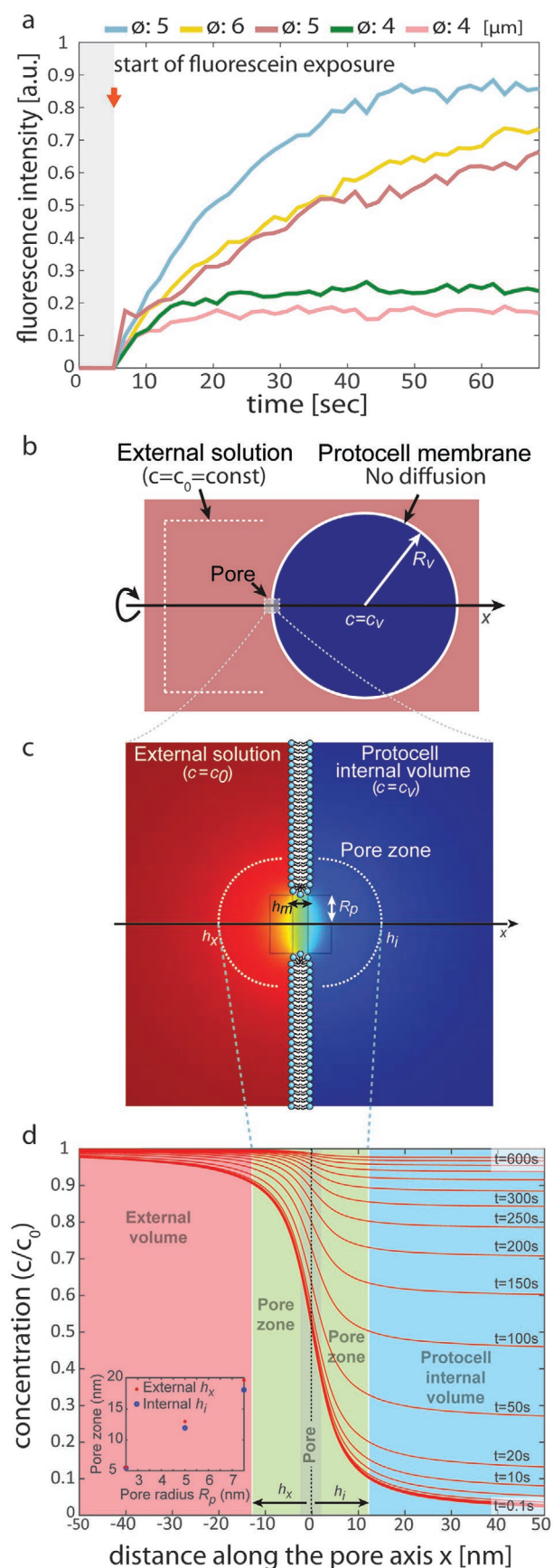


Figure 3. Encapsulation and compartmentalization of fluorescein in model protocells. a) Confocal micrograph of a model protocell, reconstructed in 3D, after pulsing with fluorescein. One of the four subcompartments maintains fluorescein content. Schematic representation of the fluorescein exposure experiment: b) The microfluidic superfusion pipette creates a fluorescein exposure zone around the model protocell. c) Semi-grown subcompartments encapsulate fluorescein during the exposure through the space at the membrane-surface interface. d) Temperature increase, together with fluorescein exposure, results in sealed subcompartments encapsulating the fluorescein. e–g, i–k, m–o) Confocal micrographs (*xy* cross section) showing the fluorescence intensity inside the subcompartments and the primary volume during fluorescein pulsing (cf. Movie S2, Supporting Information). h, l) Plots showing the fluorescence intensity of different regions versus time during the experiments shown in (e)–(g) and (i)–(k), respectively. The temperature increase during (i)–(k) is synchronized with fluorescein pulsing (gray zones in l)). The plots in green color represent the average intensity of the stock fluorescein buffer (circle indicated by white dashed line in (f)). The plot in orange color in (h) is the arithmetic mean intensity of the subcompartments versus time. The plot in black color in (h) is the intensity of the primary volume of the protocell (circle indicated by yellow dashed line in (f)). In (l) the average intensity of each compartment have been depicted individually (orange-spectrum graphs). The color plot in (p) shows the intensity of fluorescein in (o). Black arrows show the position of the two sealed subcompartments corresponding to the entities indicated with white arrows in (o). The sealed compartments display higher fluorescence intensity compared to the other subcompartments and to the primary protocell volume. The membranes in this figure are composed of PE-PG-CA, and the surface is Al_2O_3 .



can have multiple pores further apart with no overlapping pore zones where the transport from each pore contributes linearly. The calculations for different container and pore sizes can be found in Section S4, Supporting Information.

2.5. Pseudo-Division

In some occasions we observe extensive contraction and rupturing of the distal membrane (Movie S3, Supporting Information) which results in disintegration of the original protocell, leaving behind only the intact subcompartments, that is, daughter cells (Figure 5). Figure 5a shows an xz cross section of two subcompartments with the distal membrane in direct contact. Figure 5b,c shows the xz cross section and the perspective view of daughter cells remaining after the original enveloping membrane is disintegrated. The light circular region in Figure 5c consists of a single bilayer, which is also visible in Figure 5b. A double lipid membrane surrounds this region (dark red region in Figure 5c), indicating lipid spreading around an originally isolated intact cell. Figure 5d–f shows the schematic representation of the process in Figure 5a–c. We observe daughter protocells as long as 12 hours after the addition of chelators (Figure S5, Supporting Information). Note that the earlier observations of exchange of material between the primary volume and the ambient buffer on one hand, and the possibility of exchange between the primary volume and the subcompartments on the other hand (Figure 5d), will be discussed in the context of primitive protocell division in the following section.

3. Discussion

3.1. Compartmentalization Mechanism

Figure 1 shows that the spontaneous compartmentalization occurs when the strength of the adhesion of the protocell to the solid substrate decreases. Adhesion is mediated by the Ca^{2+} ions at the interface of the protocell membrane with the solid surface (depicted by purple spheres in Figure 1g,h). Ca^{2+} ions are known to have a fusogenic effect by binding to the lipid head groups,^[21] mediating membrane-surface,^[15,16,22] or membrane-membrane pinning.^[23] The adhesion of membranes to a solid substrate does not necessarily require Ca^{2+} in the solution,^[24–26] although its presence on the surface promotes adhesion. There

Figure 4. Uptake through transient pores. a) Fluorescein intensity inside the surface-adhered, non-compartmentalized model protocells, over time. b–d) Finite element model (FEM) of fluorescein uptake by a model protocell from the external solution through a nano-sized membrane pore. b) A single circular pore (toroidal gap) with a radius of $R_p = 5$ nm is located in the membrane of a giant compartment with radius of $R_v = 5$ μm . c) Concentration across the membrane in the vicinity of the pore depicted in (b). The liquid volume near and inside the pore is determined to be the “pore zone” (yellow-green area). d) Concentration profile of fluorescein at the pore zone and inside the protocell at selected time points changing from 100 ms to 600 s. The inset in (d) shows the relation between the concentration gradient (extent of the pore zone) and the pore radii of 2.5, 3, 5, and 7.5 nm. The membrane of the vesicles used in (a) are composed of PC-DOPE; the surface is Al_2O_3 .

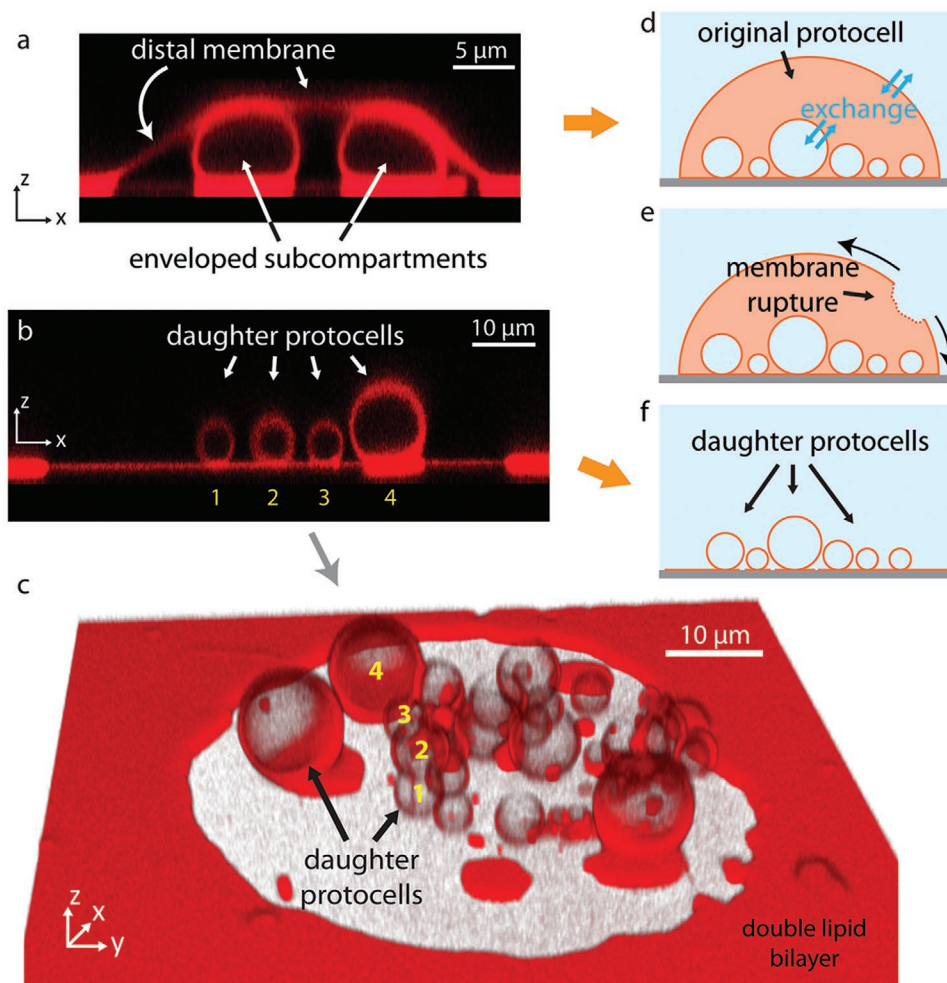


Figure 5. Pseudo-division. a) Confocal micrograph of a subcompartment (xz cross section) with the distal membrane in direct contact. b,c) Confocal micrographs of daughter cells remaining after the original enveloping membrane is disintegrated. b) xz cross section and c) the perspective view (xyz). c) Light circular region consists of a single bilayer, which is also visible in (b). d–f) Schematic representation of the process in (a)–(c). d) Material between the primary volume and the ambient buffer, and between the primary volume and the subcompartments can be exchanged. The membranes of the vesicles shown in this figure are composed of PC-DOPE; the surface is Al (with a native oxide layer).

are several Ca^{2+} -rich early Earth minerals, which might have acted as a source.^[27–29] The vesicles adhere to the substrate in a dome-like shape.^[30] Addition of chelators leads to gradual depletion of Ca^{2+} from the aqueous medium including the space between the surface and the membrane, leading to the removal of pinning points. This causes partial de-wetting at the membrane-surface interface.^[31] BAPTA which is one of the two chelators we utilized, has been shown to act as a shuttle buffer, driving Ca^{2+} out of the membrane and decreasing the Ca^{2+} concentration specifically at the membrane interface.^[32] Intercalation of EDTA, another chelator we use at mM concentrations, into the lipid head groups has been proposed to cause membrane bending and formation of invaginations.^[33] We do not think that direct interactions of BAPTA or EDTA with the membrane is the main cause of the compartmentalization, as in that case the compartments would not only form at the surface but also along the liquid interface to the protocell membrane. Formation of the compartments specifically on the solid substrate is a strong indication that the mechanism is surface

adhesion dependent. EDTA and BAPTA are strong metal chelators which were certainly not present on the early Earth. However, clay minerals were abundant in the prebiotic environment which could have played the role of the chelators in our experiments. Clay minerals are known to efficiently adsorb mono- or divalent ions including Ca^{2+} .^[34] These phyllosilicates, resemble in surface quality (flatness, homogeneity, surface potential) the synthetic surfaces used in our study.^[26] J. Szostak and co-workers showed enhanced vesicle formation upon adsorption of sheets of amphiphiles on various types of solid particle surfaces, among them clays.^[35,36]

The creases can also form spontaneously in membranes with low tension.^[22,37,38] Once the invaginations form, the transformation of these highly curved membrane regions into larger spherical compartments occurs through a self-driven process, during which the membrane curvature is reduced.^[39] A similar study, where the pinning/de-pinning occurs by means of streptavidin-biotin coupling, reports on this phenomenon.^[9] A high membrane curvature in the area of nucleation causes an

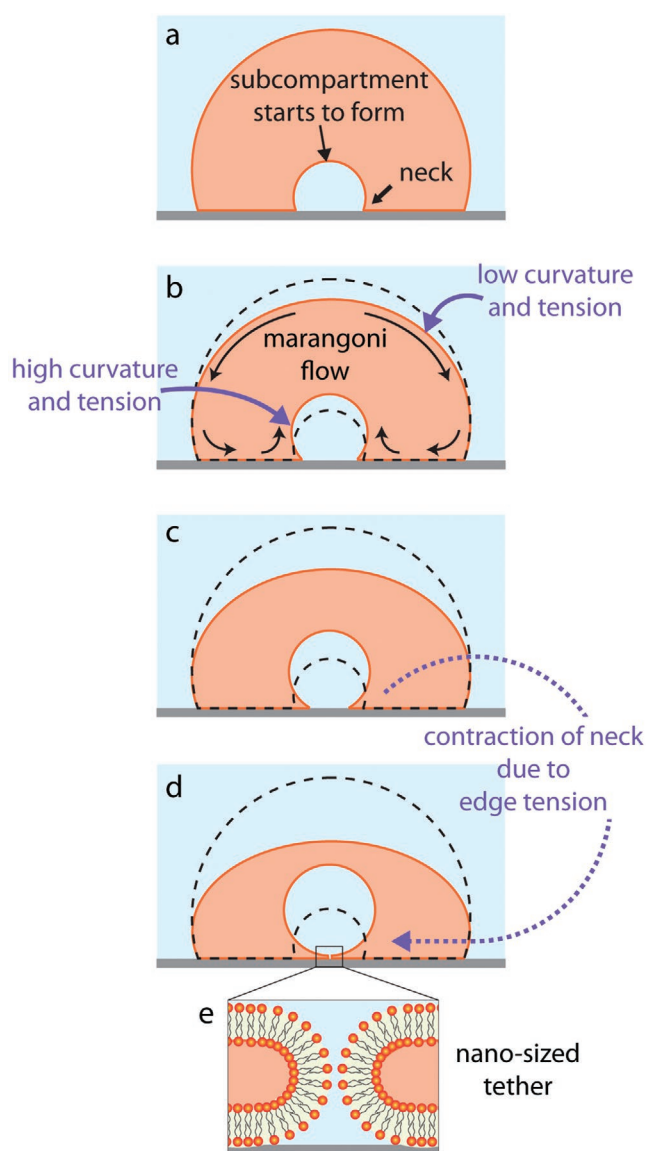


Figure 6. Subcompartmentalization mechanism. a–d) Growth of a subcompartment enveloped in a surface-adhered protocell. During growth the distal membrane is consumed. e) As pinning is removed from the contact line between the newly formed subcompartment and the surface, the contact line will contract due to edge tension transforming to a nano-sized pore or tether. The subcompartment stays connected to the basal membrane through a nano-sized pore or nanotube.

increase in the membrane tension, which leads to Marangoni flow of lipids from the region of relatively low membrane tension, that is, the distal membrane of the protocell, towards the region of higher tension. The distal membrane of the protocell is consumed as depicted in **Figure 6** (also in **Figure 1**, inset in **Figure 2m**). Additionally, an attached MLV (**Figure 1c**) can serve as a lipid source.

After a subcompartment has matured (**Figure 6b–d**), it stays connected to the basal membrane through a nano-sized pore-like connection (**Figure 6e**) as the force requirement for disconnecting the vesicle is very large: in the order of $\approx \text{mN}$ ^[16,40] versus $\approx \text{pN}$ ^[14] for pulling a membrane tether that can remain

connected through the neck. As pinning is removed from the contact line between the newly formed subcompartment and the surface, the contact line will contract due to edge tension transforming to a nano-sized pore or tether (**Figure 6e**). The area under the newly formed compartment re-wets even without the adhesion promoter Ca^{2+} lowering the surface free energy of the substrate.

We have not investigated the effect of pH and other factors, such as membrane composition or surface roughness, on compartmentalization. However, it is plausible that such factors would have a measurable impact on membrane deformations, for example due to acido-basic properties of lipids. It has been shown that pH gradients induce surface tension asymmetry, cause shape deformations and induce the formation of membrane invaginations reminiscent of mitochondrial cristae.^[41]

3.2. Temperature-Enhanced Formation

The role of temperature has been intensely discussed in the origins of life context, in particular whether high temperatures could have been beneficial or detrimental to protocell formation.^[42,43] The hydrothermal vent hypothesis which has been criticized for allowing excessively high temperatures, salinity and pH gradients is, after the discovery of “Lost City”-type hydrothermal fields (LCHFs), being reconsidered.^[43] LCHFs accommodate temperatures between 40 and 90 °C, which could have promoted the formation of prebiotic membrane compartments.^[44]

In our study, temperature increase weakens membrane-surface adhesion and causes immediate surface de-wetting,^[17] facilitating the subcompartment formation. Furthermore, it causes the membrane fluidity to increase, and enhances fusion.^[45,46] This results in accelerated growth of the subcompartments (**Movie S1**, Supporting Information). While the time scale in the case of subcompartmentalization induced by Ca^{2+} depletion ranges from several tens of minutes to an hour (**Figure 1**), it only takes a few minutes to form the compartments when the temperature is increased to 40 °C (**Figure 2a–l**). A nucleated compartment can rapidly mature and be internalized by the protocell (**Figure 2m**, inset) where some of them coalesce upon physical contact. A recent study has reported on the merging of lipid vesicles if they are in close proximity in a locally heated zone.^[47] Note that in order to elevate the temperature locally under avoidance of strong convection, we used an optical fiber and IR-B radiation (1470 nm, *cf.* Section S2 and S3, Supporting Information, for the details of the setup).

3.3. Encapsulation and Compartmentalization of External Compounds

Confining the reactants inside a membrane enclosed space and thereby bringing them into the close proximity can enhance reaction rates^[48] which is a benefit of compartmentalization in modern cells. We used anionic fluorescein as a model molecule to identify the mechanism of compartmentalization and encapsulation events. We have observed the internalization of fluorescein molecules inside the semi-grown subcompartments,

delivered locally by superfusion with a microfluidic pipette, by laser scanning confocal microscopy (Figure 3). A negatively charged dye was used to avoid electrostatic charge-based adsorption of the dye to the negatively-charged membrane.^[49] When the protocell is repeatedly pulsed with fluorescein, the fluorescence intensity inside the compartments instantly follows the external aqueous environment (Figure 3e–h and Movie S2, Supporting Information). The compartments take up fluorescein which immediately leaks out when the superfusion is terminated. This indicates that the subcompartments encapsulate the compound through the open interface to the surface, which exposes the compartments' interior to the external aqueous space. Encapsulation of the liquid at a membrane-surface interface by the invaginations has been previously reported. In that system, a protein–ligand coupling has been employed to promote the formation of the invaginations.^[9] If the subcompartment encapsulating the compound is suddenly sealed or its opening significantly reduced in size, the instant leakage of fluorescein is prevented and the fluorescence intensity decreases slowly (Figure 3l). While the leakage from the subcompartments is rapid in the initial superfusion cycles throughout the experiment, after $t \approx 8$ min the leakage from one particular subcompartment slows down (dark orange plot). Most importantly, the leakage from the subcompartments induced by heating is considerably slower, compared to the Ca^{2+} depletion-induced case (Figure 3l vs Figure 3h). Higher temperatures increase membrane fluidity, causing faster compartment growth. The compartments mature faster, likely resulting in contraction of the opening at the surface interface (Figures 3c,d and 6) to a nanosize pore or a nanotube (Figure 6e) and, accordingly, prolonged containment of internalized content (Figure 3i–l). This is in agreement with the finite element model. A single nanopore allows the equilibration of material in 600 s. (Figure 4, cf. FEM discussion below). This is confirmed by earlier studies on fluorescein diffusion through nanosized conduits.^[50]

3.4. Evidence for Pore-Mediated Encapsulation in the Primary Volume

The primary volume of the model protocell encapsulates fluorescein during multiple cycles of fluorescein exposure (Figure 3). We performed identical superfusion experiments on model protocells without subcompartments, that is, without the involvement of chelators. For different model protocells of comparable size under identical exposure conditions, the amount of encapsulated fluorescein at a given time varies from less than 20% to almost 90% of the concentration in the external medium (Figure 4a). This indicates that the means of transport through the membrane is not diffusion, which would result in each experiment in similar concentrations of the encapsulated compound at a given time. Our results are consistent with the presence of transient nano-sized pores in the membrane through which the fluorescein is diffusively internalized. It is well established that osmotic swelling of lipid vesicles causes an increase in membrane tension which leads to the formation of transient pores in the membrane.^[19,22] The adhesion of protocells to the substrate can cause a similar tension increase.^[16,22] The finite element method (FEM) simulations in Figure 4b–d

shows that transport through a single or a few nano-sized pores in the lipid membrane of a container of 5 μm size can lead to similar fluorescein concentrations inside the protocells shown in Figure 4a. According to the FEM simulations, during 100 s of uptake through a single pore, the concentration of the encapsulated fluorescein inside the protocell reaches 50% of the concentration of fluorescein in the external medium (Figure 4d). In one of the experiments (red plot in Figure 4a), the internal volume reaches 50% of the concentration of the stock fluorescein solution in 20–30 s. This corresponds to 3–5 membrane pores. It is reasonable that since 3–5 pores of nm size belong to a protocell of micron size, the pores would not overlap, and the pores would not jeopardize the integrity of the vesicle.

3.5. Implications for the Origins of Life

Origin of life studies often focus on a compartment as a whole—the (model) protocell. The possibility of consistent formation of organelle-like structures inside a protocell has not been considered plausible due to the lack of proteins and membrane-shaping machinery, which would transform the original membrane material to modular subcompartments and further stabilize them.^[10] Solid surfaces, which were abundant on the early Earth in the form of minerals, could to some extent have mimicked the role of sophisticated machinery. Surfaces intrinsically possess energy, which can promote membrane-surface interactions in several different ways.^[26] Previous studies have reported on the enhancing effects of surface associated bio- and organic chemistry relevant to the *RNA world*,^[13] including the synthesis of prebiotic peptides,^[12] nitrogen reduction, lipid self-organization, condensation-polymerization reactions, selection and concentration of amino acids and sugars as well as chiral selection.^[51] The reported surface-dependent phenomenon might pose an advantage over multi-vesiculation observed at the compartment membranes in bulk solution.^[52] Mineral surfaces have recently been shown to also induce protocell formation.^[35,36,39] Our findings reveal the capabilities of high energy surfaces, which are able to induce subcompartmentalization of adherent model protocells. We selected components which have direct representations in the prebiotic environment on the early Earth.

3.6. Flat Solid Oxide Substrates as Mineral Models

The solid model substrates Al_2O_3 and Al (with a native oxide layer) as well as SiO_2 , represent constituents of rock forming minerals on the early Earth.^[53] Al_2O_3 occurs naturally as Corundum, a mineral which has been studied and shown to amplify lipid bilayer formation.^[53] Sputtered SiO_2 corresponds to Quartz, which was associated with amino acid adsorption and peptide synthesis.^[13,54]

3.7. Protocell Models

We used giant unilamellar vesicles as protocell models. They consist of phospholipid molecules which are part of the origins

of life discussion. Several types of phospholipids have been synthesized in the laboratory under prebiotic conditions.^[55–58] Their precursor molecules were found in fluid inclusions in minerals relevant to the early Earth.^[54] A detailed list of the lipid membrane compositions and the surfaces leading to phenomena we describe in this study is provided in Section S1, Supporting Information.

The findings revealing more complex abilities of model protocells may also be important for the development of artificial cells^[59] and tissue-like materials,^[60,61] potentially in the context of drug delivery formulations and technology to produce such. Multi-compartmentalized liposome or polymerosome formulations have indeed been in the focus of biomedical investigations for improved drug and gene delivery as well as biosensing.^[62–64]

3.8. Pseudo-Division

Figure 3I reveals similar intensity levels of encapsulated fluorescence in the primary volume of the model protocell, and in one of its subcompartments. It is conceivable that the encapsulated contents are transported between the subcompartment and the primary volume through transient nano-sized membrane pores. We assume that the pores are present in the protocell membrane, which we have experimentally verified. Since the membrane surrounding the primary volume and the subcompartments are connected, and pores/defects are mobile in a fluid membrane, it is reasonable to assume that the pores can also be present in the subcompartment membrane. This would allow the transport of material across the membrane from the primary volume to the sub compartment. In some occasions the distal membrane of the model protocell ruptures, leaving multiple subcompartments, that is, the daughter cells, exposed directly to the bulk solution (Figure 5). A larger number of daughter cells can form, compared to the number of subcompartments, during the rapid collapse of the protocell (Figure S6 and Movie S3, Supporting Information). This can be anticipated, since the enveloping membrane opens up and rapidly relocates, providing excess membrane material. The relocation of the rupturing membrane evidently causes the collapse of some of the subcompartments or relocates them. This can be perceived as pseudo-division as this is not a direct splitting of the initial compartment, but a two step process starting with the transfer of internalized material to the daughter cells, followed by the disappearance of the mother protocell. We suggest that the surface mediated subcompartmentalization can therefore be viewed as starting point (pre-division) for protocell replication and division.

4. Conclusion

The question of how early in evolution cells could have had membranous subcompartments came recently into focus after their existence in archaea and bacteria has been shown. In this study we report that membrane-enveloped subcompartments consistently form in model protocells adhered on mineral-like solid substrates. The formation requires a minimum set of essential components: an amphiphile compartment, a solid

surface and an aqueous environment. External compounds can be encapsulated and transported between the primary volume of the protocell and the subcompartments. We show that when a protocell disintegrates, the subcompartments remain intact, and adhered to the substrate, suggesting the possibility of a primitive form of division. Following the earlier findings on enhancing effects of surfaces in prebiotic chemistry, this advocates that protocells with membranous subunits simultaneously running multiple reactions could have existed at the origin of life. If the process can be repeated in cycles over several protocell-subcompartment generations remains an interesting question to be elucidated.

5. Experimental Section

Preparation of Lipid Vesicles: To prepare the lipid suspensions, the dehydration and rehydration method^[14,65] was used. Various types of lipids were utilized, namely $L\text{-}\alpha$ -phosphatidylcholine (Soy), 18: dioleoylphosphoethanolamine, $L\text{-}\alpha$ -phosphoethanolamine (*Escherichia coli*), $L\text{-}\alpha$ -phosphatidylglycerol (*E.coli*), Cardiolipin (*E.coli*) and *E.coli* polar lipid extract. Briefly, lipids (99 wt %) and lipid-conjugated fluorophores (1 wt %) (for a detailed list of lipid compositions cf. Table S1, Supporting Information) were dissolved in chloroform leading to a final concentration of 10 mg mL⁻¹. 300 μ l of this mixture was then transferred to a 10 ml round bottom flask and the solvent was removed in a rotary evaporator at reduced pressure (20 kPa) for 6 hours to form a dry lipid film. The film was rehydrated with 3 ml of PBS buffer (5 mM Trizma Base, 30 mM K₃PO₄, 3 mM MgSO₄·7H₂O, 0.5 mM Na₂EDTA, pH 7.4 adjusted with 1 M H₃PO₄) and stored at +4 °C overnight to allow the lipid cake to swell. The sample was then sonicated for 25 s at room temperature, leading to the formation of giant compartments with varying lamellarity. For sample preparation, 4 μ l of the resulting lipid suspension was desiccated for 20 min and the dry residue rehydrated with 0.5 ml of 10 mM HEPES buffer containing 100 mM NaCl (pH 7.8, adjusted with 5 M NaOH) for 5 min. The lipid suspension was subsequently transferred onto a solid surface submerged in 10 mM HEPES buffer with the formulation mentioned above, but with the addition of 4 mM CaCl₂.

Surface Preparation: SiO₂, Al and Al₂O₃ surfaces were fabricated in the Norwegian Micro- and Nano-Fabrication Facility at the University of Oslo (MiNaLab). All thin films were deposited on glass cover slips (Menzel Gläss #1, 100–150 μ m thickness; WillCo Wells B.V., Amsterdam, NL). No pre-cleaning was performed on glass substrates before deposition. SiO₂ and Al were deposited onto the glass substrates by E-beam and thermal PVD evaporation using an EvoVac instrument (Ångstrom Engineering, Canada), to a final thicknesses of 10 nm of Al, and 84 nm of SiO₂. Al₂O₃ was deposited onto glass substrates by atomic layer deposition (Beneq, Finland), to a final thickness of 10 nm. Surfaces were used immediately after their fabrication.

Addition of Chelators and Fluorescein Molecules: For initiation of the subcompartmentalization, ambient buffer in the sample was gently exchanged with 10 mM HEPES buffer containing 100 mM NaCl, 10 mM EDTA and 7 mM BAPTA (pH 7.8, adjusted with 5 mM NaOH), using an automatic pipette 20 min after the initial deposition of the vesicles onto the substrates. All consecutive steps of the experiments were performed at same pH.

The experiments involving fluorescein exposure were performed by using a microfluidic pipette (Fluicell AB, Sweden). The surface-adhered vesicles were superfused with HEPES buffer with 100 mM NaCl, containing 25 μ M of Fluorescein Sodium Salt (pH 7.8, adjusted with 5 mM NaOH). The HEPES buffer used in the experiments shown in Figure 4a contains Ca²⁺, but is chelator-free. The vesicles used for Figure 4a are composed of identical lipid species, and are of similar size (4–6 μ m in diameter).

Local Heating: An optical fiber coupled to an IR-B laser (cf. Section S3, Supporting Information) was assembled to locally

increase the temperature in the sample.^[47,66] A semiconductor diode laser (HHF-1470-6-95, $\lambda = 1470$ nm, Seminex), driven with an 8 A power source (4308 Laser Source, Arroyo Instruments) was used in combination with an 0.22 NA multimode optical fiber with 50 μm core diameter (Ocean Optics). The fiber was located around approx. 30–50 μm from the vesicle. The laser current utilized for experiments were in the range 0.7 A, resulting in a local temperature increase to 40 °C.^[47]

Microscopy Imaging: All microscopy images were acquired with a laser scanning confocal microscopy system (Leica SP8, Germany) using a HCX PL APO CS 40x oil, NA 1.3 objective. The excitation/emission wavelengths varied with the employed fluorophores: Rhodamine ex: 560 nm em^{-1} : 583 nm (Figure S1, Supporting Information); Texas Red DHPE ex: 595 nm em^{-1} : 615 nm (Figure 1, Figure 2, Figure 4, Figure 5); ATTO 655-DHPE ex: 655 nm em^{-1} : 680 nm (Figure 3); Fluorescein ex: 488 nm, em: 515 nm (Figure 3, Figure 4).

Image Analyses: 3D fluorescence micrographs were reconstructed in Leica Application Suite X Software (Leica Microsystems, Germany). Image enhancement of fluorescence micrographs for the figures were performed with the Adobe Photoshop CS4 (Adobe Systems, USA). The fluorescence intensity analyses shown in Figures 2m,n, 3h, 3l, 3p, and 4a, were performed by using NIH ImageJ Software. For the micrograph series represented in Figure 2m,n (Movie S1, Supporting Information), median filtering was applied with ImageJ. For each vesicle in Figure 4a, the average intensity was measured within the whole vesicle interior at each time point normalized to the intensity of the exposed ambient stock solution with constant concentration. All graphs were plotted in Matlab R2018a, which was also used to generate the linear fit in Figure 2n. Schematic drawings were created with Adobe Illustrator CS4 (Adobe Systems, USA).

Finite-Element Simulations: Finite element modeling (FEM) was performed with the COMSOL Multiphysics software, using transport of dilute species physics (chds). The authors' model assumes a membrane thickness of $h_m = 1$ nm, and fluorescein diffusion coefficient of $D = 4.25 \times 10^{-10} \text{ m}^2 \text{ s}^{-1}$.^[20] The geometry was built using cylindrical symmetry around axis x . The vesicle has a spherical shape with radius R_v , which was set to 2.5, 5, or 7.5 μm . It was assumed there was no material transport through the membrane (no flux boundary) except through one cylindrical pore (length h_p and radius R_p) positioned on the x -axis and connecting the vesicle with the external volume. The vesicle had initial internal concentration $c = 0$, while external volume had $c = c_0 = 1$. The outer boundary of the external volume was set to the constant concentration 1, mimicking a very large bath compared to the vesicle. For the simulation, the vesicle dimension was varied, while the pore dimension was set to $R_p = 5$ nm, or changed to a pore radius between 2.5 and 7.5 nm while the vesicle radius was kept $R_v = 5$ μm (cf. Section S4, Supporting Information). The simulation was transient from 0 to 600 s in 100 ms steps.

Supporting Information

Supporting Information is available from the Wiley Online Library or from the author.

Acknowledgements

This work was made possible through financial support obtained from the Research Council of Norway (Forskningsrådet), Project Grant 274433, UiO: Life Sciences Convergence Environment, the Swedish Research Council (Vetenskapsrådet), Project Grant 2015-04561, as well as the startup funding provided by the Centre for Molecular Medicine Norway (RCN 187615), and the Faculty of Mathematics and Natural Sciences at the University of Oslo. The authors thank Prof. A. Jesorka from the Biophysical Technology Laboratory at Chalmers University of Technology, Sweden, for support with the microheating setup, and for stimulating discussions.

Conflict of Interest

A.A. is a co-inventor of the multifunctional pipette, and minority share holder of Fluicell AB, the company that markets the multifunctional pipette. No payments or financial gain were a reason for, or a direct consequence of, the research contained within the manuscript.

Author Contributions

I.G. and A.A. designed the study and E.K. made the initial setup. K.S. carried out the microscopy experiments and analyzed the experimental data. A.A. developed the FEM model. I.G. suggested the investigation of the surface-induced subcompartmentalization phenomena, contributed to data evaluation, and supervised the project. All authors contributed to the writing of the manuscript.

Keywords

compartments, origin of life, protocells, solid surfaces, wetting

Received: August 28, 2020

Revised: October 15, 2020

Published online: November 23, 2020

- [1] Y. Diekmann, J. B. Pereira-Leal, *Biochem. J.* **2013**, *449*, 319.
- [2] E. Cornejo, N. Abreu, A. Komeili, *Curr. Opin. Cell Biol.* **2014**, *26*, 132.
- [3] M. J. Seufferheld, K. Kim, J. Whitfield, A. Valerio, G. Caetano-Anollés, *Biol. Direct* **2011**, *6*, 50
- [4] R. Nevo, D. Charuvi, E. Shimoni, R. Schwarz, A. Kaplan, I. Ohad, Z. Reich, *EMBO J.* **2007**, *26*, 1467.
- [5] *The Minimal Cell: The Biophysics of Cell Compartment and the Origin of Cell Functionality* (Eds: P. L. Luisi, P. Stano), Springer, New York **2011**.
- [6] M. Markström, A. Gunnarsson, O. Orwar, A. Jesorka, *Soft Matter* **2007**, *3*, 587.
- [7] L. M. Dominak, E. L. Gundermann, C. D. Keating, *Langmuir* **2010**, *26*, 5697.
- [8] M. S. Long, C. D. Jones, M. R. Helfrich, L. K. Mangeney-Slavin, C. D. Keating, *Proc. Natl. Acad. Sci. U. S. A.* **2005**, *102*, 5920.
- [9] S. Moreno-Flores, *Biochim. Biophys. Acta, Biomembr.* **2016**, *1858*, 793.
- [10] P. A. Monnard, P. Walde, *Life* **2015**, *5*, 1239.
- [11] J. F. Lambert, *Origins Life Evol. Biospheres* **2008**, *38*, 211.
- [12] V. Erastova, M. T. Degiacomi, D. G. Fraser, H. C. Greenwell, *Nat. Commun.* **2017**, *8*, 2033.
- [13] R. M. Hazen, D. A. Sverjensky, *Cold Spring Harbor Perspect. Biol.* **2010**, *2*, a002162.
- [14] M. Karlsson, K. Sott, M. Davidson, A.-S. Cans, P. Linderholm, D. Chiu, O. Orwar, *Proc. Natl. Acad. Sci. U. S. A.* **2002**, *99*, 11573.
- [15] T. Lobovkina, I. Gözen, Y. Erkan, J. Olofsson, S. G. Weber, O. Orwar, *Soft Matter* **2010**, *6*, 268.
- [16] I. Gözen, P. Dommersnes, I. Czolkos, A. Jesorka, T. Lobovkina, O. Orwar, *Nat. Mater.* **2010**, *9*, 908.
- [17] I. Gözen, M. Shaali, A. Ainla, B. Örtmen, I. Pöldsalu, K. Kustanovich, G. D. M. Jeffries, Z. Konkoli, P. Dommersnes, A. Jesorka, *Lab Chip* **2013**, *13*, 3822.
- [18] A. Ainla, G. D. M. Jeffries, R. Brune, O. Orwar, A. Jesorka, *Lab Chip* **2012**, *12*, 1255.
- [19] E. Karatekin, O. Sandre, F. Brochard-Wyart, **2003**, *52*, 486–493.
- [20] C. Culbertson, *Talanta* **2002**, *56*, 365.
- [21] A. Melcrová, S. Pokorna, S. Pullanchery, M. Kohagen, P. Jurkiewicz, M. Hof, P. Jungwirth, P. S. Cremer, L. Cwiklik, *Sci. Rep.* **2016**, *6*, 38035.

- [22] O. Sandre, L. Moreaux, F. Brochard-Wyart, *Proc. Natl. Acad. Sci.* **1999**, *96*, 10591.
- [23] K. I. Akashi, H. Miyata, H. Itoh, K. Kinoshita, *Biophys. J.* **1998**, *74*, 2973.1.
- [24] A.-L. Bernard, M.-A. Guedeau-Boudeville, L. Jullien, J.-M. Di Meglio, *Langmuir* **2000**, *16*, 6809.
- [25] C. A. Keller, B. Kasemo, *Biophys. J.* **1998**, *75*, 1397.
- [26] S. Jõemetsa, K. Spustova, K. Kustanovich, A. Ainla, S. Schindler, S. Eigler, T. Lobovkina, S. Lara-Avila, A. Jesorka, I. Gözen, *Langmuir* **2019**, *35*, 10286.
- [27] J. D. Toner, D. C. Catling, *Proc. Natl. Acad. Sci. U. S. A.* **2020**, *117*, 883.
- [28] J. Kazmierczak, S. Kempe, B. Kremer, *Curr. Org. Chem.* **2013**, *17*, 1738.
- [29] B. Burcar, A. Castañeda, J. Lago, M. Daniel, M. A. Pasek, N. V. Hud, T. M. Orlando, C. Menor-Salván, *Angew. Chem., Int. Ed.* **2019**, *58*, 16981.
- [30] U. Seifert, R. Lipowsky, *Phys. Rev. A* **1990**, *42*, 4768.
- [31] T. Bilal, I. Gözen, *Biomater. Sci.* **2017**, *5*, 1256.
- [32] M. Rousset, T. Cens, N. Vanmau, P. Charnet, *FEBS Lett.* **2004**, *576*, 41.
- [33] V. Prachayasittikul, C. Isarankura-Na-Ayudhya, T. Tantimongcolwat, C. Nantasenamat, H. J. Galla, *Acta Biochim. Biophys. Sin.* **2007**, *39*, 901.
- [34] H. Hashizume, in *Clay Minerals in Nature*, Intech Open, London **2012**.
- [35] M. M. Hanczyc, S. S. Mansy, J. W. Szostak, *Origins Life Evol. Biospheres* **2007**, *37*, 67.
- [36] M. M. Hanczyc, S. M. Fujikawa, J. W. Szostak, *Science* **2003**, *302*, 618.
- [37] C. Monzel, D. Schmidt, U. Seifert, A. S. Smith, R. Merkel, K. Sengupta, *Soft Matter* **2016**, *12*, 4755.
- [38] K. Ogłęcka, P. Rangamani, B. Liedberg, R. S. Kraut, A. N. Parikh, *eLife* **2014**, *3*, e03695.
- [39] E. S. Köksal, S. Liese, I. Kantarci, R. Olsson, A. Carlson, I. Gözen, *ACS Nano* **2019**, *13*, 6867.
- [40] K. Olbrich, W. Rawicz, D. Needham, E. Evans, *Biophys. J.* **2000**, *79*, 321.
- [41] M. I. Angelova, A. F. Bitbol, M. Seigneuret, G. Staneva, A. Kodama, Y. Sakuma, T. Kawakatsu, M. Imai, N. Puff, *Biochim. Biophys. Acta, Biomembr.* **2018**, *1860*, 2042.
- [42] B. K. D. Pearce, R. E. Pudritz, D. A. Semenov, T. K. Henning, *Proc. Natl. Acad. Sci. U. S. A.* **2017**, *114*, 11327.
- [43] W. Martin, J. Baross, D. Kelley, M. J. Russell, *Nat. Rev. Microbiol.* **2008**, *6*, 805.
- [44] S. F. Jordan, H. Ramm, I. N. Zheludev, A. M. Hartley, A. Maréchal, N. Lane, *Nat. Ecol. Evol.* **2019**, *3*, 1705.
- [45] G. Bolognesi, M. S. Friddin, A. Salehi-Reyhani, N. E. Barlow, N. J. Brooks, O. Ces, Y. Elani, *Nat. Commun.* **2018**, *9*, 1882.
- [46] J. Prives, M. Shinitzky, *Nature* **1977**, *268*, 761.
- [47] E. S. Köksal, S. Liese, L. Xue, R. Ryskulov, L. Viitala, A. Carlson, I. Gözen, *Small* **2020**, *16*, 2002529.
- [48] A. Küchler, M. Yoshimoto, S. Luginbühl, F. Mavelli, P. Walde, *Nat. Nanotechnol.* **2016**, *11*, 409.
- [49] Y. Liu, E. C. Y. Yan, K. B. Eisenthal, *Biophys. J.* **2001**, *80*, 1004.
- [50] K. Sott, T. Lobovkina, L. Lizana, M. Tokarz, B. Bauer, Z. Konkoli, O. Orwar, *Nano Lett.* **2006**, *6*, 209.
- [51] M. Preiner, S. Asche, Becker, S. Betts, H. C. Boniface, A. Camprubi, E. Chandru, K. Erastova, V. Garg, S. G. Khawaja, N. Kostyrka, G. Machné, R. Moggioli, G. Muchowska, K. B. Neukirchen, S. Peter, B. Pichlhöfer, E. Radványi, Á. D. Rossetto, Salditt, A. Schmelling, N. M. Sousa, F. L. Tria, F. D. K. Vörös, D. Xavier, J. C., *Life* **2020**, *10*, 20.
- [52] A. L. Bernard, M. A. Guedeau-Boudeville, L. Jullien, J. M. Di Meglio, *Biochim. Biophys. Acta, Biomembr.* **2002**, *1567*, 1.
- [53] P. Dalai, N. Sahai, *Trends Biochem. Sci.* **2019**, *44*, 331.
- [54] U. Schreiber, C. Mayer, O. J. Schmitz, P. Rosendahl, A. Bronja, M. Greule, F. Keppler, I. Mulder, T. Sattler, H. F. Schöler, *PLoS One* **2017**, *12*, e0177570.
- [55] W. R. Hargreaves, S. J. Mulvihill, D. W. Deamer, *Nature* **1977**, *266*, 78.
- [56] M. Rao, J. Eichberg, J. Oró, *J. Mol. Evol.* **1982**, *18*, 196.
- [57] M. Rao, J. Eichberg, J. Oró, *J. Mol. Evol.* **1987**, *25*, 1.
- [58] D. E. Epps, E. Sherwood, J. Eichberg, J. Oró, *J. Mol. Evol.* **1978**, *11*, 279.
- [59] C. Xu, S. Hu, X. Chen, *Mater. Today* **2016**, *19*, 516.
- [60] H. Bayley, I. Cazimoglu, C. E. G. Hoskin, *Emerging Top. Life Sci.* **2019**, *3*, 615.
- [61] Q. Li, S. Li, X. Zhang, W. Xu, X. Han, *Nat. Commun.* **2020**, *11*, 232.
- [62] Y. Ai, R. Xie, J. Xiong, Q. Liang, *Small* **2020**, *16*, 1903940.
- [63] J. W. Hindley, R. V. Law, O. Ces, *SN Appl. Sci.* **2020**, *2*, 593.
- [64] Y. Elani, R. V. Law, O. Ces, *Nat. Commun.* **2014**, *5*, 5305.
- [65] E. S. Köksal, P. F. Belletati, G. Reint, R. Olsson, K. D. Leitl, I. Kantarci, I. Gözen, *JoVE* **2019**, *143*, e58923.
- [66] C. Billerit, I. Wegrzyn, G. D. M. Jeffries, P. Dommersnes, O. Orwar, A. Jesorka, *Soft Matter* **2011**, *7*, 9751.



Supporting Information

for *Small*, DOI: 10.1002/sml.202005320

Subcompartmentalization and Pseudo-Division of Model
Protocells

*Karolina Spustova, Elif Senem Köksal, Alar Ainla, and Irep
Gözen**

Supplementary Information for:

Subcompartmentalization and pseudo-division of model protocells

Karolina Spustova¹, Elif Senem Köksal¹, Alar Ainla², Irep Gözen^{1,3,4*}

¹ Centre for Molecular Medicine Norway, Faculty of Medicine, University of Oslo, 0318 Oslo, Norway

² International Iberian Nanotechnology Laboratory, 4715-330 Braga, Portugal

³ Department of Chemistry, Faculty of Mathematics and Natural Sciences, University of Oslo, 0315 Oslo, Norway

⁴ Department of Chemistry and Chemical Engineering, Chalmers University of Technology, SE-412 96 Göteborg, Sweden

*To whom correspondence should be addressed. Email: irep@uio.no

Table of contents

S1 Lipid compositions and surfaces

S2 Experimental setup

S3 Heating system

S4 Finite element simulations

S5 Stability of daughter protocells

S6 Product efficiency of pseudo-division

S1. Lipid compositions and surfaces

Surface	Lipid species	wt% percentage	Fluorophore (1%)	Associated figure
Al ₂ O ₃	PC:DOPE	69:30	Texas Red-DHPE ATTO 655-DHPE	Fig. 1a-b, e-f Fig. 2a-l Fig. 4a
	PE:PG:CA	67:23:9	16:0 Liss Rhod PE	Fig. 3a, e-p Fig. 1c-d
Al	PC:DOPE	69:30	Texas Red-DHPE	Fig. 5a-c Fig. S5a-f
	E.coli Ext. Pol.	99	16:0 Liss Rhod PE	Fig. S5g-j
	PE:PG:CA	67:23:9	16:0 Liss Rhod PE	Fig. S1a
SiO ₂	PE:PG:CA	67:23:9	16:0 Liss Rhod PE ATTO 655-DHPE	Fig. S1b

Table S1. Lipids, lipid-conjugated fluorophores and solid surface combinations

Abbreviations used in the table are as following:

PC : L- α -phosphatidylcholine (Soy)
 DOPE : 18:1 Dioleoylphosphoethanolamine
 PE : L- α -phosphoethanolamine (E.coli)
 PG : L- α -phosphatidylglycerol (E.coli)
 CA : Cardiolipin (E.coli)
 E.coli Ext. Pol. : E.coli polar lipid extract

All lipid products and 16:0 Liss Rhodamine PE were purchased from Avanti Polar Lipids, USA. Texas Red-DHPE was purchased from Sigma-Aldrich, USA. ATTO 655-DHPE was purchased from ATTO-TEC, Gmbh Germany.

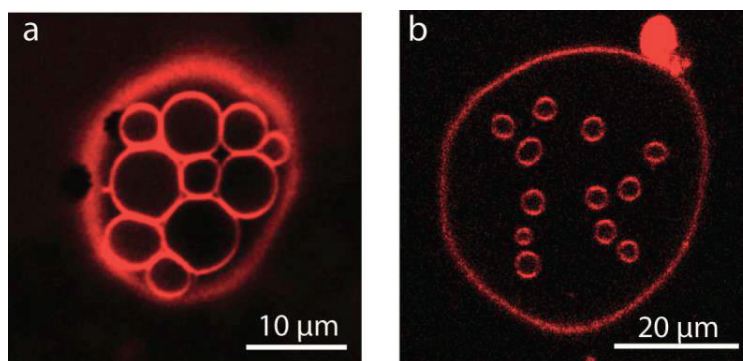


Figure S1. Subcompartmentalized model protocells made from PE-PG-CA lipids on (a) an Al surface with a native oxide layer, (b) SiO₂ surface.

S2. Experimental setup

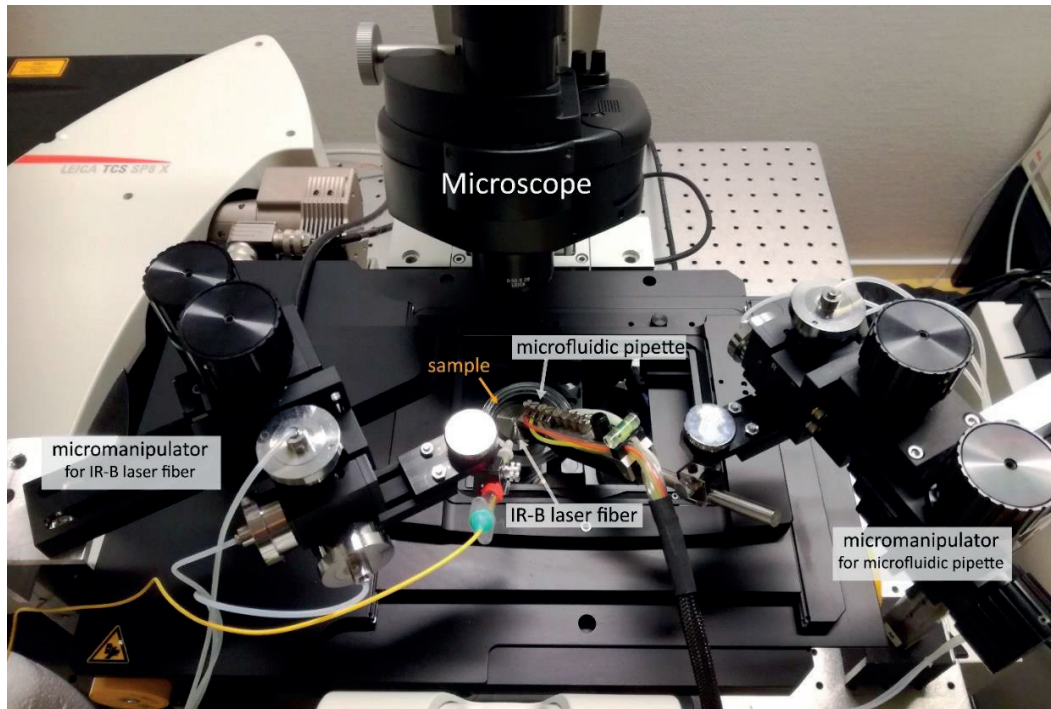


Figure S2. For the simultaneous heating and pulsing of fluorescein, an optical fiber coupled to an IR-B laser and a microfluidic pipette were positioned above the model protocells in the sample chamber, using 3-axis water hydraulic micromanipulators. The tip of the fiber and the tip of the pipette were placed in close proximity to target the same model protocell.

S3. Localized heating

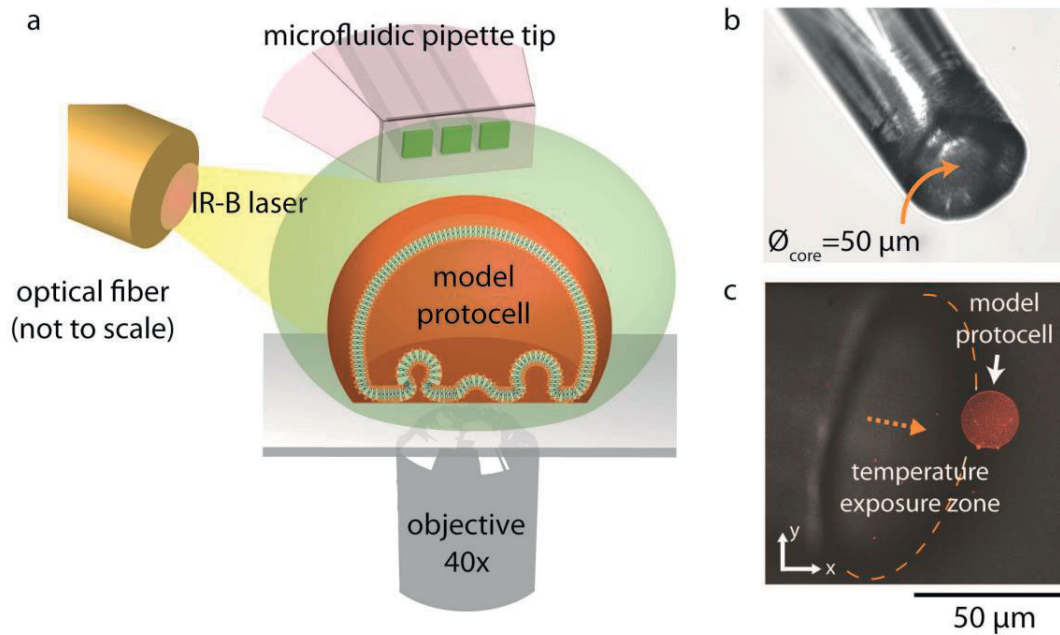


Figure S3. Localized heating. **(a)** The optical fiber is positioned above the surface near the model protocell of interest. Upon activation of the laser, the temperature in the vicinity of the protocell is increased to 40 °C. The heating can be applied with **(Fig. 3)** and without **(Fig. 2)** simultaneous fluorescein pulsing. Both the optical fiber tip and the microfluidic pipette tip are submerged into the sample buffer (not shown). **(b)** Micro-photograph of the optical fiber tip employed in the experiments. **(c)** Close up of the optical fiber tip while heating a model protocell.

S4. FEM simulations

Fig. S4 shows the concentration change in vesicles of varying size and with varying pore sizes over time, according to the FEM simulations described in the main article (**Fig. S4a**). Data sets are fitted with the function $1-e^{-kt}$, where the k is a loading rate. This is analogous to charging a capacitor through a resistor (RC circuit), where the vesicle internal volume will take the place of capacitor, and the pore will be the resistance for the loading. As expected, the loading rate increases with pore radius (**Fig. S4b**) and it is inversely proportional to the vesicle volume (**Fig. S4c**).

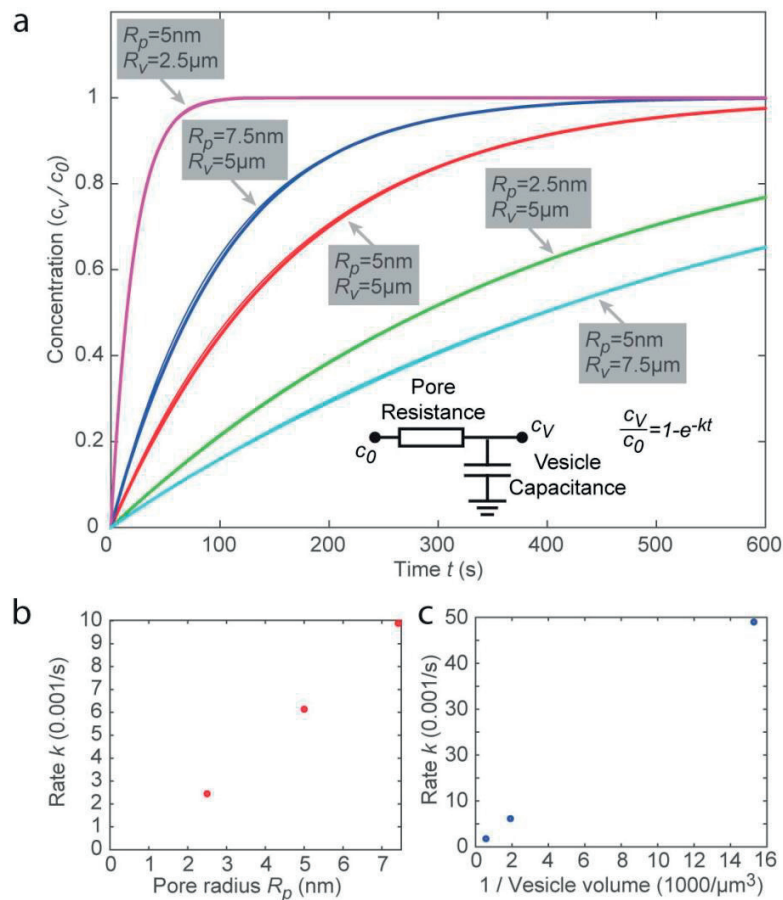


Figure S4. (a) FEM simulations showing encapsulation of fluorescein in vesicles of varying size and pore size, over time. (b) loading rate vs. pore radius, (c) loading rate vs. vesicle volume.

S5. Stability of daughter protocells

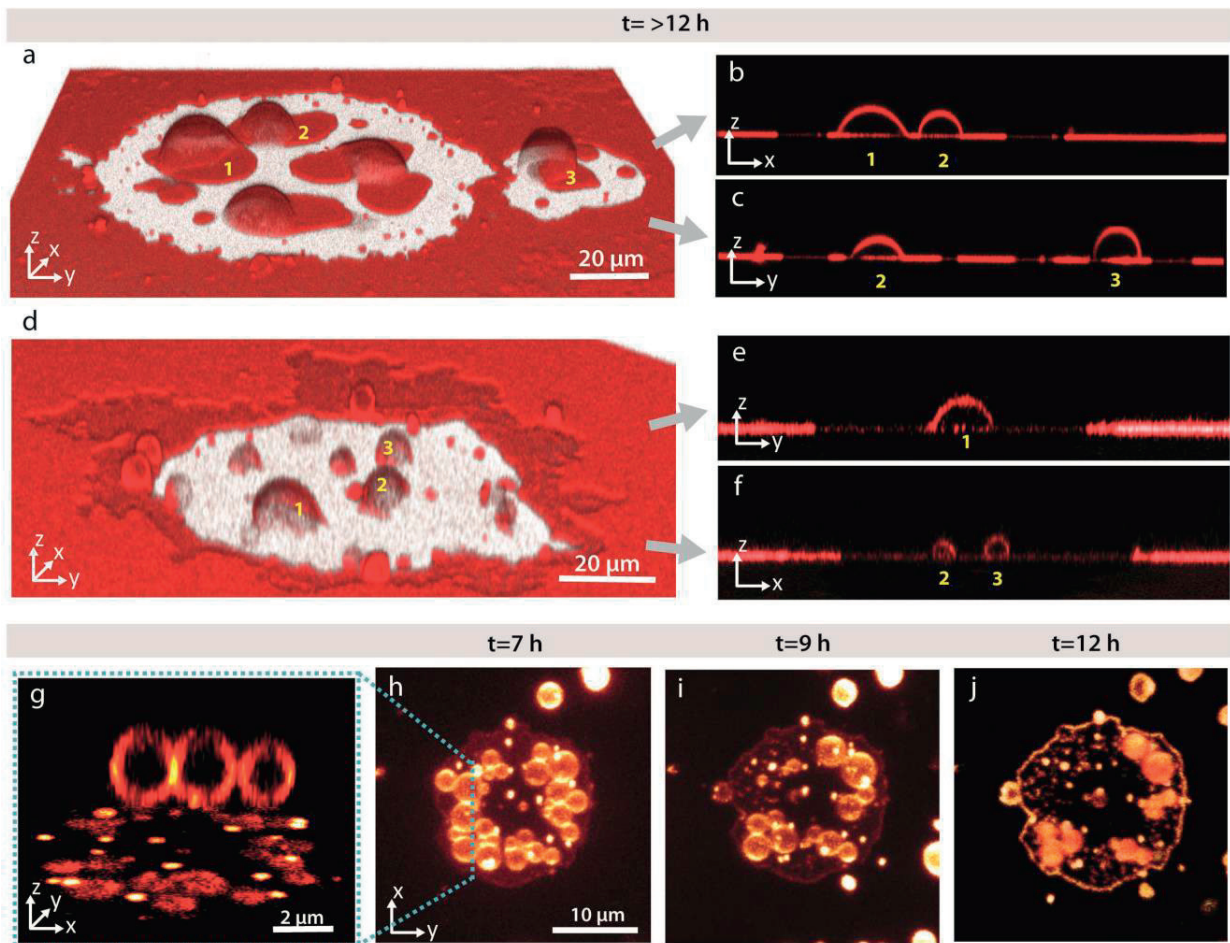


Figure S5. (a-j) Confocal micrograph of daughter protocells remaining after pseudo-division. **(a, d)** 3D reconstructed, perspective view (x-y-z) **(b-c, e-f)** cross-sections, side views (x-z/y-z). Micrographs were taken 12 hours after the addition of chelators to the ambient solution. Confocal micrographs of daughter protocells from profile view **(g)** and top view **(h-j)**. The micrographs have been acquired 7 h **(h)**, 9 h **(i)** and 12 h **(j)** after chelator addition. The membranes of the vesicles shown in this figure are composed of (a-f) PC-DOPE or (g-j) E.coli Ext. Pol.; all of the surfaces are Al (with a native oxide layer).

S6. Product efficiency of pseudo-division

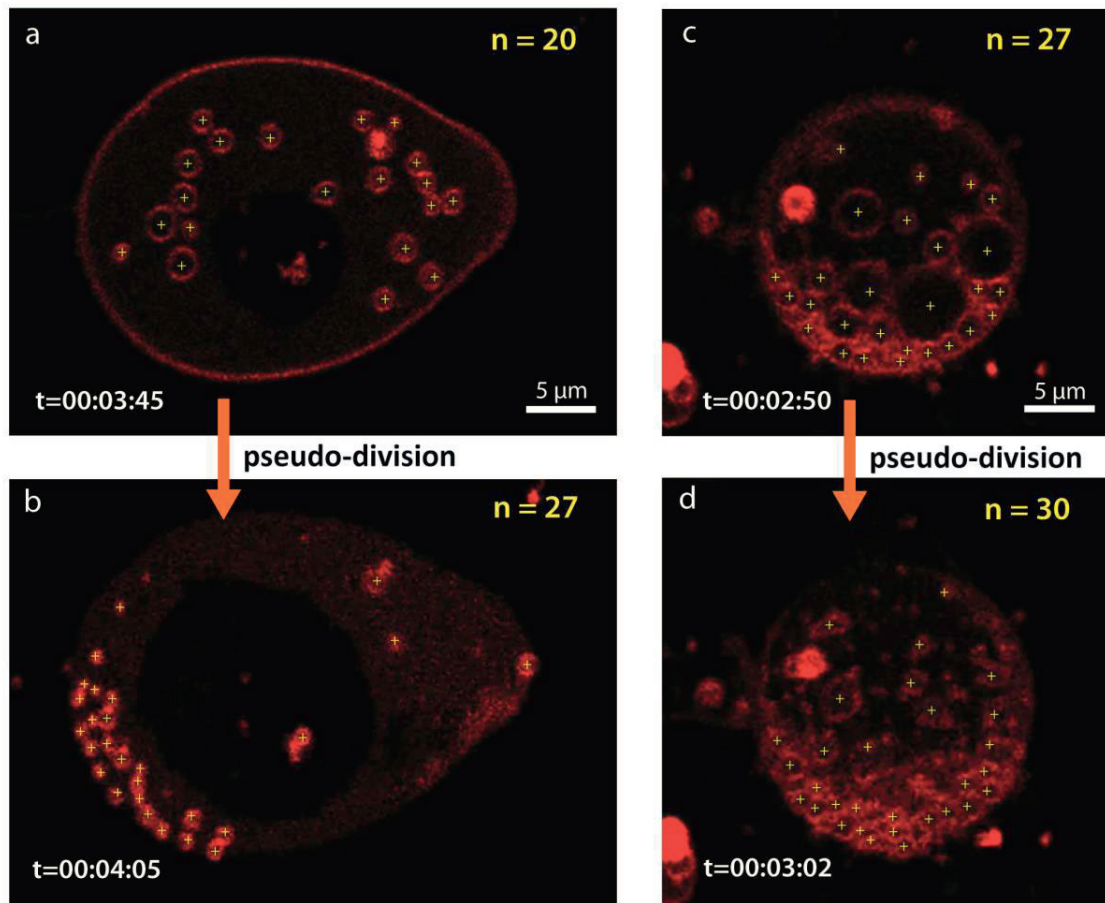


Figure S6. (a-d) Confocal micrographs showing two different experiments (a-b, c-d) where pseudo-division occurred. The number of subcompartments increase after the rupturing of the enveloping (distal) membrane (**Mov. S3**).

Supplementary Videos

Movie S1. Subcompartmentalization at increased temperature. Laser scanning confocal microscopy time series showing the temperature-induced formation, growth and fusion of the subcompartments.

Movie S2. Encapsulation and compartmentalization of fluorescein. Laser scanning confocal microscopy time series showing the encapsulation and release of the fluorescein by the subcompartments and the primary volume of the protocell. Part I: room temperature, Part II: increased temperature (40 °C).

Movie S3. Pseudo-division. Laser scanning confocal microscopy time series showing process of the pseudo-division upon disintegration of the distal membrane of the compartmentalized protocell.